Monitoring Bluff Erosion Rates Using Terrestrial Laser Scanning on Minnesota's North Shore Streams

A Thesis
SUBMITTED TO THE FACULTY
OF THE UNIVERSITY OF MINNESOTA
BY

Leah R. Hall

IN PARTIAL FULFILLMENT OF THE REQUIREMENTS
FOR THE DEGREE OF MASTER OF SCIENCE
IN NATURAL RESOURCES SCIENCE AND MANAGEMENT – FOREST HYDROLOGY AND WATERSHED MANAGEMENT

Dr. Joe Magner, Advisor

May 2016

Acknowledgements

This project could not have been completed without the support of many parties. I would like to extend my gratitude to my advisor, Dr. Joe Magner for his help throughout my graduate school process. I would also like to sincerely thank Dr. Karen Gran for her extensive guidance, time, and support she gave to me throughout this project. Additionally, I would like to thank Dr. Chris Lenhart and Brad Hansen for their advice, expertise and assistance.

Thank you to Grant Cooper, Blair Kelly, Lesley Gerberding, and Aaron Knowlton for all of your help in the field collecting data. Thank you also to all the fellow graduate students who helped me think through various aspects of my thesis, gave advice, helped with editing, and with moral support.

Thank you to the Minnesota Pollution Control Agency through a research assistant from the University of Minnesota Department of Biosystems and Bioproducts Engineering for providing funding for me to work on this project.

Lastly, I would like to thank my parents Jim and Allison, my sister Kelly, Brian, and all my other family and friends for their support and love.

Abstract

Portions of ten streams along Minnesota's North Shore currently are listed on the Environmental Protection Agency's 303(d) list as impaired for turbidity, due to excess sediment. Bluff erosion is a large contributor of fine sediment to Minnesota's North Shore streams; however, inadequate data are available to quantify rates of bluff erosion relative to total suspended solid (TSS) loads. This bluff monitoring project is designed to quantify site-specific bluff erosion rates at ten sites and combine them into annual fine sediment loads attributed to bluff erosion.

Bluff erosion rates are quantified using terrestrial laser scanning (TLS), which allows for the creation of high resolution digital elevation maps (DEMs) of bluff surfaces. DEMs can be used to quantify geomorphic change over time on riverine bluffs. In this study, we assessed multi-year bluff erosion rates on a series of bluffs on Amity Creek and Lester River. We compared previously scanned and analyzed data from 2011 and 2012 on eight bluffs along Amity Creek and Lester River with scans collected from these same bluffs in fall 2013, fall 2014, and spring and fall 2015.

The second component of the study involved comparing erosion rates from natural bluffs with bluffs that have undergone stabilization work. Two bluffs on Amity Creek were stabilized in 2009 and these bluffs have been scanned at least once a year since 2012. One more site on Amity Creek and one on the Knife River were stabilized in 2014. These two bluffs were scanned in fall 2014, spring 2015 and fall 2015. Retreat rates from stabilized bluffs were compared with natural bluffs to analyze the initial effectiveness of these stabilization efforts.

This study used a Faro Focus 3D phase-shift laser scanner to collect TLS point cloud datasets. Post-processing of the data involved using Faro Scene, Topographic Point Cloud Analysis Toolkit (ToPCAT) and ArcGIS software, which included using the Geomorphic Change Detection (GCD) Add-in. Data produced were used to calculate average retreat rates between successive scanning campaigns of each bluff and to determine an overall average retreat rate over the entire study period.

Geomorphic change was measured on eight of the study sites over a four-year period and change was detected in seven to nine periods for these bluffs. The time periods between scans ranged from one month to one year. Geomorphic change was differentiated on these eight bluffs over a three-year period, November 2012 to November 2015, to obtain an average retreat rate. The average annual retreat rate, determined from a weighted average based on bluff area, is -0.08 m/yr.

Since most of the study sites are in Amity Creek watershed, we extrapolated this erosion rate to bluffs throughout the watershed to determine a total mass of sediment that is being contributed to the stream by bluff erosion. It is estimated that bluffs contributed 564,000 kg of fine sediment to Amity Creek annually, which when compared to total suspended solid (TSS) load estimates in Amity Creek from previous years, is anywhere from 40-558% of the total. Results show that high flow events, such as the 500-year flood that occurred on June 19-20, 2012, and resulted in 7.25 inches of precipitation, have the greatest impact on bluff erosion. However, detectable geomorphic change was measured even when there were no high flow events, showing that other processes, such as freeze-thaw cycles influence bluff erosion.

This study also looked at four stabilized bluffs, where sediment reduction was attempted to be quantified. This was not possible on two of the stabilized bluffs. However, on the two other bluffs, stabilized in 2014 and scanned over a 14-month period, results show that stabilization efforts have worked to slow erosion rates and retain eroded sediment that does occur. Due to these results and the evidence that bluffs are contributing a large portion of the total TSS to Amity Creek and therefore likely other watersheds in the North Shore region, it is clear that controlling bluff erosion is an effective measure to improving water quality in these turbidity impaired streams.

Table of Contents

List of Tables

List of Figures

1.0 INTRODUCTION

Lake Superior South and North watersheds are located in northeastern Minnesota, adjacent to Lake Superior, and include parts of St. Louis, Cook, and Lake Counties. This area is known as Minnesota's North Shore and is a relatively undeveloped region, compared to the rest of the state. However, stream impairments exist. Portions of ten streams along the North Shore currently are listed on the Environmental Protection Agency's 303(d) list as impaired for turbidity due to excess sediment (Lahti et al., 2013). The impaired streams include the Knife, Sucker, Beaver, Poplar, Flute Reed, French, Talmadge, Skunk, Amity and Lester (Lahti et al., 2013).

Bluff erosion is a large contributor of fine sediment to Minnesota's North Shore streams; however, inadequate data are available to quantify rates of bluff erosion relative to total suspended solid (TSS) loads. This bluff monitoring project is designed to quantify site-specific bluff erosion rates at ten sites and combine them into annual fine sediment loads attributed to bluff erosion.

Light detection and ranging (LiDAR) is currently at the forefront of techniques to analyze bluff erosion (Heritage and Hetherington, 2007; Milan et al., 2007; Buckley et al., 2008; Nasermoaddeli and Pasche, 2008; Resop and Hession, 2010; Day et al., 2012). Most LiDAR scans are taken aerially; however, to analyze bluff erosion, terrestrial laser scanning (TLS) was utilized to create digital elevation models (DEMs) of each bluff. Repeat TLS scans were then used to quantify geomorphic change over time (Buckley et al., 2008).

This project has several components. First, we assess multi-year bluff erosion rates on a series of bluffs on Amity Creek and Lester River. We compare previously scanned and analyzed data from 2011 and 2012 on eight bluffs along Amity Creek and

Lester River with scans collected from these same bluffs in fall 2013, fall 2014, and spring and fall 2015. These combined datasets provide four years of continuous data on bluff changes.

The second component involves comparing erosion rates from natural bluffs with bluffs that have undergone bank stabilization work. Two bluffs on Amity Creek were stabilized in 2009 and these bluffs have been scanned at least once a year since 2012. One more site on Amity Creek and one on the Knife River were stabilized in 2014. These two bluffs were scanned in fall 2014, spring 2015 and fall 2015. Analysis of the four stabilized bluffs will provide preliminary results for comparing the erosion/deposition rates of stabilized bluffs to bluffs that have not been stabilized.

By combining multiple years of bluff erosion data, we can determine the contribution of bluff erosion to the fine sediment loads in North Shore streams. Although the bluffs being analyzed are only on three of the impaired North Shore streams, many streams in this region have similar geomorphic characteristics and the results here may be transferable to other streams in the region. In addition, the data can then ultimately be used to determine the effectiveness of bluff stabilization projects in terms of trapping fine sediment that would otherwise be input into the stream, thus reducing turbidity.

2.0 FIELD SITE

The bluffs being monitored in this study are along Amity Creek, Lester River and Knife River (Figure 2.1). These streams lie in northeastern Minnesota, in what is referred to as Minnesota's North Shore. Amity Creek and Lester River are located in the northeastern section of Duluth, Minnesota (Figure 2.1). Amity Creek flows southwest of Lester River, and the two streams converge just before their water discharges into Lake

Superior. The Knife River is located approximately ten miles north of Duluth, Minnesota, and is approximately ten miles south of Two Harbors, Minnesota (Figure 2.1). It also drains into Lake Superior.

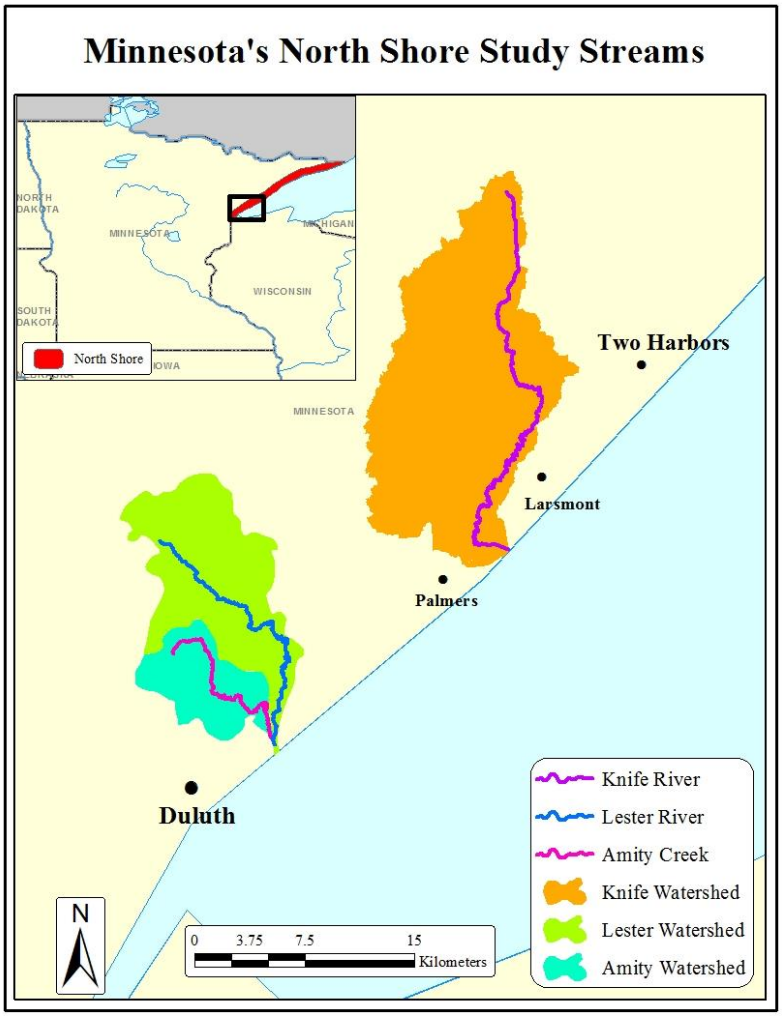

Figure 2.1: Location of Amity Creek, Lester River, and Knife River within the North Shore region.

The geological characteristics and glaciation history of the North Shore have a large influence on the processes occurring today within the Amity Creek, Lester River and Knife River watersheds. The bedrock geology of this region was primarily emplaced approximately 1.1 billion years ago, when the Lake Superior Basin was created by a midcontinental rift system (Sims and Morey 1972). The bedrock in the area is composed

of stacked basalt flows and igneous intrusions, which formed during the rifting (Sims and Morey 1972).

Minnesota's North Shore was also impacted by numerous glaciation events. This includes the Superior Lobe, which was a lobe of the Laurentide ice sheet and one of many lobes that developed in the late Wisconsinan (Figure 2.2) (Farrand and Drexler 1985). The Superior Lobe was present in the Lake Superior Basin up to 10,000 years before present (BP) and the ice lobe experienced numerous advancements and retreats (Farrand and Drexler 1985). During the last glacial maximum, approximately 21,000 years BP the Superior Lobe occupied the Lake Superior Basin and extended southwest as far as the St. Croix terminal moraine in southeastern Minnesota (Wright 1971).

As the Superior Lobe retreated to the northeast approximately 11,000 years BP, glacial Lake Duluth formed due to the meltwater produced from this retreating glacial lobe (Wright 1971). Glacial Lake Duluth at its highest level was about 1,100 feet above sea level (Farrand 1969). Glacial Lake Duluth drained to the south until the Superior Lobe retreated to a point, approximately 9,500 years BP, which allowed meltwater to drain to the east (Farrand 1969; Wright 1971). When this eastern drainage opened through the Sault St. Marie, the water level of glacial Lake Duluth fell to its lowest level of around 400 feet above sea level (Farrand 1969).

Due to further retreat of the vast Laurentide ice sheet, isostatic uplift of the North Shore began around 9,500 years BP and continues today (Farrand 1969). The uplift led to an increase in lake levels. Around 5,000 years BP the level of the glacial lake reached the current level of Lake Superior, 602 feet above sea level (Farrand 1969). However, the overall drop in base level of Lake Superior from 1,100 feet above sea level, created

instability in the streams that drain into the Lake, since the drop in base level at the mouth has not yet propagated throughout the watersheds (Andrews *et al*. 1980). Today, the streams continue to down-cut as they attempt to reach equilibrium with the lowered base level of Lake Superior, which leads to higher erosion rates in streams.

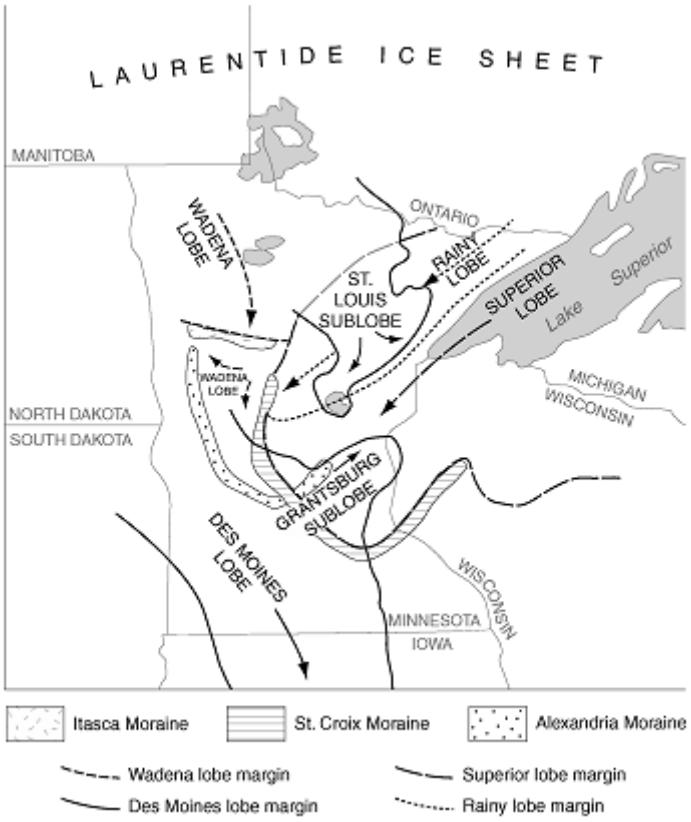

Figure 2.2: Location and extent of the Laurentide ice sheet lobes in Minnesota during the late Wisconsinan (Hobbs and Breckenridge 2011).

The soil of the North Shore is comprised of tills deposited by glaciations, interspersed with fine-grained lacustrine sediments deposited by glacial Lake Duluth. The lacustrine deposits can be seen in a narrow band along the shores of Lake Superior (Hobbs and Goebel 1982). The glacial tills deposited along the North Shore consist of two identified formations, the Cromwell and the Barnum formations (Hobbs 2004). The

Cromwell formation is the oldest Wisconsinan glacial sediment in the region (Hobbs 2004). It has a loam matrix, contains an average of 12% coarse-grained fragments (Hobbs 2003, Hobbs 2004) and is reddish-brown, 5YR 4/4 (Munsell Color 1975). It originated from glacial advancement in the Superior basin and obtained its reddish color from pulverized red sedimentary rocks, including sandstone, siltstone and shale, from the floor of the Superior basin (Hobbs 2004). It also contains other red rock fragments, which have a northeast origin and are mostly igneous rocks, including basalt, rhyolite, diabase and gabbro (Hobbs 2004).

The Barnum formation is a clayey till that overlies the Cromwell formation (Hobbs and Breckenridge 2011). The Barnum formation is broken up into member till units. These include the Lakewood, Moose Lake and the Knife River members. The Lakewood is the lowest till in the formation (Hobbs 2004). It is a reddish-brown color, 5 YR 4/3 to 3/4 (Munsell Color 1975), and has a silt loam matrix with about 6-12% coarse-grained fragments (Hobbs 2003, Hobbs 2004). The Moose Lake member is the middle till (Hobbs 2004). It is reddish-brown, 5 to 2.5 YR 5/3 to 4/4 (Munsell Color 1975), has a clay loam to silty clay loam matrix and approximately 3-6% coarse-grained fragments (Hobbs 2004). The uppermost till in the Barnum formation is the Knife River member (Hobbs 2004). This till is reddish-brown, 2.5 YR 5/3 to 4/4 (Munsell Color 1975), has a clay matrix and contains 1-3% coarse-grained fragments (Hobbs 2004). The till deposits, as well as the lacustrine deposits are composed of 40-100% fine-grained particles (i.e. silt and clay) within this region (Hobbs 2004). Therefore, when these deposits are eroded into waterbodies, due to the small particle sizes, they travel primarily as washload, thus contributing to turbidity.

All of the study watersheds are composed of multiple till formations. However, in general, the upper portion of the watersheds are comprised of the Cromwell formation and the middle portion of the watersheds are primarily composed of the Lakewood and Moose Lake members of the Barnum formation, with older units below (Neitzel 2014). The bottom section of the watersheds, as the streams near Lake Superior, are comprised of the Knife River member of the Barnum formation on top, with Moose Lake and Lakewood members below and Cromwell formation at the bottom. There are also pockets of fine-grained lacustrine sediments interspersed among the till deposits in the middle and lower reaches of the watersheds.

As Amity Creek begins, flowing through the Cromwell till formation, it is a low-gradient, meandering channel and evolves into a high-gradient, bedrock-dominated channel before converging with Lester River and Lake Superior. Amity Creek watershed is approximately 43.25 square kilometers and is comprised of lowland forest (69%), grassland (9%), developed land (7%), upland forest (7%), lowland shrubs (5%), cropland (2%) and upland shrubs (1%) (Fitzpatrick *et al*. 2006). Lester River also begins as a low-gradient, meandering channel and develops into a higher-gradient, bedrock-dominated channel before draining into Lake Superior. Lester River watershed is approximately 93.24 square kilometers and is comprised of lowland forest (68%), lowland shrubs (11%), upland forest (7%), grassland (5%), developed land (3%), cropland (2%), upland shrubs (2%), marsh (1%), and water (1%) (Fitzpatrick *et al*. 2006).

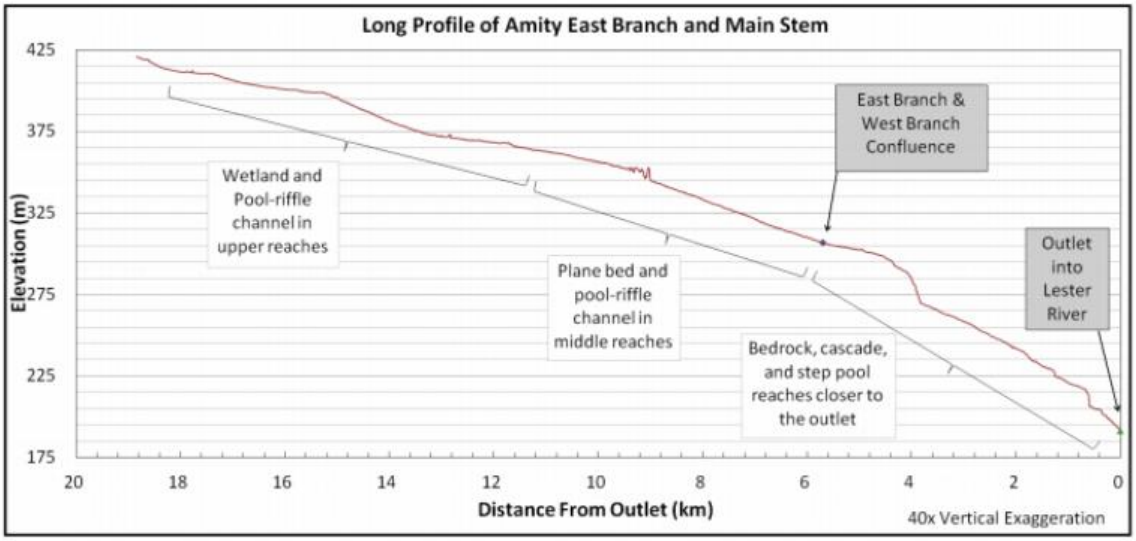

Figure 2.3: Annotated longitudinal profile of Amity Creek, showing a concave-down shape, with increasing slopes near the outlet. This longitudinal profile shape is common of North Shore streams (Wick, 2013).

Unlike most of the other North Shore streams, which run perpendicular to Lake Superior, much of the main channel of Knife River flows relatively parallel to the Lake (Figure 2.1). Therefore, the slope of the upper as well as the middle reaches of the stream are slightly more gradual than other North Shore streams. The slope of the lower reach still intensifies as it nears its outlet into Lake Superior, and this lower reach is dominated by bedrock. The Knife River watershed is approximately 216.52 square kilometers (Nieber *et al*. 2008). The land-use in the watershed is forest (72%), wetland (16%), grassland (6%), cropland (5%), and developed (1%) (Lake Superior Streams 2009).

Seven of the bluffs that were studied are on Amity Creek (Figure 2.3), two are on Lester River (Figure 2.4) and one is on the Knife River (Figure 2.5). The bluffs all are accessible by road or trail and generally lack vegetation. The bluffs range in size from approximately 30 to 700 m^2 and all lie on the outside of channel meanders.

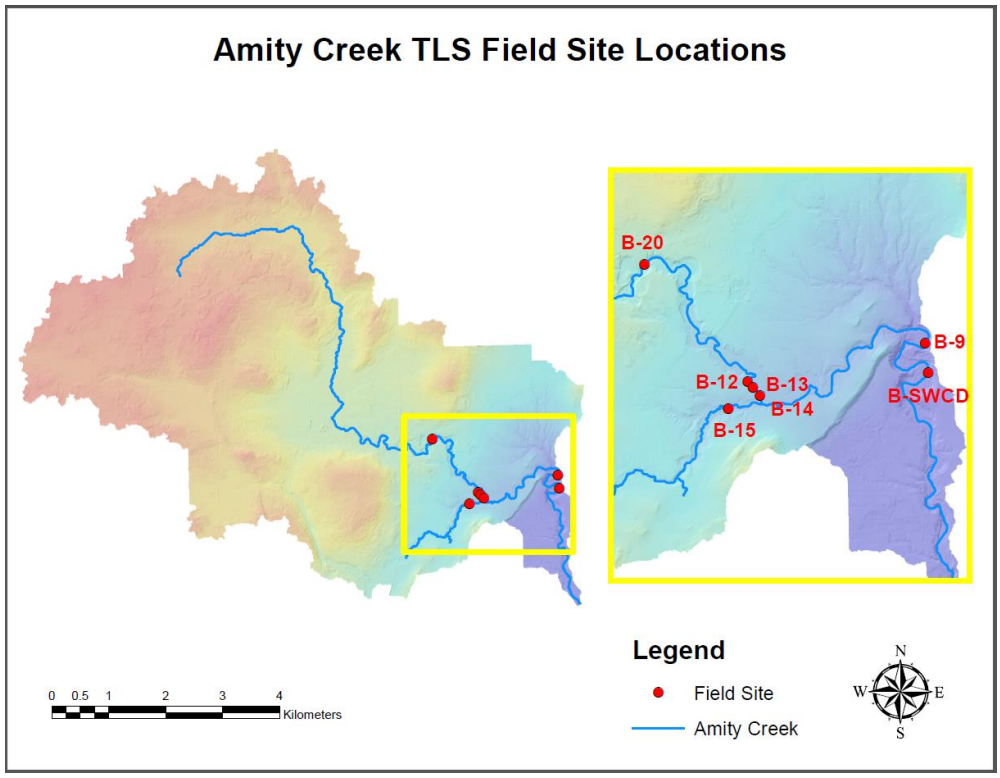

Figure 2.4: TLS field site locations within the Amity Creek watershed.

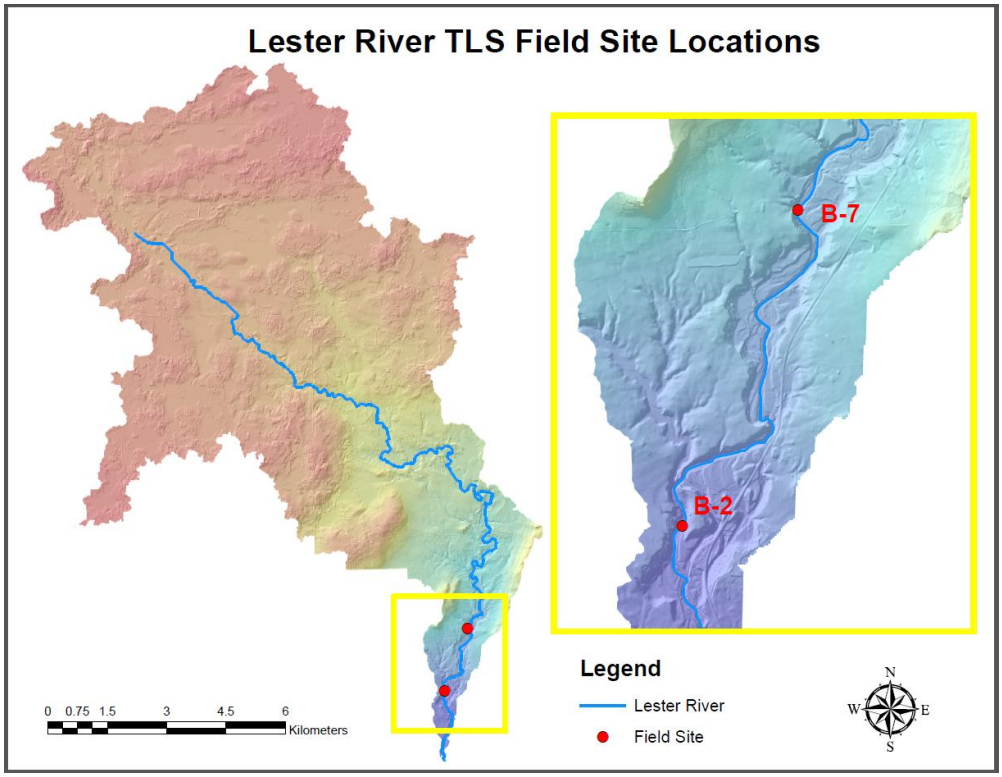

Figure 2.5: TLS field site locations within the Lester River watershed.

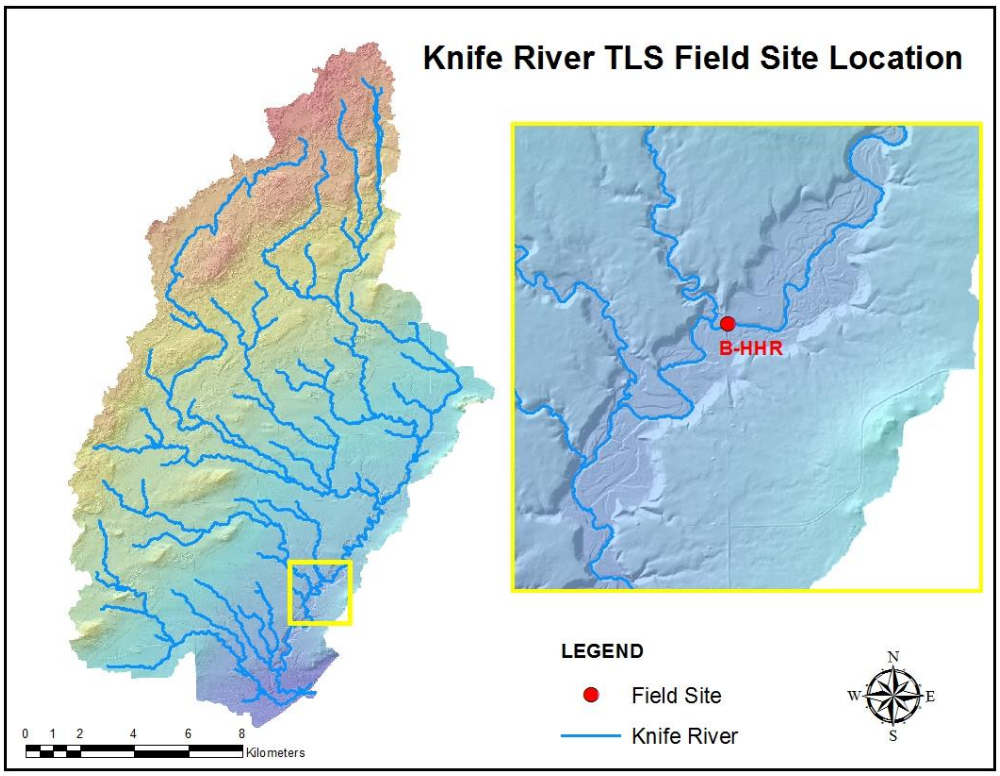

Figure 2.6: TLS field site locations within the Knife River watershed.

3.0 BACKGROUND

3.1 Terrestrial Laser Scanning

Terrestrial laser scanning (TLS), often called ground-based or terrestrial LiDAR, is a portable, tripod-based system that rapidly collects spatially-dense point cloud datasets (Buckley *et al*. 2008, Day *et al*. 2012). It uses pulse laser technology, which calculates the distance from the device to a point by measuring the time between the transmission of the laser pulse to the return of the reflected pulse (Letortu *et al*. 2014). TLS is able to collect three-dimensional geometry of objects and terrain surfaces ranging from forests, to industrial facilities, to riverine bluffs (Vosselman and Maas 2010). The data collected from this system can be used to generate digital elevation models, capturing unprecedented detail of surfaces (Buckley *et al*. 2008, Olsen 2014). Using the high spatial

resolution data collected from TLS, retreat rates and measurements can be made of geomorphic change, even on vertical surfaces such as bluffs (Day *et al*. 2012).

Other techniques that have been used to detect geomorphic change include erosion pins, total station instruments, Real-Time Kinematic Global Positioning Systems, terrestrial photogrammetry and aerial photogrammetry. Erosion pins provide high point resolution data at a relatively low cost (Couper *et al*, 2002) but have low spatial and temporal resolution, can be affected by operator bias, can only be used in areas that are accessible and can cause physical disturbance to the surface (Lawler 1993, Pyle *et al*. 1997, Day *et al*. 2012). Total station instruments and Real-Time Kinematic Global Positioning Systems allow for more spatial coverage than erosion pins but have lower resolution, can have sensor error and operator bias (Lawler 1993). Terrestrial photogrammetry collects dense and accurate datasets but offers low spatial resolution data due to reduced aerial coverage (Heritage and Hetherington 2007). Aerial photogrammetry can also be used and provides more spatial coverage but does not provide high elevation accuracy (Heritage and Hetherington 2007).

Airborne terrestrial laser mapping or airborne LiDAR has also been used to measure bluff erosion but due to the orientation of the airplane to the near vertical bluff surfaces it is difficult to capture and requires multiple flight lines and regular spacing between each flight line to produce an accurate model (Day *et al*. 2012). Additionally, a motion compensation correction has to be applied to data collected by airborne LiDAR and therefore can only produce DEMs with an accuracy of 15 cm (Charlton *et al*. 2003).

Terrestrial laser scanning was used in this study because it allows for the collection of data points across a large surface area (Resop and Hession 2010). Therefore,

it provides more information about the spatial variability and volume of a surface (Resop and Hession 2010) for the spatial scale (a meter to a kilometer) and time scale (a few days to many years) (Heritage and Hetherington 2007) that are necessary based on bluff sizes in this study and likely erosion rates. Terrestrial laser scanning also provides high spatial resolution analysis of the surface with millimeters to centimeters accuracy, is less time-consuming to collect data, does not require physical disturbances to the bluff surface (Day *et al*. 2012), removes operator bias associated with other techniques (Resop and Hession 2010) and is cheaper than other methods, such as airborne LiDAR mapping (Nasermoaddeli and Pasche 2008).

There are limitations of TLS. Vegetation on the surface of interest has to be removed digitally from the dataset during post-processing, because it conceals the surface (Grayson *et al.* 2012). This process is time-consuming and creates holes in the dataset in the location where vegetation was eliminated. Additionally, TLS cannot be run during precipitation events or in windy and dusty conditions, because these conditions will force the laser to scatter (Heritage and Hetherington 2007, Wawrzyniec *et al.* 2007). The TLS datasets are also very large, which require a computer with high processing speeds to analyze the data. A single TLS scan can contain several million points, with each point having a unique x, y, z coordinate and intensity value (Buckley *et al.* 2008).

Terrestrial laser scanning is a relatively new technology; however, it has been used in other geomorphic studies. These studies have ranged in scale from measuring individual rock breakdown (Bourke et al., 2008) to measuring landslides (Bitelli *et al.* 2004, Teza *et al*. 2008, Blasone 2014). Terrestrial laser scanning used for detecting geomorphic change has also ranged in environmental setting, having been used to

monitor dynamic erosion of beach berms in southern California (Schubert *et al.* 2015), to measure erosion across a bog in the United Kingdom (Graysen *et al*. 2012) and to measure slip-surface geometry of faults in central Greece (Jones *et al*. 2009). Terrestrial laser scanning has also been used before to measure geomorphic change of bluffs, river banks and cliffs. For example, Neitzel (2014) successfully utilized TLS to investigate the relationship between peak flow rates and stream bluff erosion in Amity Creek and Lester River watersheds. Day *et al*. (2012) used TLS to find the rates and processes of bluff erosion on Le Sueur River in southern Minnesota. Terrestrial laser scanning has also been used to measure the retreat rate of sea cliffs (Rosser *et al*. 2005, Lim *et al*. 2010, Letortu *et al*. 2014) and Resop and Hession (2010) as well as O'Neal and Pizzuto (2010) used TLS to analyze stream bank retreat in two different river systems in Virginia.

3.2 Bluff Erosion Processes

Bluff erosion has been shown to be a primary contributor of sediment loading in many watersheds (Cancienne *et al.* 2008, Nasermoaddeli and Pasche 2008, Fox *et al*. 2007), including in some watersheds along Minnesota's North Shore (Andrews *et al*. 1980, Wick 2013, Neitzel 2014). Excess sediment is a concern in streams due to the potential health impacts on aquatic organisms. Increased turbidity can raise water temperatures, restrict primary production, lower dissolved oxygen levels, clog fish gills, affect egg and larval development, and make it more challenging for visual hunters to find prey (Grabbelaar 2009). Excess sediment can also lead to deposition, resulting in changes to stream and lake morphology (Grabbelaar 2009). Additionally, erosion of sediment can attach to and result in the transport of undesirable quantities of heavy

metals and nutrients into the stream, which can lead to a variety of undesirable stream conditions (Andrews *et al.* 1980, Brooks *et al*. 2013).

The main controls affecting bluff erosion are soil characteristics, near surface processes, hydrologic processes and mass failures (Lawler 1992, Couper and Maddock 2001, Wynn and Mostaghimi 2006, Resop and Hession 2010). Soil characteristics have a strong influence on bluff erodibility potential. Bulk density, which is a measure of soil compaction and is calculated by dividing the dry weight of soil by its volume, has been shown to affect soil erosion rates (Wynn and Mostaghimi 2006). As bulk density increases, shear strength of a soil also increases (Asare *et al*. 1997). High bulk density therefore decreases the likelihood of erosion. Soil texture, which is the proportion of sand, silt and clay in a soil, also influences soil behavior. This is because soil texture influences the size and amount of pore spaces in a soil. Pore space influences the water content and bulk density, which then affects critical shear strength. Therefore, due to smaller pore spaces and more surface area, soils composed of smaller particles, such as clay are more cohesive than soils composed of larger particles such as sand. It is then more probable for erosion rates to be higher in soils with high proportions of sand (Wynn and Mostaghimi 2006).

Soil water content also has a strong influence on erodibility potential. In general, saturation reduces shear strength of a soil (Day and Axten, 1989). When a soil is not saturated, pore spaces are filled with air and water and negative pore-water pressure is present. A negative pore-water pressure results in positive matric suction, which is the difference between the air pressure and the water pressure, and when positive, results in increased shear strength (Casagli *et al*. 1999, Simon *et al*. 2000). However, when the

pore-water pressure is positive, the matric suction is negative, which reduces the frictional resistance of a soil and increases the probability of erosion (Brooks *et al*. 2013). Bluff erosion or failure have been commonly observed on the falling limb of a storm hydrograph, when the positive pore-water pressure is no longer offset by the pressure provided by the higher flow water levels in the channel (Simon *et al*. 1999, Rinaldi *et al*. 2004, Wilson *et al*. 2007).

Near-surface processes also influence erodibility. Surface erosion, which is the detachment and removal of soil particles by water or wind (Brooks *et al*. 2013), tends to result in the greatest erosion rates in spring and early summer, when snowmelt is occurring and rain events are common (Wick 2013). These events result in water running over the surface of the bluffs, which can cause soil particles to detach from the bluff.

Freeze-thaw cycles are another near-surface process that is an important component to bluff erosion rates. Water expands when it freezes and this expansion reduces granular interlocking between particles (Dietrich and Gallinatti 1991). Experiments in a lab setting and in the field have shown that repeated freeze-thaw cycles result in a reduction of the soil's shear strength and a reduction in bulk density (Kok and McCool 1989, Asare *et al*. 1997). Therefore, erosion will increase as freeze-thaw cycles increase. In Minnesota, the erosion effects from this process will be most significant in late winter and spring when freeze-cycles have occurred.

Another component of bluff erosion includes groundwater-driven processes, such as seepage erosion. Seepage erosion occurs when water infiltration rates are high and a perched water table is formed above less permeable layers or between layers with different hydraulic conductivity (Fox *et al*. 2007, Cancienne *et al*. 2008). The rise of the

perched water table creates a hydraulic gradient and results in lateral subsurface flow, which is especially seen on the falling limb of a storm hydrograph when the water table is rapidly declining (Fox *et al*. 2007). Bluffs are a key point for water to exit the soil profile (Wilson *et al*. 2007). This lateral flow or seepage has the potential to entrain soil particles and to undercut bluffs as the amount of soil particles eroded increases (Fox *et al.* 2007, Cancienne *et al*. 2008).

Bluffs differ from stream banks in that bluffs extend beyond the height of the floodplain and are composed of in-situ material, while stream banks are composed of alluvial deposits (Neitzel 2014). Therefore, bluffs are considered "hydrologically disconnected" from the current stream channel (Day *et al*. 2012). However, fluvial processes do still influence bluffs, such as during high flow events when the stream exceeds the height of its floodplain and by fluvial scour. Fluvial scouring at the basal zone of a bluff loosens sediment and detaches it from the bluff. The rate at which basal material is removed depends on the cohesiveness of the soil as well as the stream discharge. Fluvial erosion can lead to undercutting and over-steepening at the basal zone of bluff, which increases soil shear stress and increases the probability of a mass failure event (Brooks *et al*. 2013). A mass failure refers to an erosion event where a mass of soil and rock material quickly detach and move (Brooks *et al*. 2013). Mass failure events occur whenever shear stress factors are larger than shear strength factors (Brooks *et al*. 2013). Therefore, mass failures events not only increase in likelihood due to fluvial processes, but also are influenced by soil characteristics, near-surface processes and groundwater-driven processes.

3.3 Bluff Stabilization

One bluff on Amity Creek, BSWCD (Figure 2.4) and one bluff on the Knife River, BHHR (Figure 2.6) have had restoration projects completed on them in effort to reduce erosion rates and sediment inputs into the streams. BSWCD and BHHR were both stabilized in 2014. The stabilization method used for these bluffs was the Toe Wood Structure approach (Figure 3.1, 3.2) (Rosgen 2011). This method involved moving the stream channel away from the bluffs and a bench was installed at the base of the bluffs, at bankfull height (Rosgen 2011). The stabilization projects began by reshaping the channel, then foundation logs were laid on the lower one-third to one-half of the bluffs (Rosgen 2011). Next, root wads were added to provide roughness and additional aquatic habitat, and filler material, such as branches, brush and soil, was put on top (Rosgen 2011). "Burrito" soil lifts, made of soil rolled up in coir fabric, then were installed to lift the bench up to bankfull stage (Rosgen 2011). Finally, sod and/or fabric were laid down to stabilize the bench and live tree stakes were installed to provide more stabilization as well as to start the revegetation process (Rosgen 2011).

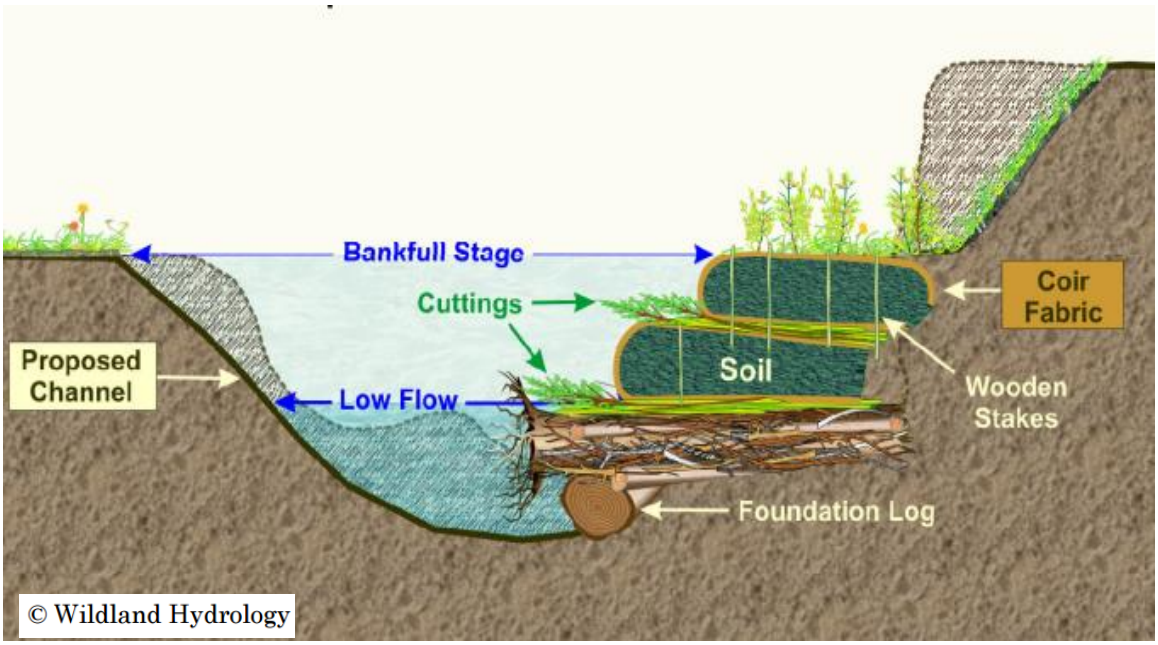

Figure 3.1: Toe Wood Structure design (Rosgen 2011).

The Toe-Wood Structure bluff design of moving the stream and building a protective bench, intends to stabilize the bluff by no longer allowing fluvial scour to undercut the basal bluff zone. This design also aims to be beneficial to the stream by enhancing fish habitat with the addition of woody debris to the stream, providing stability in the channel to maintain a low width/depth ratio and restoring a stream's connection to a floodplain with the bankfull bench (Rosgen 2011). Additionally, this design intends to enhance the riparian zone with the addition of native vegetation, which increases terrestrial habitat (Rosgen 2011). This design is meant to be versatile, being shown to be capable for use on all sediment types and on small to medium streams (Rosgen 2011).

Figure 3.2: Toe Wood Structure at BHHR in November 2015.

Two bluffs on East Branch Amity Creek, B13 and B14, also were stabilized. These bluffs were stabilized in 2009. At the downstream bluff, B14, the creek was moved to create a bench at bankfull height, root wads were placed in front of this bench to add habitat, coconut blanket was installed on the bench to provide erosion short-term erosion control and native seedlings were planted on the bench to provide longer-term erosion control (Anderson 2010). The design on this earlier project differed in that the bankfull bench was constructed of only sediment. At both B13 and B14, three j-hook vane features were installed, constructed of large rocks (Figure 3.3) (Anderson 2010). These vanes are intended to decrease stream power, velocity and near-bank slope in order to reduce stress applied to the bluff and promote the formation of a scour pool (Rosgen 2006). The bluffs were also regraded in order to reduce the slopes (Anderson 2010). This allowed for native vegetation to be planted on them, with the intent to further promote stabilization.

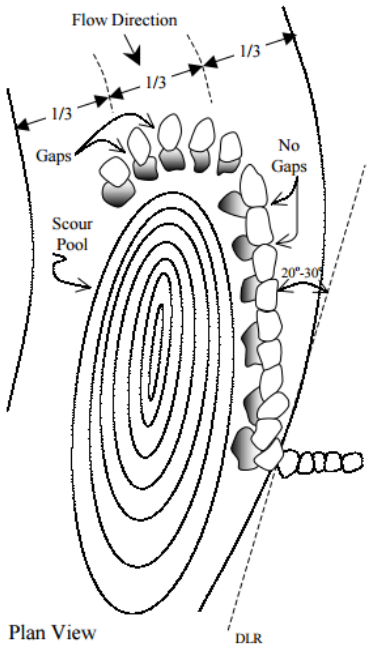

Figure 3.3: J-hook vane design (Rosgen 2006).

4.0 METHODS

4.1 Terrestrial Laser Scanning

This study used terrestrial laser scanning (TLS) technology to investigate an average annual bluff erosion rate. In order to obtain this average erosion rate, previously scanned and analyzed data from 2011 and 2012 of eight bluffs along Amity Creek (Figure 2.4) and Lester River (Figure 2.6) were compared with scans collected from these same bluffs in fall 2013, fall 2014, and spring and fall 2015. These combined datasets provide four years of data on geomorphic bluff changes.

The second component of this study involves comparing erosion rates from natural bluffs with bluffs that have undergone bank stabilization work. Four stabilized bluffs are included in this study. Two of the stabilized bluffs, B13 and B14 (Figure 2.4) are on Amity Creek and have scanning data available from November 2011 to November

2015. One additional stabilization project was completed on Amity Creek in 2014 and scanning of this bluff, BSWCD, began following the completion of the project (Figure 2.4). Another bluff was stabilized in the region in 2014. This bluff, BHHR, is on Knife River (Figure 2.6). The bluff was scanned following completion of the project in fall 2014, spring 2015 and fall 2015.

Table 4.1: Study Bluff Scan Dates

Stream	Bluff Name	2011	2012	2013	2014	2015
Amity	B9	November	April, May, June, November	November	September	April, November
Amity	B12	November	April, May, June, November		September	April, November
Amity	B13	November	April, May, June, November	November	September	April, November
Amity	B14		April, May, June, November	November	September	April, November
Amity	B15	November	April, May, June, November	November	September	April, November
Amity	B20		April, May, June, November	November	September	April, November
Lester	B2		April, May, June, November	November	September	April, November
Lester	B7		April, May, June, November	November	September	April, November
Knife	BHHR				September	April, November
Amity	BSWCD				September	April, November

4.1.1 Data Collection

The selection of TLS scanning sites to obtain an average bluff erosion rate were selected based on sites where a previous TLS study occurred. Neitzel (2014) used TLS to

investigate the relationship between peak flow rates and stream bluff erosion in Amity Creek and Lester River watersheds. This study selected eight bluffs within these watersheds based on relative ease of access and general lack of vegetative cover (Neitzel 2014). Neitzel (2014) collected TLS scans of the eight bluffs, providing bluff scan data back to spring 2012 for all the bluffs and scans from fall 2011 for four of the bluffs. The same eight bluffs were scanned again in fall 2013 and 2014 by Dr. Karen Gran and her students. These bluffs were then scanned as part of this study in spring and fall 2015.

Four bluffs are included in the study that have undergone stabilization work. As of fall 2014, when bluff study sites were selected, these were all the bluffs within the study watersheds where stabilization bluffs projects were complete. There was another bluff stabilized on the Knife River in summer 2015. This bluff was scanned in spring 2015, before the stabilization project began and in fall 2015, following completion of the project. Additionally, one bluff upstream and one bluff downstream of the most recently restored bluff on the Knife River, were scanned. These bluffs are similar in size, material and percent of vegetative cover to the stabilized Knife River bluff prior to the restoration work. However, with only two scans of each of these three bluffs, it was determined that it was not enough data to accurately determine an average geomorphic change rate. The data from these bluffs will not be included in this study but will hopefully be the start of a longer dataset that can provide more information on the effectiveness of stabilization projects for reducing geomorphic change rates.

At the three bluff sites added in 2015, three to four control points were established at each site. The control points consist of 1.5-centimeter-diameter rebar posts that were installed around and on the bluff and which stand 0.7 to 1.5 meters above the land

surface. On the rebar a sphere can be attached, with the use of a magnet. Spheres are automatically detectable objects in the post-processing software. Therefore, established control points can be used in post-processing to register scans taken from different locations along a bluff on a particular day and scans taken of the same bluff from different time periods into the same framework. Similar control points were already installed at all the bluffs scanned prior to 2015.

A Faro Focus 3-D laser scanner was used to perform TLS for this project. This is a phase-shift laser system with a range of 0.6 – 130 m. The Faro Focus 3-D works by emitting a laser that reflects off of a rotating mirror towards the area being scanned. The beam is reflected back to the scanner when it comes in contact with an object. The amount of time for the beam to return is then measured by the scanner to obtain the distance and relative vertical and horizontal angles of an area. The Faro Focus 3-D is able to collect up to 976,000 points per second. The instrument has a scanning range of 360° horizontally and 300° vertically, where 60° is lost from the vertical range due to a circular footprint created at the base of the scanner.

The Faro Focus 3-D scanner also allows for the resolution, quality and scope of the scan to be changed by the operator. In this study, the scanning parameters that were used to scan each bluff are 1/4 resolution, quality 4x, using the full-window (360 degree) scan option. The resolution options range from 1/1 to 1/32 and the quality options range from 1x to 8x. There is also an option to select a smaller area to be scanned but the full-window scan option allows data points to be collected from the full vertical and horizontal range of the scanner. The parameters chosen meant that each scan took just over nine minutes.

The Faro Focus 3-D scanner was set up at each bluff study site on a tripod. Five spheres were placed on and around the bluff. Spheres were placed on rebar control points when available and other spheres were placed in highly visible locations that were spread across the whole of the scan and at varying elevations. In order to use spheres to register scans together, a minimum of three control spheres have to be visible between scans to accurately triangulate and align. However, it was attempted to have more than three spheres visible between scans to increase registration accuracy.

In order to capture the whole bluff, due to the range limit of the scanner and irregular bluff surfaces, multiple scans were taken along the length of each bluff in the study. The number of scans taken at each study bluff varied from two to six, based on the length of the bluff and the angles present on the bluff face. A set of scans, conducted at one study site on the same day, is considered a campaign.

Campaigns were generally collected at study sites in late fall and early spring, during a time when most of the deciduous foliage was lost and in the absence of snow. Vegetation and snow data points have to be manually removed during the post-processing stage, which is a time-consuming process and leaves holes in the dataset. Therefore, these selected times to scan were chosen to reduce the post-processing workload and to obtain more complete point clouds. In addition to scanning campaigns from the early spring and late fall, Neitzel (2014), who examined the influence of peak flow events on bluff erosion, scanned the original eight bluff study sites following two large precipitation events. These events occurred May 23-28, 2012 and June 19-20, 2012 (Neitzel 2014).

4.1.2 Data Analyses

Once the raw point cloud data were gathered from all the bluffs, post-processing work was done in order to determine the quantity of erosion and deposition occurring on the study bluffs. The three major steps in determining geomorphic change of a bluff are aligning individual scans within a single campaign, preparing individual scans by removing vegetation from the surface of interest, and merging successive scanning campaigns from throughout the experiment to determine volumetric change.

Post-processing involved the use of three software programs. Faro Scene, a proprietary laser scanner software designed specifically to be used for scans collected using the Faro Focus 3-D scanner, was used for preliminary post-processing. This included registering individual campaigns together, trimming point cloud extents, removing vegetation, and registering campaigns of each bluff taken throughout the experiment. Topographic Point Cloud Analysis Toolkit (ToPCAT), which is a decimation software, was used to reduce the TLS point cloud file size and allow for the bluff axes to be managed. The final stage of measuring geomorphic change used ArcMap and the Geomorphic Change Detection ArcGIS Add-In developed by Joe Wheaton and his colleagues at Utah State University (Wheaton *et al.* 2009).

4.1.2.1 Faro Scene

The first stage of post-processing TLS point cloud data was registering scans together taken of the same study bluff on the same day. This was primarily accomplished automatically in Faro Scene, using spheres, which are automatically detectable objects in the software for reference. A minimum of three common reference spheres are needed to automatically register scans together. In many scans, additional reference spheres were

available to make registration more accurate since five spheres were placed on each bluff. In cases where three spheres were not detectable due to distance from the scanner or an obstruction in line of sight, scanning campaigns were manually registered. Manual registration was accomplished in Faro Scene by finding and creating common reference points between scans, such as corners of larger rocks.

Once scans were registered by campaigns, the campaigns were trimmed, deleting all the points that were not of the bluff face. After trimming the scans, vegetation could be removed from each bluff. Vegetation is removed from the point cloud manually by using a basic select and delete process. In order to best view vegetation present in Faro Scene, individual bluff scans are viewed in a planer view and vertical bluff slices are selected and examined in 3-D view. The 3-D view of a thin bluff section allows the section to be rotated and the vegetation can be selected without deleting bare-earth surface points. This procedure was developed based on the method used by Neitzel (2014) who processed the bluff scans taken in 2011 and 2012 that are used in this study. The method used by Neitzel (2014) drew heavily from a method used by Day (2012) to remove vegetation from scans collected from river bluffs in Southern Minnesota.

Following the removal of vegetation, campaigns taken from the same bluff throughout the experiment were linked together to create a point cloud composed of all the scans collected of a site in a common coordinate system. In scans where adequate reference points were available, i.e. where rebar stakes were available throughout the experiment, Faro Scene was automatically able to detect these common points and register the campaigns together. However, in most of the scans these reference points were not available. Control points, composed of rebar stakes were installed at all the

bluffs before their initial scan but many of these stakes were lost or moved over the years. In June 2012, Duluth and the surrounding area experienced a 500-year flood event. Many of the rebar control points were likely harmed in this event. Other stakes were damaged by other high flow events, erosion/deposition events and river migration. Therefore, no study site that has scanning campaigns going back to 2011, 2012 and 2013 could be automatically registered together. Manual targets, such as rocks and trees, were found and used to establish common reference points to register scans together. Manual targets are inherently not as accurate as control points and introduce some additional alignment error. The point clouds of individual campaigns were then each exported as ".pts" files, within which each point has an x, y, z position showing its location in a local coordinate system (Neitzel 2014).

4.1.2.2 ToPCAT Decimation Software

Due to the immense size of TLS point cloud datasets, it is necessary to reduce the file size before the file can be imported to ArcMap. ToPCAT is a decimation software specifically designed for processing TLS datasets. In this study, the 32-bit version of the software was used to reduce the file size of TLS datasets. The software works by separating the data points into a two dimensional grid of square cells that can be specified by the user and then a spatial algorithm extracts terrain products, such as minimum, maximum and mean elevation, from each cell (Brasington *et al*. 2012). The resolution used by ToPCAT can also be changed and in this study a resolution of 0.05 meter was selected. The product produced from ToPCAT that this study used was minimum elevation or z_{min}. This provided the bare surface points existing in each cell, effectively

removing any remaining vegetation and providing the most accurate representation of the bluff surface.

Additionally, the product of this process are text files, which is a file type that allows the bluff axes to be switched when importing the data into ArcMap. Switching the axes, ensures that geomorphic change is being calculated on the bluff faces.

4.1.2.3 ArcMap/GCD

The last step involved in post-processing the TLS point cloud data was completed using ArcMap GIS. Once the raw point cloud data was decimated in ToPCAT, the output of the procedure was a ".txt" file and this file was imported to ArcMap. During the importing stage, the axes were re-oriented so that the z-axis would be perpendicular to the face of the bluff and the y-axis would be perpendicular to the Earth's surface. Once in ArcMap, the ".txt files" were converted to shapefiles and the area over which geomorphic change will be detected was identified with a polygon overlapping the surface of all the bluff scans being compared to one another. This was accomplished by first creating a polygon shapefile clipped to match the extent of the scan campaigns. The point shapefiles of each scan campaign were then overlaid onto the polygon shapefile and holes in the data, such as where dense vegetation was present, were cut out of the polygon. Due to a desire to obtain accurate data in an efficient manner, voids in the dataset approximately 0.50 by 0.25 meters or larger were removed and smaller voids were left (Day *et al*. 2012, Neitzel 2014). Next, Triangular Irregular Networks (TINs) were generated. The resulting trimmed polygon shapefile along with the TLS point shapefile were used as inputs to create TINs of each scan campaign. From the TINs, Digital Elevation Models (DEMs) were created (Neitzel 2014). When creating the first DEM in a scan series, the polygon

shapefile showing the extent of the scan campaigns, without holes removed, was used to define the processing extent. The processing extent was then modified, by rounding the top and right extents up to the nearest whole number and rounding the bottom and left extents down to the nearest whole number (Neitzel 2014). This ensured that no portion of the TIN was omitted during the DEM conversion. The generation of subsequent DEMs for a series used the original DEM created for the processing extent in order to create a concurrent series of DEMs (Neitzel 2014).

The above steps generated a DEM of each individual scanning campaign for each study bluff, which then could be compared using Geomorphic Change Detection. Geomorphic Change Detection (GCD) is an ArcGIS Add-In and allows for two DEMs, representing the same surface at different times, to be differentiated. It calculates volume of erosion, deposition and no net change over the bluff surface and produces a DEM of Difference (DoD). To obtain these calculations, DEMs from a given study bluff were added to the Add-In's "Survey Library," the "single method survey" was selected and "TLS" was selected under the "single method survey". Next, any two DEMs from different periods of the same bluff were chosen for comparison. Overlapping cells from the two DEMs were differentiated by subtracting the old DEM from the new DEM, which gave erosion values as negative and deposition values as positive. Once the DoD was produced, a threshold value of 0.10 meter was applied to filter out any "noise" from the calculation (Day *et al*. 2012, Neitzel 2014). This threshold effectively removed any cells in the DoD ranging from -0.10 to 0.10 meter and was done in order to remove cumulative error or uncertainty in the dataset generated from each stage of the process (i.e. errors from the TLS scanner, vegetation removal, registration, TIN creation and

DEM creation). With the threshold set, net volume difference between each set of scans could be calculated with the equation:

$$(1)\ V_{net} = V_d - V_e$$

where V_{net} is the thresholded net volume difference, V_d is the total thresholded volume of deposition and V_e is the total thresholded volume of erosion.

Once the net volume difference was determined for each pair of scans, the average retreat distance could be calculated with the equation:

$$(2)\ D = \frac{V_{net}}{A}$$

where *D* is the average retreat distance (m), V_{net} is the thresholded net volume difference (m^3), and *A* is the area over which change was detected (m^2).

4.2 Bluff Characterization

Bulk density samples were collected at the stabilized bluff study site on the Knife River (Figure 2.6) in April 2015. The samples were collected using an AMS bulk density sampler with a compact slide hammer. Three samples were taken just above the bluff toe, at the soil surface. The volume of the soil samples were determined by calculating the volume of the sampling canisters, obtaining a constant volume of 370.68 cm^3. The samples were then dried for 24 hours in a hot-air oven at approximately 105 degrees Celsius (°C). Once dried, the soil was ground and small stones were removed from the mixtures. The soil and the stones were weighed separately. The volume of the stones were determined by measuring the volume of water displacement when the stones were added to a graduated cylinder filled partially with water. Bulk density was calculated using the equation:

$$(3)\quad \rho_{bulk} = \frac{W_{soil} - W_{st}}{V_{soil} - V_{st}}$$

where ρ_{bulk} is bulk density, W_{soil} is oven dry weight of soil, W_{st} is the weight of stones, V_{soil} is the volume of soil solids and pores, and V_{st} is the volume of stones.

Bulk density values used for riverine bluffs within Amity Creek and Lester River watersheds were previously obtained, calculated by Neitzel (2014). Neitzel (2014) collected bulk density samples from five Amity Creek study bluffs (Figure 4.1), in the summer of 2012 and 2013 using an ICT International 0200 soil bulk density sampler. The procedure for calculating bulk density was the same as the above described procedure (Neitzel 2014).

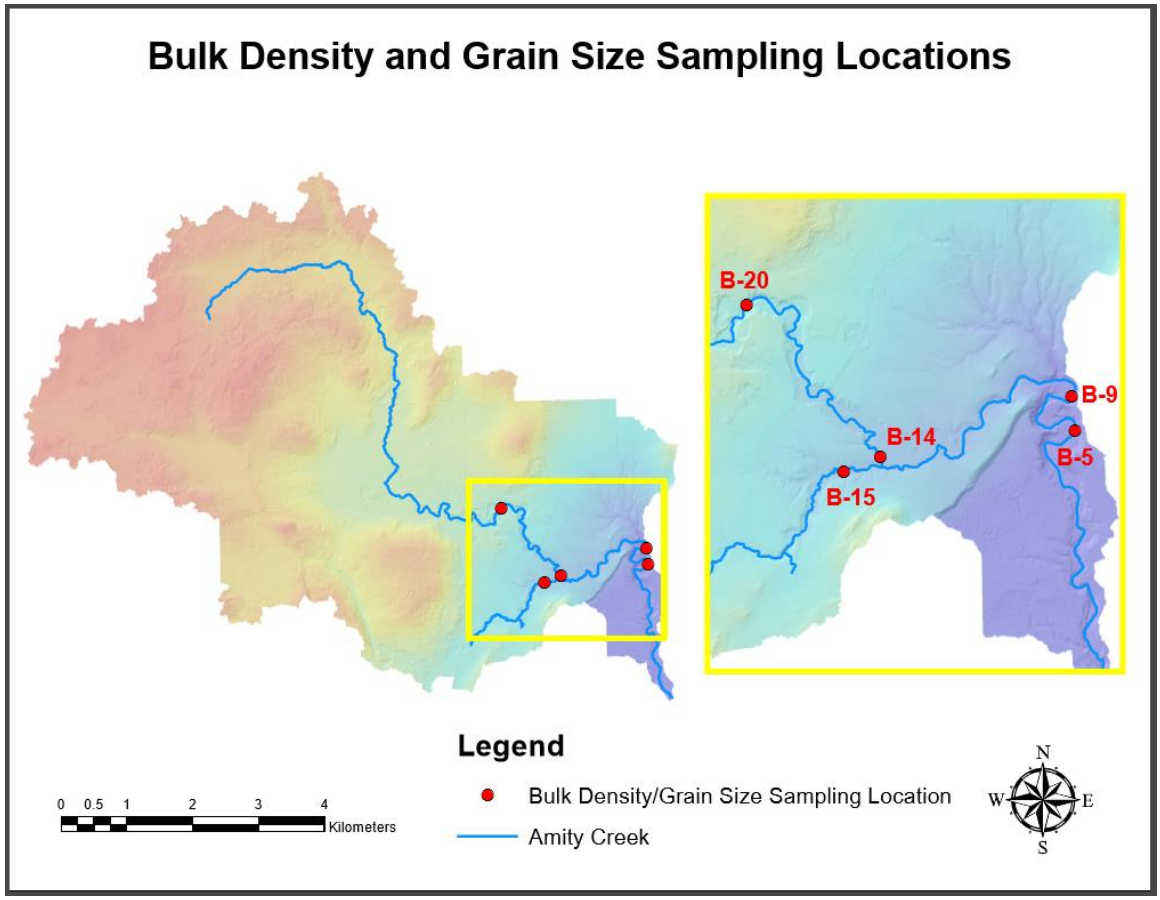

Figure 4.1: Bulk density and grain size sample locations taken on Amity Creek by Neitzel (2014).

Soil texture or the proportion of sand, silt and clay of a soil, impacts soil behavior, including erodibility. Therefore, a soil sample was collected at the Knife River study bluff (Figure 2.6) and a grain size analysis was run on this sample. The hydrometer method was used to determine the distribution of small particles (Bouyoucos 1927, Bouyoucos 1928a, Bouyoucos, 1928b). The hydrometer method is based on the fact that at a given time and depth, the suspension density is a result of particle suspension (Bedaiwy 2012). Hydrometers readings of the soil solution and the calibration solution as well as temperature readings were taken at total elapsed time intervals of 3, 10, 30, 60, 90 and 120 minutes and again at approximately 24 hours. After the 24 hour reading, the soil solution was remixed and poured over a No. 200 sieve (Bouyoucos 1962). The remaining particles on the sieve were then dried for 24 hours in a hot-air oven at approximately 105°C.

In order to determine the distribution of larger particles, the oven-dried particles were sieved through a combination of screens having decreasing mesh sizes (Bedaiwy 2012). For this study, the dried soil sample material was placed on top of a set of sieves containing U.S. Bureau of Standards Sieve Nos. 20, 40, 80, 140 and 200. The particles were shaken for four minutes and the sample retained on each sieve was weighed (Bedaiwy 2012). From the results of the sieve retention weights and the hydrometer readings the percentage of sand, silt and clay were calculated for the soil sample (Bouyoucos 1927).

Particle size distributions used for riverine bluffs in the Amity Creek and Lester River watersheds were obtained from samples taken by Neitzel (2014). Neitzel (2014) collected samples from the same five bluff study sites (Figure 4.1) where bulk density

samples were taken on Amity Creek (Neitzel 2014). The soil grain size distribution was analyzed using a Beckman Coulter LS13 320 laser diffractometer at the Large Lakes Observatory in Duluth, Minnesota (Neitzel 2014). This instrument determines particle sizes by sending a beam of light at a given sample and measuring the patterns of light that are scattered when this beam comes in contact with a soil particle (Neitzel 2014). For example, large soil particles scatter light at small angles and small particles scatter light at large angles (Beckman Coulter 2003). Results from this analysis are given as percentage of the soil sample consisting of sand, silt, clay and percent washload – silt and clay (Neitzel 2014).

4.3 Extrapolating Results

Once the volume of sediment that is eroded and deposited at each of the study bluffs was determined, an average retreat rate was calculated and these results were extrapolated across Amity Creek watershed to determine the total mass of sediment that can be attributed to bluff erosion. In order to complete this calculation, it was necessary to know the total area of unvegetated bluffs in the watershed. Neitzel (2014) conducted a field survey of Amity Creek in 2013 where the total area of unvegetated bluff were determined. This study was conducted recently and based on standard geomorphic principles, over a short timescale the total area of bluffs in a watershed tends to not change. Some bluffs may erode and grow larger, while other bluffs may become more stable and vegetation will grow. Neitzel (2014) walked the entirety of Amity Creek and at each bluff measured the height and length of unvegetated area using a laser altimeter as well as a rangefinder. Neitzel (2014) and this study were concerned with just unvegetated bluffs since vegetated bluffs are known to be more stable and are less likely to erode and

contribute sediment to the streams. Additionally, an average erosion rate was determined based on TLS scans conducted on unvegetated bluffs only. If this rate was applied to vegetated bluffs, it would overestimate bluffs' contribution to sediment loading within the watershed. By only using unvegetated bluffs in the watershed, the calculation for bluff attributed sediment loads will likely be conservative.

In order to determine the total volume of sediment that unvegetated bluffs in Amity Creek contribute to the stream channel, the average retreat rate determined from the eight study bluffs where data are available since 2012 was multiplied by the total area of unvegetated bluffs in the watersheds. This provided the total volume of sediment contributed by unvegetated bluffs. The total volume of sediment was then multiplied by the average bulk density, which determined the mass of sediment attributed to bluff erosion. Next, the total mass was multiplied by the average percent of fine-grained particles, silt and clay, to get a total mass of fine sediment that enters the streams due to bluff erosion.

4.4 Precipitation data

In order to determine the effect that total precipitation and high-magnitude precipitation events, which largely determine the stream discharge, have on bluff erosion in Amity Creek, precipitation amounts need to be compared with change detection calculations. Ideally, a stream gage would be available in Amity Creek to report daily discharge; however, the gage was taken out in August 2012. Therefore, precipitation data were used as a proxy for stream flow. Precipitation data were obtained from the Western Lake Superior Sanitary District (WLSSD) using their daily readings from the Endion Station rain gage. This regional rain gage (Lat: 46.80N, Long: -92.06) is located

approximately 3.5 miles south of the confluence of Amity Creek and Lester River, at roughly the same elevation.

Neitzel (2014) showed through differencing bluffs from just before and following large rain events that large precipitation events significantly affect bluff erosion rates. From May 23 to 28, 2012, 4.75 inches of rain fell and induced "major slumping" on bluffs, and a precipitation event of 7.25 inches from June 19-20, 2012 resulted in "severe erosion" (Neitzel 2014). In this study, we looked at precipitation from four different periods (November 2012 to November 2013, November 2013 to September 2014, September 2014 to April 2015, and April 2015 to November 2015). The total precipitation amount was calculated for each period to determine whether precipitation period totals have an effect on bluff erosion.

Despite knowing from Neitzel (2014) that extremely high storm events affect geomorphic change on bluffs, this study examined if more typical large rain events have an effect on bluff erosion. The threshold given for a more typical rain event was an inch or greater. For each period, the number of days with precipitation amounts one inch or greater were calculated and the highest one-day rain event in each period was reported. Precipitation events producing one inch or more of rain were also recorded. These were consecutive periods where a number of days in a row all reported precipitation amounts, which together totaled over an inch. The numbers reported for "precipitation events" include the single days as well as a group of consecutive days where there was an inch or more of rain.

5.0 ERROR ANALYSIS

Terrestrial laser scanning (TLS) allows geomorphic change to be detected at a high resolution. However, errors are introduced throughout the process, from the data collection stage through post-processing the data. These errors are considered when obtaining results. Sources of this error came from the initial scanning process, aligning campaign scans, aligning scans from successive campaigns, removing erroneous points (i.e. vegetation) from the point cloud, and from calculating erosion and deposition volumes (Day *et al.* 2012).

In order to minimize the inherent error when aligning/registering scans from a single campaign and from successive campaigns, Faro Scene has an internal scan manager that provides the "mean tension" between scans. This allows the user to determine how well fit the scans are to one another. When the "mean tension" is zero the scans are perfectly fit together and as the mean tension gets larger, the greater the error in fit is between the scans. Faro Scene also provides "reference tension" values, which show the pairs of control points and reference points that are being used for registration and provides the tension between the two points. Pairs of points with large tension values show low accuracy of fit. An "anti-correspondence" can be set between points with a large "reference tension" so that particular pairs will no longer be used to align the scans.

Vegetation on the bluff surface can also add error to the procedure since it can prevent the DoD from detecting change of the bluff surface. In this study, it was attempted to remove all the vegetation that could be detected in the point cloud data of each bluff. Many of the bluffs in this study were selected due to their lack of vegetation. However, every study site had at least patches of vegetation and the stabilized bluffs, in

particular B13 and B14, had significant areas of ground vegetation. All vegetation on the bluffs was removed liberally due to the known errors that vegetation present can generate in the geomorphic change detection calculations (Coveney and Fotheringham 2011, Day *et al.* 2012). When the vegetation was removed it created holes in the dataset and resulted in less area for geomorphic change to be detected. However, holes generated from this process existed in areas where there is vegetation and due to the stabilization potential of plants, these areas are less likely to change as much over short timescales (Day *et al.* 2012).

Errors generated when calculating erosional and depositional volumes are highlighted in a summary file generated by the GCD ArcGIS Add-In when creating a DoD. This summary file provides information such as the total volume of erosion and deposition and the total area over which erosion and deposition occurred for each DoD generated. The raw values of each of these are provided, along with the thresholded values, which were created due to the error surface value of 0.10 meter that was applied to all the DoD maps. This file also provides the uncertainty in the calculated erosion and deposition volumes, given as +/- error volume and corresponding percent error. The GCD software generates error volume by multiplying the area of the non-thresholded cells with the error surface area and shows whether there is a clear sign of erosion and deposition (Neitzel 2014).

The Geomorphic Change Detection (GCD) ArcGIS Add-In also creates a colorized geomorphic change map of each bluff for all the periods over which geomorphic change was analyzed. The maps show in red the location of erosion, in blue the location of deposition and in grey locations where the measured change was within

the threshold (-0.10 to 0.10 m). The shade of red and blue on the map vary depending on the amount of erosion and deposition that has occurred. The darker the tone, the greater the amount of erosion and deposition. Photos were also taken of the bluffs by the Faro Focus 3-D scanner during every scan campaign and in April and November 2015 photos were also taken with a digital camera. The areas showing significant erosion or deposition on the geomorphic change maps were checked with these photos to confirm that geomorphic change occurred or whether there was an issue in scan registration.

6.0 RESULTS

6.1 Bluff Characterization Results

The average bulk density for Amity Creek and Lester River was determined by Neitzel (2014) to be 1.426 ± 0.280 g/cm^3 (Table 6.1). Neitzel (2014) took two bulk density samples at each bluff, one at the surface and another 30-40 cm below the surface. The samples were collected in summer 2012 and again in spring 2013. Samples were taken at different depths to investigate whether bulk density increases with soil depth and samples were taken in different seasons to determine if the freeze-thaw cycle influences bulk density (Neitzel 2014). It was hypothesized that bulk density values would increase with depth and would decrease in the spring due to the freeze-thaw cycle lessening the soil particles interlocking structure (Neitzel 2014). However, bulk density sampling results did not conclusively support this hypothesized trend (Neitzel 2014). Therefore, Neitzel (2014) used an average bulk density value. Three bulk density samples were taken at the surface of the Knife River bluff and the average bulk density was determined to be 1.99 g/cm^3.

The particle size analysis completed on Amity Creek, Lester River and Knife River all show that there is a high concentration of fine-grained particles, silt and clay, in the soil that composes the study bluffs. Grain size analyses conducted by Neitzel (2014) were used for Amity Creek and Lester River watersheds. Neitzel (2014) found the average ratio of sand, silt and clay to be approximately 2/28/70 with the clay content in the samples ranging from 47-90% of the overall sample (Table 6.2). The ratio of sand, silt and clay of the Knife River bluff was found to be 1.5/17.5/81 respectively.

Table 6.1: Amity Creek Bulk Density Samples (Neitzel 2014)

	Bulk Density (g/cm^3)	
Site/Sample	**Summer 2012**	**Spring 2013**
B5A[a]	1.143	1.767
B5B[b]	1.083	1.022
B9A[a]	1.290	1.653
B9B[b]	1.774	1.627
B14A[a]	1.108	0.967
B14B[b]	1.876	1.471
B15A[a]	1.186	1.417
B15B[b]	1.345	1.485
B20A[a]	1.686	1.614
B20B[b]	1.701	1.312
Average	1.419	1.434
Overall Average	1.426	
Standard Deviation	0.280	

[a]Sample collected at surface
[b]Sample collected 30-40 cm deep

Table 6.2: Amity Creek Grain Size Analysis (Neitzel 2014)				
Sample #	**% Sand**	**% Silt**	**% Clay**	**% Silt/Clay**
B5-1	1.1	29.9	69.1	98.9
B5-2	1.0	29.8	69.2	99.1
B5-3	0.9	29.7	69.4	99.1
B5–4	1.3	21.4	77.3	98.7
B5–5	1.1	21.3	77.6	98.9
B5–6	1.0	21.1	77.8	99.0
B9-1	0.0	5.8	94.3	100.0
B9-2	0.0	5.7	94.3	100.0
B9-3	0.0	5.7	94.3	100.0
B9-4	0.0	17.1	82.9	100.0
B9-5	0.0	17.0	83.0	100.0
B9-6	0.0	17.0	83.0	100.0
B14-1	3.6	49.0	47.4	96.4
B14-2	3.5	49.0	47.6	96.5
B14-3	3.4	48.9	47.7	96.6
B14-4	3.5	49.2	47.3	96.5
B14-5	3.3	49.2	47.5	96.7
B14-6	3.3	49.1	47.6	96.7
B15-1	7.4	38.6	54.0	92.6
B15-2	7.2	38.5	54.3	92.8
B15-3	7.2	38.5	54.3	92.8
B15-4	2.4	30.9	66.7	97.6
B15-5	2.3	30.8	66.9	97.7
B15-6	2.3	30.8	67.0	97.7
B20-1	0.0	12.6	87.4	100.0
B20-2	0.0	12.6	87.4	100.0
B20-3	0.0	12.6	87.4	100.0
B20-4	0.7	31.3	68.0	99.3
B20-5	0.6	31.3	68.1	99.4
B20-6	0.7	31.3	68.1	99.4
Average	**1.9**	**28.5**	**69.6**	**98.1**

6.2 TLS/GCD Results

Terrestrial laser scanning was conducted on ten study bluffs during this experiment (Table 4.1). Six of the study bluffs were natural (i.e. not stabilized) and four stabilized artificially.

Net volume of erosion and deposition (net change) was determined for the natural bluffs and the stabilized bluffs by comparing subsequent scanning campaigns (Table 6.3, 6.4). Average retreat distance was then calculated for all the study bluffs (Table 6.5, 6.6,

6.7). This was determined by dividing the net change by the total area of erosion and deposition on each study bluff (Table 6.8). The net change and area were determined using a summary file produced using the Geomorphic Change Detection ArcGIS Add-In. Table 6.9 summarizes the outputs of this summary file. For this study the thresholded net change, which is the difference between erosion and deposition with a 0.10 meter threshold applied, and the non-thresholded area were used to calculate the average retreat distance. This provided the total area over which change was measured and excluded areas of the bluff that were removed due to vegetation.

Table 6.3: Natural Bluffs DoDs – Net Change with 0.10 meter threshold applied (m^3)

Site #	Nov. 2011 to Apr. 2012	Apr. to May 2012	May to June 2012	June to Nov. 2012	Nov. 2012 to Nov. 2013	Nov. 2013 to Sep. 2014	Sep. 2014 to Apr. 2015	Apr. to Nov. 2015	Nov. 2012 to Nov. 2015
B9	-83	32	-247	10	-17	-87	28	-20	-90
B12	-7	2	-1	0	n/a	n/a	0	-2	-8
B15	-1	-6	-6	0	0	0	1	1	2
B20	n/a	-5	-27	0	0	-1	1	0	-3
B2	n/a	-23	-347	-1	-50	-176	-19	-65	-158
B7	n/a	-10	-141	-8	-84	-36	-96	-81	-51

Table 6.4: Stabilized Bluffs DoDs – Net Change with 0.10 meter threshold applied (m^3)

Site #	Nov. 2011 to Apr. 2012	Apr. to May 2012	May to June 2012	June to Nov. 2012	Nov. 2012 to Nov. 2013	Nov. 2013 to Sep. 2014	Nov. 2013 to Apr. 2015	Sep. 2014 to Apr. 2015	Apr. to Nov. 2015	Sep. 14 to Nov. 15	Nov. 2012 to Nov. 2015
BHHR	n/a	n/a	n/a	n/a	n/a	n/a	n/a	30	8	29	n/a
BSWCD	n/a	n/a	n/a	n/a	n/a	n/a	n/a	-28	25	14	n/a
B13	-11	-2	-3	0	2	4	n/a	-10	0	n/a	-5
B14	n/a	0	-8	1	-1	n/a	3	n/a	-1	n/a	5

Table 6.5: Natural Bluffs DoDs – Average Retreat Distances (m)

Site #	Nov. 2011 to Apr. 2012	Apr. to May 2012	May to June 2012	June to Nov. 2012	Nov. 2012 to Nov. 2013	Nov. 2013 to Sep. 2014	Sep. 2014 to Apr. 2015	Apr. to Nov. 2015	Nov. 2012 to Nov. 2015
B9	-0.25	0.10	-0.86	0.03	-0.09	-0.25	0.08	-0.09	-0.30
B12	-0.32	0.09	-0.05	0.00	n/a	n/a	0.00	-0.13	-0.53
B15	-0.06	-0.24	-0.26	0.01	0.00	0.00	0.07	0.07	0.25
B20	n/a	-0.07	-0.44	0.00	0.00	-0.02	0.01	0.00	-0.06
B2	n/a	-0.05	-0.84	0.00	-0.20	-0.38	-0.04	-0.11	-0.63
B7	n/a	-0.02	-0.30	-0.01	-0.13	-0.06	-0.16	-0.16	-0.08
Period Average	-0.21	-0.03	-0.46	0.01	-0.08	-0.14	-0.01	-0.07	-0.23

Table 6.6: Stabilized Bluffs – Average Retreat Distances (m)

Site #	Nov. 2011 to Apr. 2012	Apr. to May 2012	May to June 2012	June to Nov. 2012	Nov. 2012 to Nov. 2013	Nov. 2013 to Sep. 2014	Nov. 2013 to Apr. 2015	Sep. 2014 to Apr. 2015	Apr. to Nov. 2015	Sep. 14 to Nov. 15	Nov. 2012 to Nov. 2015
BHHR	n/a	n/a	n/a	n/a	n/a	n/a	n/a	0.15	0.04	0.14	n/a
BSWCD	n/a	n/a	n/a	n/a	n/a	n/a	n/a	-0.04	0.04	0.02	n/a
B13	-0.25	-0.05	-0.08	0.00	0.09	0.07	n/a	-0.14	0.00	n/a	-0.19
B14	n/a	0.01	-0.47	0.02	-0.02	n/a	0.05	n/a	-0.02	n/a	0.11
Period Average	-0.25	-0.02	-0.28	0.01	0.04	0.07	0.05	-0.01	0.02	0.08	-0.04

Table 6.7: Bluffs scanned since at least Nov. 2012 – Average Retreat Distance (m)

Site #	Nov. 2011 to Apr. 2012	Apr. to May 2012	May to June 2012	June to Nov. 2012	Nov. 2012 to Nov. 2013	Nov. 2013 to Sep. 2014	Sep. 2014 to Apr. 2015	Apr. to Nov. 2015	Nov. 2012 to Nov. 2015
B9	-0.25	0.10	-0.86	0.03	-0.09	-0.25	0.08	-0.09	-0.30
B12	-0.32	0.09	-0.05	0.00	n/a	n/a	0.00	-0.13	-0.53
B13	-0.25	-0.05	-0.08	0.00	0.09	0.07	-0.14	0.00	-0.19
B14	n/a	0.01	-0.47	0.02	-0.02	n/a	n/a	-0.02	0.11
B15	-0.06	-0.24	-0.26	0.01	0.00	0.00	0.07	0.07	0.25
B20	n/a	-0.07	-0.44	0.00	0.00	-0.02	0.01	0.00	-0.06
B2	n/a	-0.05	-0.84	0.00	-0.20	-0.38	-0.04	-0.11	-0.63
B7	n/a	-0.02	-0.30	-0.01	-0.13	-0.06	-0.16	-0.16	-0.08
Period Average	-0.22	-0.03	-0.41	0.01	-0.05	-0.11	-0.03	-0.06	-0.18

Table 6.8: GCD Area (m^2)

Site #	Nov. 2011 to Apr. 2012	Apr. to May 2012	May to June 2012	June to Nov. 2012	Nov. 2012 to Nov. 2013	Nov. 2013 to Sep. 2014	Nov. 2013 to Apr. 2015	Sep. 2014 to Apr. 2015	Apr. to Nov. 2015	Sep. 14 to Nov. 15	Nov. 2012 to Nov. 2015
B9	339	318	287	310	197	345	n/a	345	215	n/a	305
B12	23	17	21	25	n/a	n/a	n/a	16	15	n/a	15
B13	43	42	42	43	23	61	n/a	74	26	n/a	26
B14	n/a	23	16	42	48	n/a	63	n/a	43	n/a	44
B15	23	26	24	25	10	15	n/a	15	15	n/a	8
B20	n/a	64	62	66	54	64	n/a	68	63	n/a	50
B2	n/a	447	412	417	250	464	n/a	465	584	n/a	251
B7	n/a	488	461	626	633	613	n/a	598	507	n/a	671
BHHR	n/a	n/a	n/a	n/a	n/a	n/a	n/a	205	226	206	n/a
BSWCD	n/a	n/a	n/a	n/a	n/a	n/a	n/a	683	655	656	n/a

Table 6.9: GCD Outputs Summary

GCD Output:	Description:
Total Area of Erosion (m^2)	Total area of cells having negative change
Total Thresholded Area of Erosion (m^2)	Total area of cells having negative change > 0.10 m
Total Area of Deposition (m^2)	Total area of cells having positive change
Total Thresholded Area of Deposition (m^2)	Total area of cells having positive change > 0.10 m
Total Volume of Erosion (m^3)	Total volume of cells having negative change
Total Thresholded Volume of Erosion (m^3)	Total volume of cells having negative change > 0.10 m
Total Volume of Deposition (m^3)	Total volume of cells having positive change
Total Thresholded Volume of Deposition (m^3)	Total volume of cells having positive change > 0.10 m
Total Net Volume of Difference (m^3)	Net volume difference among all cells
Total Thresholded Net Volume of Difference (m^3)	Net volume difference among all cells with >0.10 m of change
+/- Error Volume (total volume of erosion)	Thresholded total area of erosion ÷ spatially uniform error surface (0.10 m)
+/- Error Volume (total volume of deposition)	Thresholded total area of deposition ÷ spatially uniform error surface (0.10 m)
+/- Error Volume (total net volume difference)	Thresholded total area of change ÷ spatially uniform error surface (0.10 m)
% Error (total volume of erosion)	+/- Error Volume ÷ Thresholded volume of erosion
% Error (total volume of deposition)	+/- Error Volume ÷ Thresholded volume of deposition
% Error (total net volume difference)	+/- Error Volume ÷ Thresholded net volume difference

In this experiment, the original intent was to compare each scan campaign with the scanning campaign which it preceded and then compare the newest scanning campaign (November 2015) with the oldest scanning campaign (November 2011, April 2012 or September 2014). Scanning campaigns for each bluff were compared with the scanning campaign in which it preceded except in a few instances. The exceptions are

that there is no scan of B12 available in 2013, and B14 had too much vegetation present when it was scanned in September 2014 that it was not possible to determine a geomorphic change rate. For the study site B14 a geomorphic change rate was instead determined from November 2013 to April 2015, instead of November 2013 to September 2014 and September 2014 to April 2015.

Additionally, it was not possible in most instances to compare November 2015 bluff scans with scans taken in November 2011 and April 2012. This was due to two large precipitation events that occurred in the Duluth area in May 2012 and June 2012. From May 23 to 28 the area received 4.75 inches of rain and from June 19 to 20 the area received 7.25 inches of rain, which resulted in a 500-year flood event (Neitzel 2014). This precipitation event resulted in high erosion rates mainly due to intensive fluvial scour and greatly changed the size and appearance of most of the bluffs in this study (Neitzel 2014). Therefore, an insufficient number of common points could be located to reference together scanning campaigns from before the May and June 2012 precipitation events to scanning campaigns from November 2015. For this reason, bluff scans from November 2015 were compared with bluff scans from November 2012 for eight of the study bluffs (Table 6.7). This provided a three-year period over which geomorphic change was detected.

Geomorphic change detected from November 2012 to November 2015, shows an overall average retreat distance that is negative, meaning there was net erosion during this period for the eight bluffs that were compared in this time range (Table 6.7). However, two bluffs, B14 and B15 show positive retreat distances, which means that there was more deposition over this three-year period than erosion. Study bluffs B12 and B2 show

the highest negative retreat distances over this period, with both over -0.50 m. Of the other, shorter periods compared, May to June 2012 showed the highest average retreat distances. This is the period that captured a 500-year flood event and the eight bluffs compared in this period all showed negative (i.e. erosional) retreat distances. November 2011 to April 2012 also was a period where all the bluffs showed negative retreat distances; however, only four bluffs were scanned during this period. September 2014 to November 2015 shows a period of overall deposition, but only two stabilized bluffs were compared during this period. All the other periods show a mix of negative (i.e. erosional) and positive (i.e. depositional) retreat distances among the bluffs. Additionally, eight of the ten bluffs used in this study showed a variety of negative retreat distances, positive retreat distances and/or no detectable retreat distance between compared periods. The exception to this was B7, which showed a negative retreat distance in every period where scans were compared and BHHR, which had all positive retreat distances over three periods where geomorphic change was differentiated.

The Geomorphic Change Detection (GCD) ArcGIS Add-In also creates a colorized geomorphic change map of each bluff for all the periods over which geomorphic change was analyzed. These maps show the locations of erosion and deposition, which helps to interpret the process that is causing the geomorphic change. Figure 6.1, 6.2, 6.3 contain examples of three of the geomorphic change maps produced using the GCD ArcGIS Add-In. These maps show the longest period over which change was detected for each of the respective bluffs. Appendix A contains colorized geomorphic change maps for all the study bluffs.

Figure 6.1 shows the geomorphic change detected on study bluff B9, from November 2012 to November 2015. The average retreat distance for this period is -0.30 m. Study bluff B9 is approximately 370 m^2 and is located on Amity Creek, roughly 3.4 km upstream from the confluence with Lester River (Figure 2.4). The geomorphic change detection map shows a large area of erosion on the downstream (right) side of the bluff. This is likely due to a large slump that occurred, possibly due to over-steepening caused by fluvial scour. A photo taken of that region of the bluff in November 2012 shows that the bluff face is very steep in the basal zone and has a convex shape above (Figure 6.1). A November 2015 photo of this same area of the bluff shows that the basal zone now has a more gradual slope and the upper region is more of a concave shape.

There is minimal deposition visible below this area of erosion, showing that the eroded material was carried away by the stream. There is also a band of erosion running across the upper, middle portion of the bluff and another band of erosion running across the lower, upstream (left) side of the bluff. These appear to be slides and the material from the slides is deposited below, having not been carried away by the stream. There are also some deposition areas showing at the top of the bluff, which is likely due to material falling or being washed onto the bluff from above. Lastly, there are small area scattered across the bluff of erosion and deposition. These could be the result of processes such as small slides, rockfalls, overland flow or freeze-thaw action.

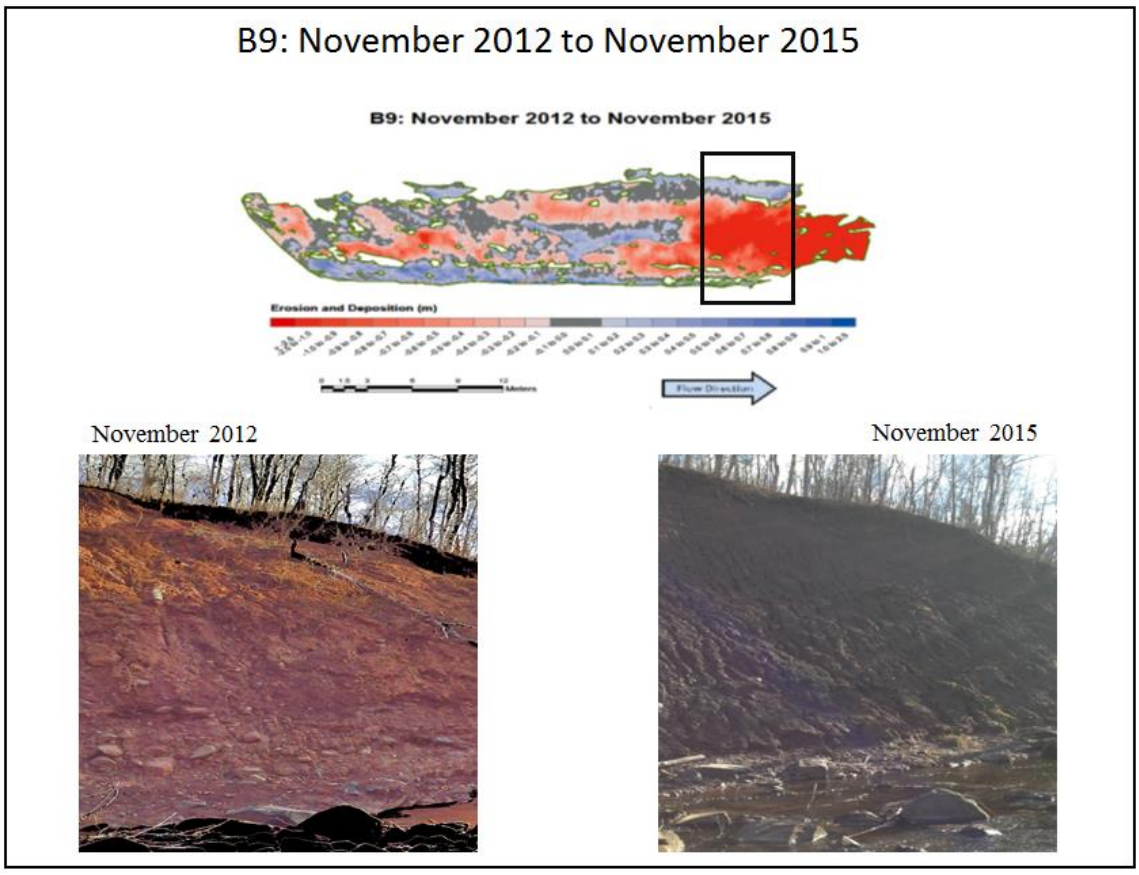

Figure 6.1: Colorized geomorphic change detection map of study bluff B9, with a black square marking the area of a slump. The below photos show the marked area in November 2012 and November 2015.

Geomorphic change that occurred on study bluff B7 is shown in Figure 6.2. B7 is one of the two bluffs in this study that are on Lester River (Figure 2.5). The bluff is approximately 736 m^2 and is located about 4 km upstream of the confluence with Amity Creek. Figure 6.2 shows the geomorphic change from November 2012 to November 2015 and during this period the average retreat distance was -0.08 m. The geomorphic change detection map shows erosion occurring linearly down much of the bluff face. This is due to rill erosion likely caused by water coming off the land above the bluff and running down, over the surface of the bluff. A photo of the bluff from November 2012 shows only some small rills on the bluffs surface but a photo of the same spot in November 2015 shows a greater amount and deeper cut rills.

There are depositional areas at the bottom of the bluff, where sediment from the rills appears to be gathering and has not been removed by fluvial action. On the bottom, right (upstream) side of the bluff and on the bottom, left (downstream) side of the bluff there are areas of erosion that are not in a linear direction. These areas are likely slumps, possibly caused by over-steepening of the basal zone due to fluvial scour.

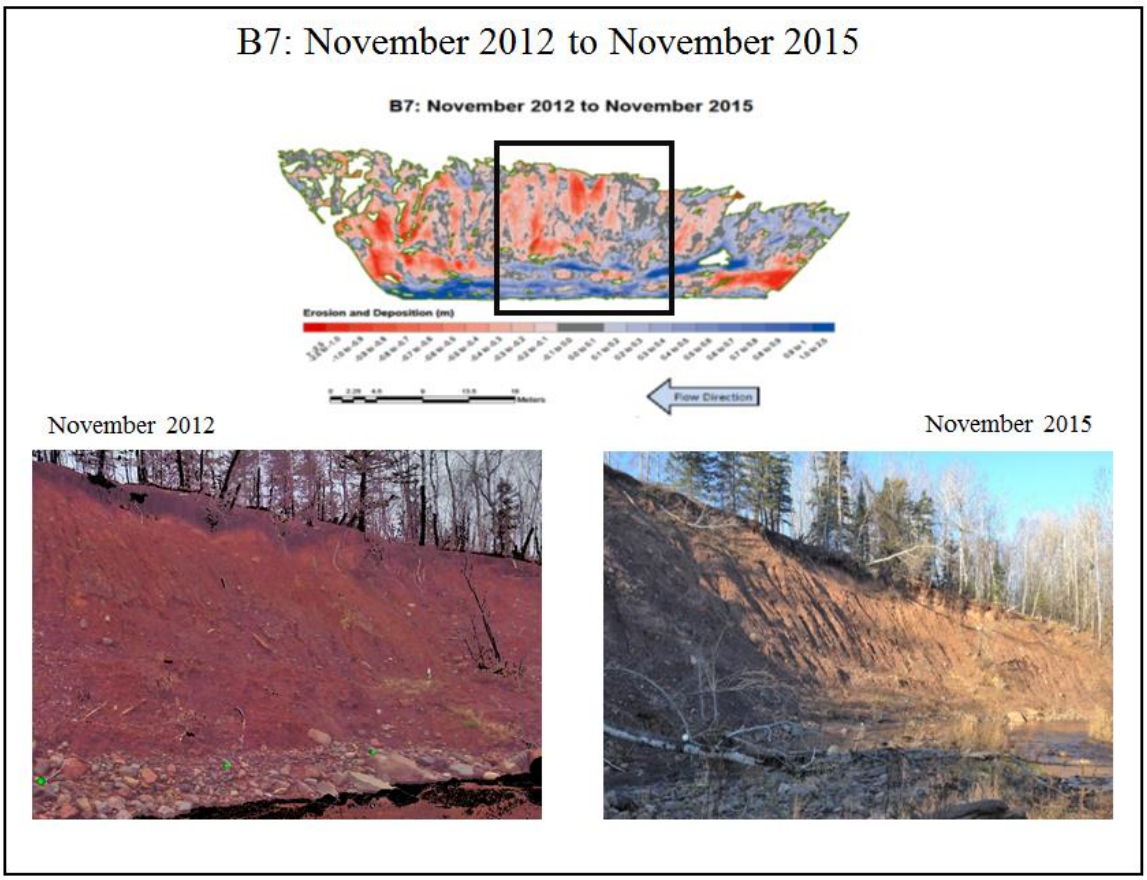

Figure 6.2: Colorized geomorphic change detection map of study bluff B7, with a black square marking the area of rill formation. The photos below show the marked area in November 2012 and November 2015.

Figure 6.3 shows the geomorphic change that occurred on study bluff BHHR from September 2014 to November 2015. The average retreat distance for this period is 0.14 m, meaning that there was more deposition than erosion occurring. This bluff is the only bluff in this study located on the Knife River (Figure 2.6) and is one of the two bluffs in the study that was stabilized with a Toe Wood Structure design. BHHR is

approximately 226 m^2 and located 6.6 km upstream from where the Knife River discharges into Lake Superior. The geomorphic change map shows what appears to be a slump in the center, left of the bluff and a band of erosion running along the top, right (downstream) side of the bluff. Both of these locations are marked on the geomorphic change map with a black rectangle and photos taken of the site in September 2014 and November 2015 show the area and extent of this erosion. Eroded material from these sites can then be seen deposited directly below. There is a large area of deposition along the bottom, center of the bluff. This sediment is piling up on the bench that is now located here and since the Knife River has not reached flood stage since September 2014, this sediment has not been moved by the river's flow.

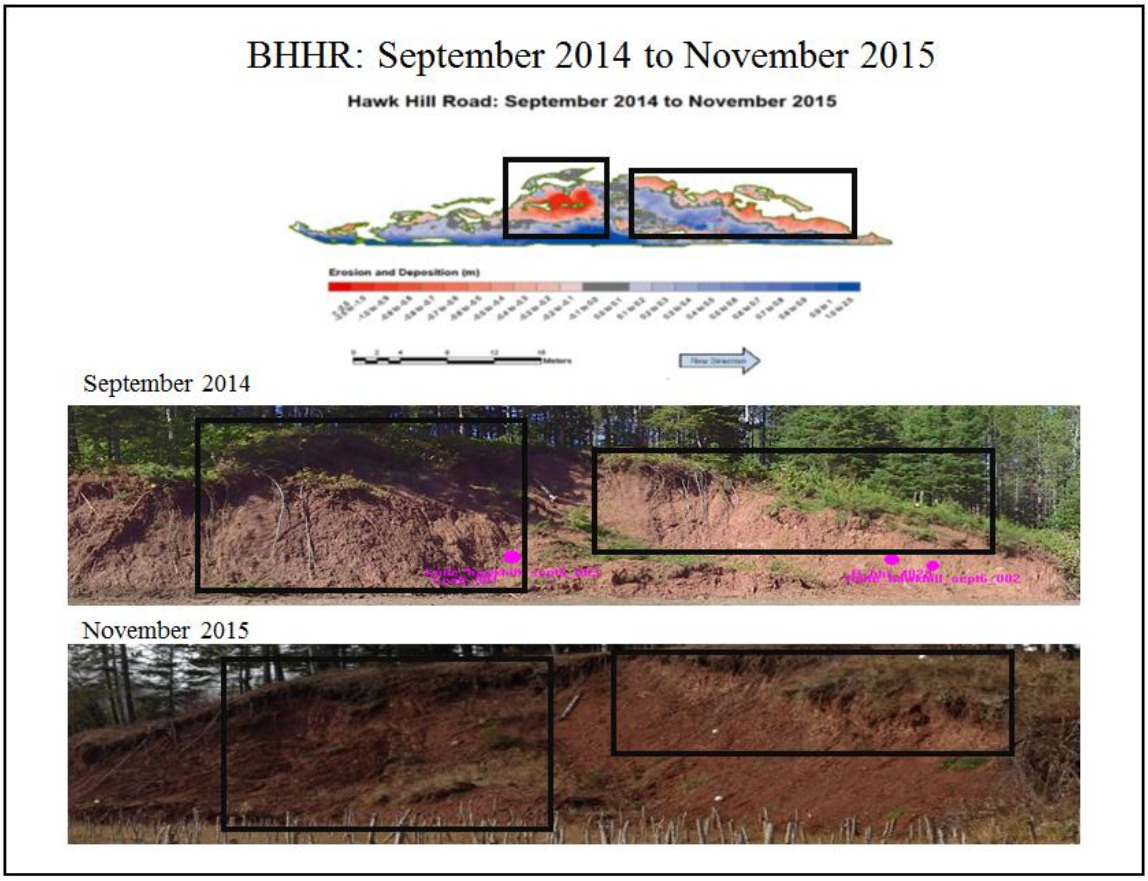

Figure 6.3: Colorized geomorphic change detection map of study bluff BHHR, with black squares marking the two largest areas of erosion. The below photos show the study site in September 2014 and November 2015 with the erosional areas marked.

6.2.1 Faro Scene/GCD Error Results

Errors were found and analyzed at multiple stages in this study, which is further discussed in the Error Analysis section (5.0) of this paper. In Faro Scene the mean tension values, which provide the error in registration and alignment, were generated when registering multiple scans taken of a particular bluff on the same day and when registering scans of the same bluff taken in different periods. Table 6.10 gives the mean tension results for registering same-day scanning campaigns together. The mean tension for individual scan campaigns ranged from 0.0008 m to 0.0221 m, while the average at each study bluff ranged from 0.0017 m to 0.0077 m. The average mean tension for each

period ranged from 0.0023 m to 0.0045 m. Table 6.10 also gives the standard deviation in tension at each study bluff site, showing an overall average of 0.0026 m. The mean tension resulting from registering successive scanning campaigns together is reported in Table 6.11. The mean tension when aligning successive bluff campaigns together ranged from 0.0112 m to 0.067 m.

Table 6.10: Faro Scene Scan Manager Mean Tension Results (m) and Standard Deviation

Site #	Nov. 11	Apr. 12	May 12	June 12	Nov. 12	Nov. 13	Sep. 14	Apr. 15	Nov. 15	Site Average	Standard Deviation
B9	0.0024	0.0023	0.0033	0.0027	0.0021	0.0045	0.0036	0.0040	0.0090	0.0038	0.0021
B12	0.0036	0.0012	0.0010	0.0019	0.0008	n/a	0.0018	0.0016	0.0020	0.0017	0.0009
B13	0.0022	0.0032	0.0016	0.0017	0.0018	0.0034	0.0017	0.0020	0.0024	0.0022	0.0007
B14	n/a	0.0023	0.0090	0.0090	0.0019	0.0035	0.0013	0.0028	0.0026	0.0041	0.0031
B15	0.0011	0.0013	0.0012	0.0010	0.0012	0.0031	0.0022	0.0018	0.0116	0.0027	0.0034
B20	n/a	0.0018	0.0023	0.0029	0.0031	0.0028	0.0014	0.0013	0.0025	0.0023	0.0007
B2	n/a	0.0011	0.0022	0.0011	0.0013	0.0030	0.0030	0.0212	0.0042	0.0046	0.0068
B7	n/a	0.0221	0.0129	0.0057	0.0070	0.0050	0.0016	0.0025	0.0049	0.0077	0.0067
BHHR	n/a	n/a	n/a	n/a	n/a	0.0011	0.0032	0.0039	0.0025	0.0027	0.0012
BSWCD	n/a	n/a	n/a	n/a	n/a	n/a	0.0033	0.0034	0.0037	0.0035	0.0002
Time Period Average	0.0023	0.0044	0.0042	0.0033	0.0024	0.0033	0.0023	0.0045	0.0045		
Average Standard Deviation											0.0026

Table 6.11: Faro Scene Manager Mean Tension Results Between Successive Campaigns

Site #	Mean Tension (m)
B9	0.0404
B12	0.0521
B13	0.0112
B14	0.0302
B15	0.0397
B20	0.0392
B2	0.0341
B7	0.0151
BHHR	0.0697
BSWCD	0.0262

Errors are also analyzed and reported during the GCD process. The errors are shown on a summary file produced by the GCD software for each set of successive campaigns that were compared. The 0.10 m thresholded area of erosion/deposition and

the spatially uniform error surface were used to calculate the error in net change volume. The error volume and the 0.10 m thresholded net volume difference were used to calculate the percent error present. Table 6.12 shows the net volume change, the calculated error volume and the percent error. The percent error ranged from 3% to 655%, tending to be lower when retreat distance was highest and higher when geomorphic change was negligible. GCD summary files for each compared campaign are provided in Appendix B. These summaries provide the information listed in Table 6.12, in addition to showing the thresholded and non-thresholded total area, the volume of erosion and deposition, and the corresponding error volume and percent error associated with the volume of erosion and deposition.

Table 6.12: DoDs – Net Change and Associated Uncertainties

	Nov. 2011 to Apr. 2012			Apr. to May 2012			May to June 2012		
Site #	Net Change (m^3)	±Error (m^3)	% Error	Net Change (m^3)	±Error (m^3)	% Error	Net Change (m^3)	±Error (m^3)	% Error
B9	-83	31	37%	32	14	45%	-247	26	10%
B12	-7	2	26%	2	0	3%	-1	0	31%
B13	-11	4	38%	-2	1	58%	-3	3	94%
B14	n/a	n/a	n/a	0	0	4%	-8	1	17%
B15	-1	1	56%	-6	2	37%	-6	2	31%
B20	n/a	n/a	n/a	-5	2	33%	-27	3	12%
B2	n/a	n/a	n/a	-23	13	54%	-347	23	7%
B7	n/a	n/a	n/a	-10	4	40%	-141	23	17%
BHHR	n/a	n/a	n/a	n/a	n/a	n/a	n/a	n/a	n/a
BSWCD	n/a	n/a	n/a	n/a	n/a	n/a	n/a	n/a	n/a

	June to Nov. 2012			Nov. 2012 to Nov. 2013			Nov. 2013 to Sep. 2014		
Site #	Net Change (m^3)	±Error (m^3)	% Error	Net Change (m^3)	±Error (m^3)	% Error	Net Change (m^3)	±Error (m^3)	% Error
B9	10	8	77%	-17	8	48%	-87	21	24%
B12	0	0	0%	n/a	n/a	n/a	n/a	n/a	n/a
B13	0	0	0%	2	1	53%	4	2	43%
B14	1	0	0%	-1	0	47%	3	3	82%
B15	0	0	0%	0	0	154%	0	0	289%
B20	0	0	0%	0	1	198%	-1	1	207%
B2	-1	1	100%	-50	15	29%	-176	43	24%
B7	-8	35	438%	-84	32	39%	-36	29	82%
BHHR	n/a	n/a	n/a	n/a	n/a	n/a	n/a	n/a	n/a
BSWCD	n/a	n/a	n/a	n/a	n/a	n/a	n/a	n/a	n/a

	Nov. 2013 to Apr. 2015			Sep. 2014 to Apr. 2015			Apr. to Nov. 2015		
Site #	Net Change (m^3)	±Error (m^3)	% Error	Net Change (m^3)	±Error (m^3)	% Error	Net Change (m^3)	±Error (m^3)	% Error
B9	n/a	n/a	n/a	28	19	67%	-20	8	40%
B12	n/a	n/a	n/a	0	1	228%	-2	1	47%
B13	n/a	n/a	n/a	-10	3	27%	0	0	331%
B14	3	3	82%	0	2	655%	-1	2	213%
B15	n/a	n/a	n/a	1	0	37%	1	1	103%
B20	n/a	n/a	n/a	1	2	191%	0	1	342%
B2	n/a	n/a	n/a	-19	21	110%	-65	28	43%
B7	n/a	n/a	n/a	-96	27	28%	-81	38	47%
BHHR	n/a	n/a	n/a	30	10	35%	8	8	108%
BSWCD	n/a	n/a	n/a	-28	13	46%	25	14	55%

	Nov. 2012 to November 2015			Sep. 2014 to Nov. 2015		
Site #	Net Change (m^3)	±Error (m^3)	% Error	Net Change (m^3)	±Error (m^3)	% Error
B9	-90	18	20%	n/a	n/a	n/a
B12	-8	1	17%	n/a	n/a	n/a
B13	-5	2	36%	n/a	n/a	n/a
B14	5	2	47%	n/a	n/a	n/a
B15	2	1	39%	n/a	n/a	n/a
B20	-3	2	65%	n/a	n/a	n/a
B2	-158	25	16%	n/a	n/a	n/a
B7	-51	41	81%	n/a	n/a	n/a
BHHR	n/a	n/a	n/a	29	13	44%
BSWCD	n/a	n/a	n/a	14	19	134%

Lastly, high intensity areas of erosion and deposition shown on the colorized geomorphic change maps were confirmed with photos taken of the bluffs to further validate the accuracy of the Faro Scene and GCD results. Figures 6.4 and 6.5 show examples of areas of geomorphic change that were verified with photography. Figure 6.4 includes the geomorphic change map of study site B2, showing significant levels of erosion, particularly in the basal zone. Photos of the bluff taken by the Faro Focus 3-D scanner in November 2012 and by a digital camera in November 2015 confirms that there was noticeable removal of sediment from the basal zone of B2 during this period. Figure 6.5 shows the geomorphic change maps of study site B20, with an area of significant erosion showing in the upper, left (downstream) side of the bluff. This area of erosion was verified with a photo taken of the bluff by the Faro Focus 3-D scanner in November 2012 and a photo of the same bluff area taken with a digital camera in November 2015. In November 2012, this region of the bluff has a convex shape and by November 2015 the region is more concave with clear undercutting visible, thereby affirming that erosion occurred in this region during the period of geomorphic change detection.

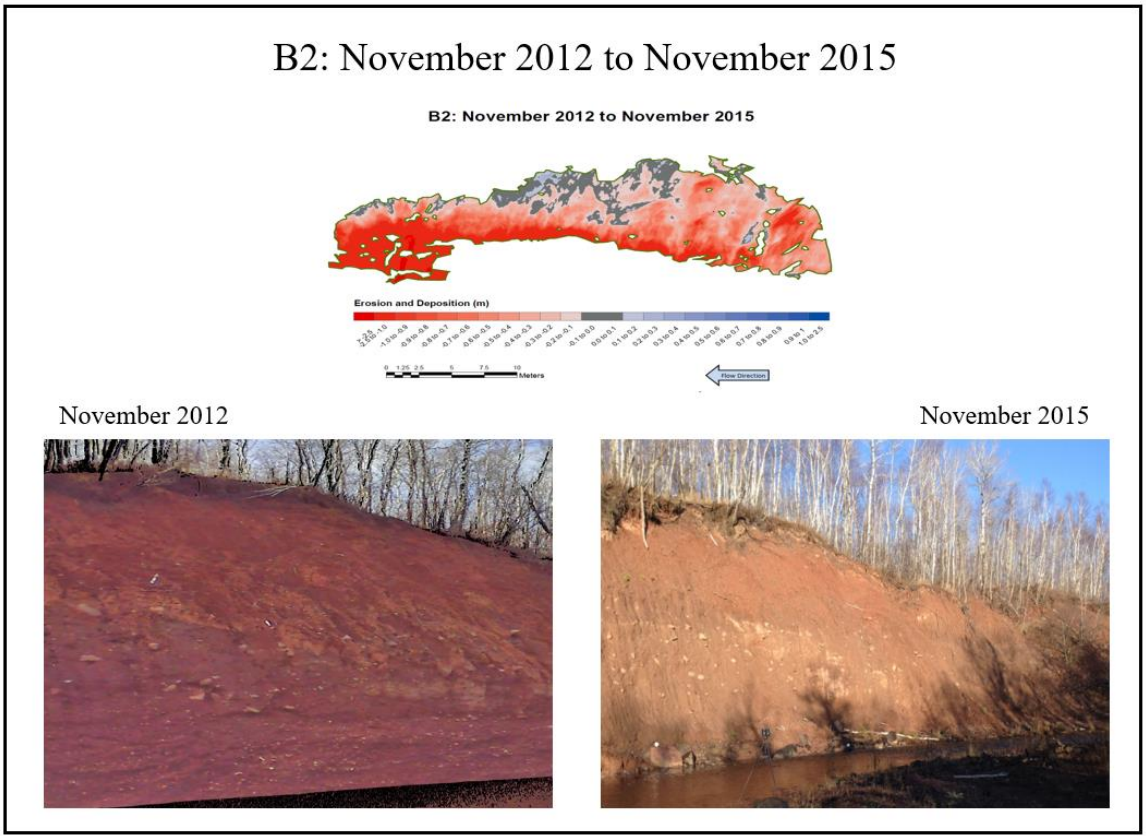

Figure 6.4: Colorized geomorphic change detection map of study bluff B2, showing high levels of erosion, particularly in the bluffs lower zone. The below photos show the study bluff in November 2012 and November 2015, illustrating a clear loss of sediment in basal zone.

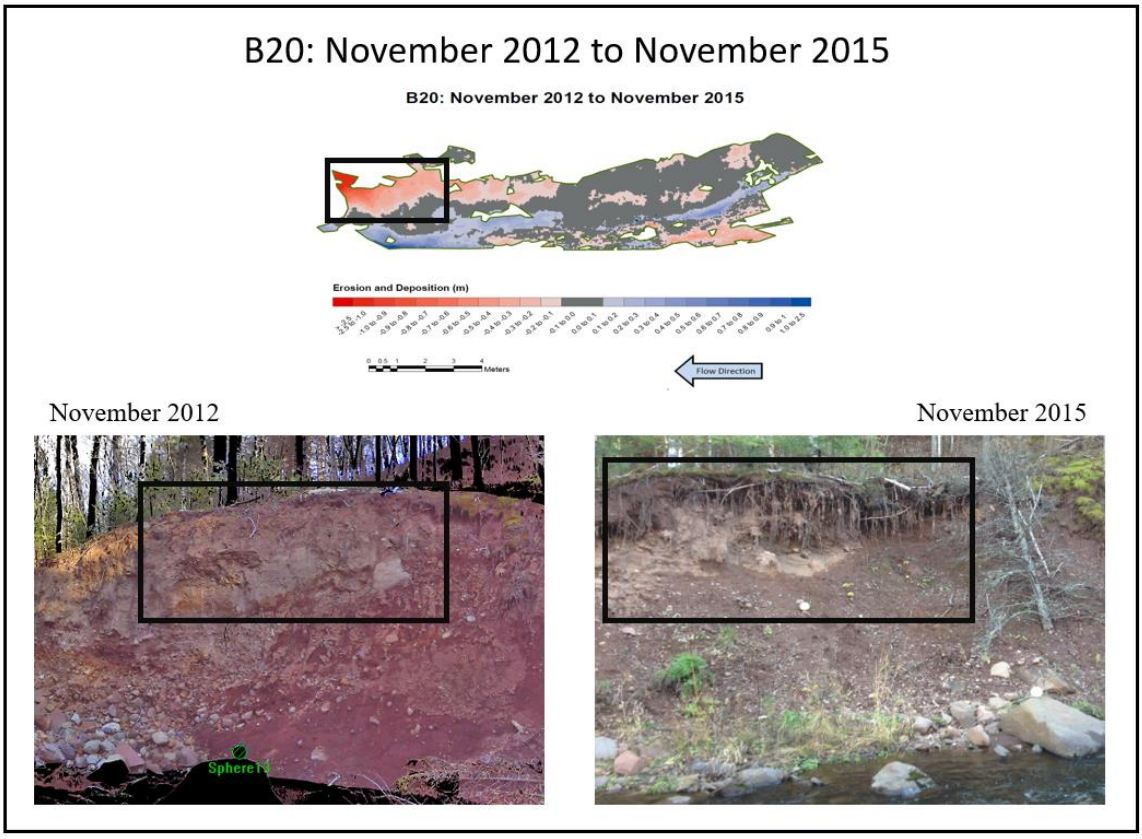

Figure 6.5: Colorized geomorphic change detection map of study bluff B20, with a rectangle marking an area of high levels of erosion. The below photos, taken in November 2012 and November 2015 show the same marked area showing that erosion did occur in this geomorphic change detection period.

6.3 Extrapolating Results

In order to determine a total mass of sediment attributed to bluff erosion within a watershed, the inventory of unvegetated bluffs, the retreat distance measurements, as well as the bulk density and grain size analyses results need to be combined. For Amity Creek watershed, which is where the majority of the study bluffs are located, the TLS/GCD results were extrapolated to obtain an approximate total mass of sediment contributed to Amity Creek due to geomorphic change of bluffs.

The total area of unvegetated bluffs in Amity Creek is 5,596 m^2 (Table 6.13), which includes 656 m^2 of study bluff area and 4,940 m^2 of additional field-inventoried

unvegetated bluff within the watershed (Neitzel 2014). Various average retreat rates were calculated in this study. The average retreat rate for natural bluffs, which are bluffs that have not been stabilized in any way, was found to be -0.08 m per year of retreat (Table 6.14). This rate was calculated by taking the average over the longest period of registered scans available for all of the natural bluffs, November 2012 to November 2015. The average retreat rate for stabilized bluffs was found to be -0.01 m per year of retreat for study bluffs B13 and B14, using the period from November 2012 and November 2015 to obtain this average rate (Table 6.15). The most recently stabilized bluffs, BHHR and BSWCD, were found to have an average retreat rate of 0.07 m per year, indicating deposition, when analyzing scans from September 2014 to November 2015 (Table 6.15). An average retreat rate was also found for all the bluffs that have scans available from November 2012. This allows for an average rate to be based on three years of geomorphic change (Table 6.16). The average retreat rate was found to be -0.06 m per year of retreat.

However, since the bluffs vary significantly in area (Table 6.8) a weighted average based on area was calculated to get a more spatially-representative rate. The area-weighted average retreat rate, using the eight bluffs where a three-year period is available to calculate geomorphic change, was found to be -0.08 m per year of retreat. Using the -0.08 m/yr. average retreat rate and the total unvegetated bluff area of 5,596 m^2, the estimated total volume of sediment attributed to bluff erosion is 448 m^3/yr.

In order to obtain a mass of fine particles entering Amity Creek through bluff erosion, the estimated total volume needs to be combined with the soil characteristics that were measured. Larger particles, anything larger than coarse sand, were removed from

the grain size samples before they were analyzed. These larger particles were estimated to be 10% of the total volume. Therefore, the estimated total sediment volume was reduced by 10%, giving a total volume of 403 m^3 of fine particles eroded from bluffs within Amity Creek watershed. By multiplying the volume of sediment by the calculated average bulk density of 1430 kg/m^3 for Amity Creek bluffs (Neitzel 2014), we get a mass of 576,000 kg of sand, silt and clay particles eroding from bluffs each year in the watershed. However, this study is primarily concerned with reducing turbidity, which is caused by silt and clay sized particles that are suspended in the water column. Therefore, the total sand, silt, and clay sediment load was multiplied by the average percent of silt and clay to determine an estimate of the TSS load that is caused by eroded bluff material. The average percentage of silt and clay calculated from a grain size analysis was found to be 98% (Neitzel 2014). This calculation showed that there is 564,000 kg of silt and clay particles eroding from bluffs each year in Amity Creek watershed.

Table: 6.13: Amity Creek Un-vegetated Bluff Area (Neitzel 2014)

Study Bluffs	Height	Length	% Un-vegetated	Total area (m^2)
B9	N/A	N/A	N/A	370
B12	N/A	N/A	N/A	36
B13	N/A	N/A	N/A	45
B14	N/A	N/A	N/A	91
B15	N/A	N/A	N/A	32
B20	N/A	N/A	N/A	83
Total Study Bluff	**N/A**	**N/A**	**N/A**	**656**

Field Inventory	Height	Length	% Un-Vegetated	Total area (m^2)
1	2	12	60	14
2	2.5	38	50	48
3	2	43	75	65
4	2.5	35	30	26
5	5	58	30	87
6	20	100	60	1,200
7	13	120	75	1,170
8	22	30	85	561
9	13	52	35	237
10	5	63	95	299
11	2	10	75	15
12	3.5	45	60	95
13	3.5	60	60	126
14	2.5	30	95	71
15	3	30	65	59
16	3.5	15	65	34
17	2.5	18	40	18
18	4.5	20	65	59
19	1.8	22	60	24
20	3.5	38	70	93
21	5.5	5	80	22
22	4.5	22	80	79
23	3.5	15	80	42
24	3.5	38	60	80
25	3.5	45	85	134
26	2	10	65	13
27	7	30	50	105
28	4	15	65	39
29	8	23	40	74
30	3.5	15	25	13
31	5	40	20	40
Inventory Total				4,940
Total				**5,596**

Table 6.14: Natural Bluffs - Average Retreat Rates (m/yr)

Site #	Nov. 2011 to Apr. 2012	Apr. to May 2012	May to June 2012	June to Nov. 2012	Nov. 2012 to Nov. 2013	Nov. 2013 to Sep. 2014	Sep. 2014 to Apr. 2015	Apr. to Nov. 2015	Nov. 2012 to Nov. 2015
B9	-0.60	1.20	-10.3	0.07	-0.09	-0.30	0.14	-0.16	-0.10
B12	-0.77	1.08	-0.60	0.00	n/a	n/a	0.00	-0.23	-0.18
B15	-0.14	-2.88	-3.12	0.02	0.00	0.00	0.11	0.11	0.08
B20	n/a	-0.84	-5.28	0.00	0.00	-0.02	0.03	0.00	-0.02
B2	n/a	-0.60	-10.1	0.00	-0.20	-0.46	-0.07	-0.19	-0.21
B7	n/a	-0.24	-3.60	-0.02	-0.13	-0.07	-0.28	-0.27	-0.03
Period Average	-0.50	-0.38	-5.50	0.01	-0.08	-0.17	-0.01	-0.12	-0.08

Table 6.15: Stabilized Bluffs – Average Retreat Rates (m/yr)

Site #	Nov. 2011 to Apr. 2012	Apr. to May 2012	May to June 2012	June to Nov. 2012	Nov. 2012 to Nov. 2013	Nov. 2013 to Sep. 2014	Nov. 2013 to Apr. 2015	Sep. 2014 to Apr. 2015	Apr. to Nov. 2015	Sep. 14 to Nov. 15	Nov. 2012 to Nov. 2015
BHHR	n/a	n/a	n/a	n/a	n/a	n/a	n/a	0.25	0.06	0.12	n/a
BSWCD	n/a	n/a	n/a	n/a	n/a	n/a	n/a	-0.07	0.07	0.02	n/a
B13	-0.60	-0.60	-0.96	0.00	0.09	0.08	n/a	-0.23	0.00	n/a	-0.06
B14	n/a	0.12	-5.64	0.05	-0.02	n/a	0.03	n/a	-0.04	n/a	0.04
Period Average	-0.60	-0.24	-3.30	0.03	0.04	0.08	0.03	-0.02	0.02	0.07	-0.01

Table 6.16: Bluffs scanned since at least Nov. 2012 – Average Retreat Rates (m/yr)

Site #	Nov. 2011 to Apr. 2012	Apr. to May 2012	May to June 2012	June to Nov. 2012	Nov. 2012 to Nov. 2013	Nov. 2013 to Sep. 2014	Sep. 2014 to Apr. 2015	Apr. to Nov. 2015	Nov. 2012 to Nov. 2015
B9	-0.60	1.20	-10.3	0.07	-0.09	-0.30	0.14	-0.16	-0.10
B12	-0.77	1.08	-0.60	0.00	n/a	n/a	0.00	-0.23	-0.18
B13	-0.60	-0.60	-0.96	0.00	0.09	0.08	-0.23	0.00	-0.06
B14	n/a	0.12	-5.64	0.05	-0.02	n/a	n/a	-0.04	0.04
B15	-0.14	-2.88	-3.12	0.02	0.00	0.00	0.11	0.11	0.08
B20	n/a	-0.84	-5.28	0.00	0.00	-0.02	0.03	0.00	-0.02
B2	n/a	-0.60	-10.1	0.00	-0.20	-0.46	-0.07	-0.19	-0.21
B7	n/a	-0.24	-3.60	-0.02	-0.13	-0.07	-0.28	-0.27	-0.03
Period Average	-0.53	-0.35	-4.95	0.02	-0.05	-0.13	-0.04	-0.10	-0.06

6.3.1 Estimating Sediment Loads from Stabilized Bluffs

Four of the studied bluffs have been stabilized in some capacity. Study bluffs B13 and B14 were both stabilized (see Background section of this paper for more details). However, much of the stabilization designs on these bluffs no longer remains in place, including the bankfull bench at B14. Therefore, these bluffs are still susceptible to fluvial scour and sediment that is eroded from these bluffs still enters the stream. Additionally, the average erosion rates are not significantly different than the natural bluff retreat rates. For these reasons, B13 and B14, were included with the natural bluffs to calculate an average retreat rate (Table 6.14, 6.15, 6.16).

Two of the bluffs, BHHR and BSWCD, were stabilized using a Toe Wood Structure design. This design builds a bench in front of the bluff, to eliminate fluvial scour on the bluff thereby likely reducing the rate of geomorphic change and to serve as a catchment area for sediment that still erodes from the bluffs. Therefore, even if bluff erosion occurs, this material does not enter the stream but is retained on the benches, unless there is a high flow event where the stream stage rises above bankfull height.

Due to a sample size of only two and a short period of 14 months to detect geomorphic change, results from this stabilization method could not be extrapolated throughout the watershed or be statistically compared with natural bluffs with any confidence. However, these bluffs do show an average retreat that is positive over the longest period that could be compared, showing that there is overall growth or deposition occurring. Additionally, preliminary results of the effectiveness of this stabilization design were calculated for both bluffs by determining the mass of sediment that is retained on the bankfull benches.

The mass of sediment that the bankfull benches captured was calculated using the volume of sediment that has eroded from September 2014 to November 2015. For BHHR, the total volume of erosion is 31 m^3 (Figure 6.6). Particles larger than coarse sand were removed from the soil sample prior to the grain size analysis and were estimated also to be 10% of the total sample. The volume of sediment was reduced by 10%, resulting in 27.9 m^3 of sediment erosion on this bluff. The volume of sand, silt, and clay particles was then multiplied by the bulk density of 1990 kg/m^3 that was calculated for this Knife River bluff. This calculation resulted in an estimation of 55,500 kg of sand, silt, and clay that has been eroded on BHHR. Since we are mainly concerned with the very fine particles, silt and clay, this mass was then multiplied by the percentage of these fine particles found in the soil while running a grain size analysis. The soil was found to be composed of 98.5% silt and clay. Therefore, roughly 54,700 kg of silt and clay comprised sediment has been captured on the bankfull bench at BHHR over a 14-month period instead of entering Knife River.

Attribute	Raw	Thresholded DoD Estimate:			
AREAL:					
Total Area of Erosion (m^2)	85	85			
Total Area of Deposition (m^2)	121	71			
VOLUMETRIC:				± Error Volume	% Error
Total Volume of Erosion (m^3)	31	31	±	7	23%
Total Volume of Deposition (m^3)	66	60	±	11	18%
Total Volume of Difference (m^3)	97	91	±	18	19%
Total Net Volume Difference (m^3)	35	**29**	**±**	**13**	44%

Figure 6.6: Output data from GCD software of BHHR over the longest period of scan record, September 2014 to November 2015.

For BSWCD, the total volume of eroded sediment is 27 m^3 (Figure 6.7). Particles larger than coarse sand were removed from the soil sample prior to the grain size analysis and were estimated to be 10% of the total sample. The volume of sediment was reduced by 10%, resulting in 24.3 m^3 of sediment deposition on this bluff. The volume of sand, silt, and clay particles was then multiplied by the average Amity Creek bulk density of 1430 kg/m^3. This calculation resulted in an estimation of 34,700 kg of sand, silt and clay that has eroded at BSWCD. In order to determine the mass of silt and clay particles, this mass was then multiplied by 98%, the percentage of these particles found in the soil during the grain size analysis. Therefore, roughly 34,000 kg of silt and clay comprised sediment has been captured on the bankfull bench at BSWCD over a 14-month period and not entering Amity Creek.

Attribute	Raw	Thresholded DoD Estimate:		
AREAL:				
Total Area of Erosion (m^2)	221	221		
Total Area of Deposition (m^2)	435	48		
VOLUMETRIC:			± Error Volume	% Error
Total Volume of Erosion (m^3)	27	27	± 8	29%
Total Volume of Deposition (m^3)	75	41	± 17	42%
Total Volume of Difference (m^3)	102	68	± 25	37%
Total Net Volume Difference (m^3)	48	**14**	**± 19**	134%

Figure 6.7: Output data from GCD software for BSWCD over the longest period of scan record, September 2014 to November 2015.

6.4 Precipitation data

The precipitation data show only 5.62 inches of rain from September 2014 to April 2015 and only one precipitation event that produced over an inch of rain (Table 6.17). However, there was still geomorphic change detected in this period, with the

average retreat rate being -0.04 m/yr. using the eight study bluffs scanned since at least November 2012 (Table 6.16). November 2012 to November 2013 saw 20.19 inches of precipitation, with five events and three single day events with precipitation over one inch (Table 6.17). The largest precipitation event produced 2.5 inches of rain over a four-day period and the largest single day amount of precipitation was 1.63 inches (Table 6.17). The average retreat rate for this period is -0.05 m/yr., just slightly more than for the period from September 2014 to April 2015 (Table 6.16). The total precipitation for April 2015 to November 2015 is 24.03 inches and there were ten events and seven single days with precipitation over one inch (Table 6.17). The largest amount of precipitation generated from an event is 2.44 inches falling in a two-day period from September 23-24, 2015 (Table 6.17). The largest single day precipitation amount was 2.03 inches, which fell during this event, on September 23, 2015 (Table 6.17). The average retreat rate for this period is -0.10 m/yr. (Table 6.16). The period with the most total precipitation, the largest event amount and the largest single day amount was November 2013 to September 2014. In this period, there was 25.51 inches of precipitation, nine events and four single days with precipitation amounts of an inch or more (Table 6.17). The largest precipitation event produced 2.88 inches over a three-day period from August 17 to 19, 2014, and the largest single day amount during this period is 2.58 inches, which fell on August 24, 2014 (Table 6.17). This period also had the highest average retreat rate between the four periods of -0.13 m/yr. (Table 6.16).

Table 6.17: Precipitation Data					
Period	**Total Precipitation (inches)**	**# of Events with Precipitation > 1 inch**	**Largest Event Amount (inches)**	**# of Single Days with Precipitation > 1 inch**	**Largest Single Day Amount (inches)**
Nov. 12 to Nov. 13	20.19	5	2.5 (6/20-23/13)	3	1.63 (7/21/13)
Nov. 13 to Sep. 14	25.51	9	2.88 (8/17-19/14)	4	2.58 (8/24/14)
Sep. 14 to Apr. 15	5.62	1	1.05 (10/1-4/14)	0	n/a
Apr. 15 to Nov. 15	24.03	10	2.44 (9/23-24/15)	7	2.03 (9/23/15)

The average retreat rates when compared with the number of precipitation events with greater than one inch and with total precipitation shows that these variables trend similarly. As the number of precipitation events over an inch increases, average retreat rates also tend to increase (Figure 6.8). Similarly, as the total precipitation increases, average retreat rates tend to increase (Figure 6.9).

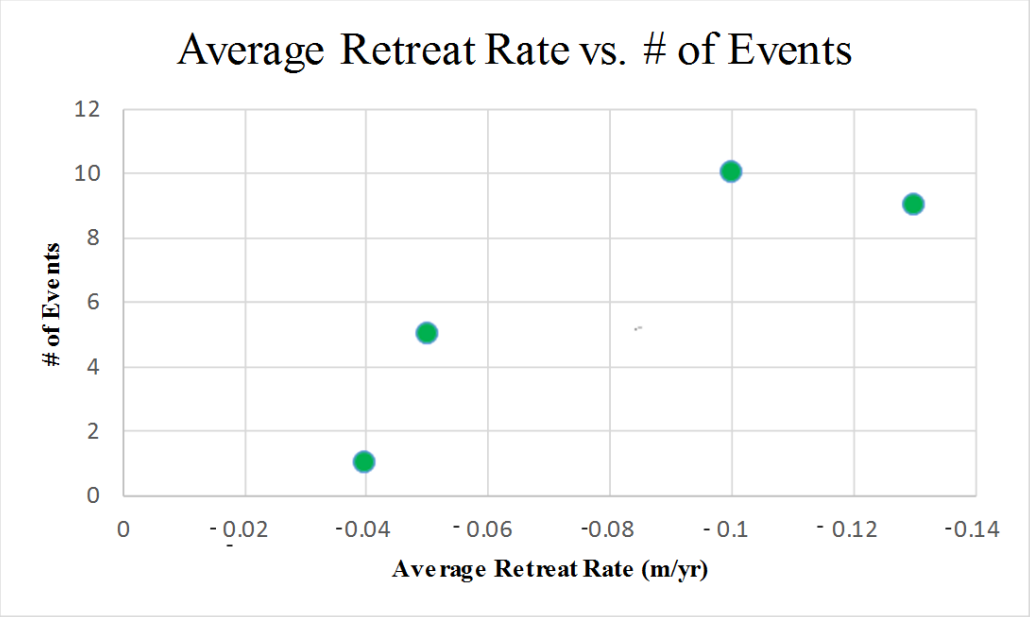

Figure 6.8: Average retreat rates compared with the number of precipitation events for four periods of geomorphic change detection.

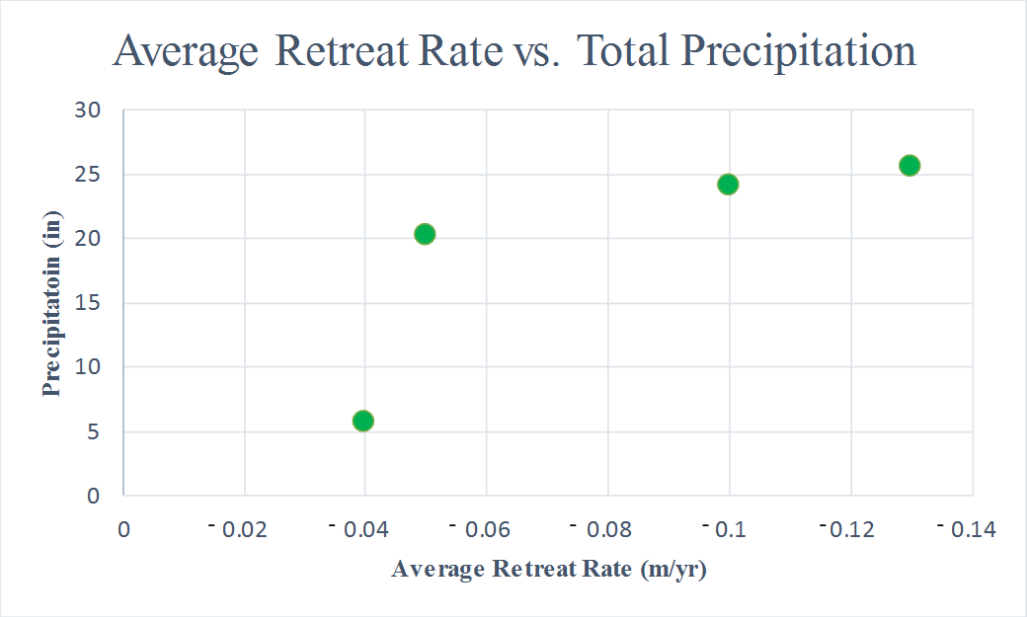

Figure 6.9: Average retreat rates compared with total precipitation for four periods of geomorphic change detection.

7.0 Discussion

This study has shown that bluffs are contributing large amounts of sediment to Amity Creek watershed and in this watershed, we have been able to estimate a quantity of sediment that is being added to the stream each year by bluffs. Through this analysis in Amity Creek watershed and by detecting geomorphic change on two Lester River bluffs and one Knife River bluff, it has been shown that natural bluffs in general are retreating. Unvegetated bluffs are likely a major contributor of sediment to streams throughout Minnesota's North Shore and are contributing to the turbidity impairment present in ten streams in this region.

All of the bluffs in this study that have been scanned since 2012 have shown periods of retreat and in the nine periods where these bluffs were compared the average retreat distance was negative (i.e. erosional) in eight of the nine periods. The greatest

period of retreat was from May to June 2012, which is the period that shows calculated geomorphic change before and after a 500-year flood. Neitzel (2014) showed that high flow events have a major effect on bluff erosion rates. However, by comparing retreat rates post-flood and over a three-year period, this study was able to show that even without historic high flow events geomorphic change is still detectable on bluffs. Our results tell us that flow rates have an effect on bluff erosion even when they are not at historic stages but also that other processes besides fluvial scour influence the geomorphic change of riverine bluffs. For example, geomorphic change was detected over winter, when flow rates were very low, showing the influence of freeze-thaw cycles on erosion rates. Additionally, surface erosional features, such as rills and gullies developed showing that surface flow is influencing geomorphic change.

In this study, we also looked at stabilized bluffs. The sample size of stabilized bluffs that were able to be analyzed is small, with only four study sites. Of these four site, two had been stabilized in 2009, and these stabilization efforts were damaged by the June 2012 flood event. The stabilization efforts are not fully functioning as designed, and vegetation was abundant on both study sites. Therefore, these stabilized bluffs were challenging to analyze for their effects on reducing TSS loads. The two other stabilized study bluffs, which were stabilized in 2014, were able to show that the average retreat distance is positive for both of these bluffs and thus the efforts are at least initially reducing TSS loads to the streams.

7.1 TSS Loads Caused by Bluff Erosion

The average retreat rate, area of unvegetated bluffs present, the soil's bulk density and the percentage of silt and clay were all used to calculate the mass of sediment that is

attributed to Amity Creek watershed due to bluff erosion. The average retreat rate used was -0.08 m/yr. This number was based on the average erosion rate of eight bluffs, where geomorphic change could be detected from November 2012 to November 2015, to get a three-year average. When taking a straight average of these eight bluffs the average retreat rate was -0.06 m/yr. (Table 6.16). The individual bluff retreat rates over this period ranged from -0.21 to 0.08 m/yr. (Table 6.16). However, the studied bluffs vary significantly in size, with study site B15 having an area of only 15 m^2 to study site B7 having an area of 671 m^2 (Table 6.8). Therefore, a weighted average based on area was taken, resulting in an average retreat rate of -0.08 m/yr. The weighted-average retreat distance calculated from our study sites was then extrapolated to all the unvegetated bluffs in the Amity Creek watershed. This resulted in an estimate that bluffs in Amity Creek watershed contribute 564,000 kg of TSS to the creek annually.

Unfortunately, TSS annual loads for Amity Creek were unavailable for the period over which this study was conducted. Therefore, the estimated annual sediment load attributed to bluff erosion, based on data from 2012 to 2015, could not be directly compared with total TSS loads from the same period. However, there are TSS load estimates available in Amity Creek from previous years (Table 7.1). These results show that the annual TSS load from bluffs is anywhere from 40-558% of the total TSS load in Amity Creek. From our study we know that bluff retreat distances vary annually based on conditions as do total TSS loads therefore a range is expected. Although it is unfortunate that we cannot compare the total annual TSS load in Amity Creek from the years during our study, it is evident that a large portion of the total TSS load in Amity Creek watershed is coming from bluffs. Due to this evidence, it is clear that controlling bluff

erosion in Amity Creek watershed will significantly reduce turbidity and improve water quality.

Table 7.1: Amity Creek TSS Load Estimates (kg)

Year	MPCA Estimated Load[a]	NRRI Estimated Load[b]	Study calculated load % of total
2002	895,000	--	63%
2003	184,000	--	307%
2004	946,000	--	60%
2005	251,000	117,000	225% / 482%
2006	168,000	101,000	336% / 558%
2007	--	679,000	83%
2008	--	--	--
2009	--	1,044,000	54%
2010	--	1,406,000	40%
Study calculated bluff contributed TSS load	**564,000**		

[a] Estimated load from Minnesota Pollution Control Agency (MPCA) North Shore Monitoring Program

[b] Estimated load from University of Minnesota Duluth Natural Resources Research Institute (NRRI)

7.2 Effectiveness of Bluff Stabilization

Completed bluff stabilization projects were analyzed in this study. However, only two study sites, BSWCD and BHHR, had stabilization projects that were intact and the bluffs were still predominantly unvegetated. Geomorphic change was only able to be detected in three periods for these bluffs and the longest period of detection was just 14 months, from September 2014 to November 2015. However, during this period retreat rates were shown to be positive, showing the geomorphic change that is occurring is more depositional than erosional. Using the total volume of erosion on each bluff, the soil's bulk density and percentage of silt and clay, it was calculated that 34,000 kg at BSWCD and 54,700 kg at BHHR have been deposited on the bluffs or bankfull benches over a 14-month period instead of accessing the stream.

These bluffs are still showing detectable geomorphic change and there are still areas of erosion. For example, at study site BHHR, there was a slump that occurred between April 2015 and November 2015; however, all the material shows to have deposited on the bench below the slump (Figure 7.1). Figure 7.1 shows that the project is still working as designed; sediment is being captured on the bankfull bench. Eventually the idea is that due to reduced fluvial scour and to this sediment deposition, the gradient of the bluff face will decrease and allow for vegetation to take hold. In the first year after these restoration projects, TLS/GCD results show that the Toe Wood Structure is working as designed by reducing the amount of sediment that is reaching the streams.

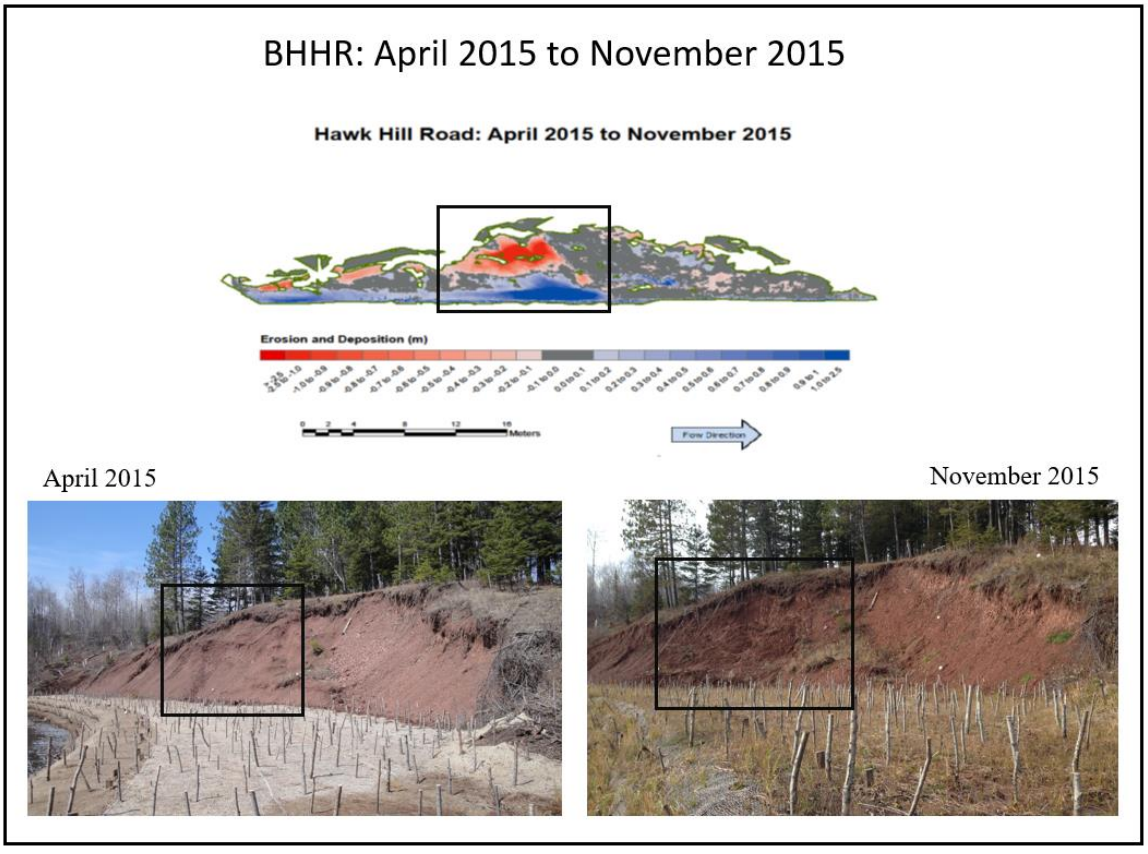

Figure 7.1: The colorized geomorphic change maps shows erosion in red and deposition in blue on site BHHR. The pictures below show the marked area in April 2015 on the left and in November 2015 on the right.

Two other bluffs, B13 and B14, were also stabilized and were analyzed in this study. Their average retreat rates did not show a consistent pattern of deposition and did not show significantly smaller retreat rates over time when compared with bluffs that had not been stabilized. However, geomorphic change was difficult to detect on these bluffs due to the fact that they were both heavily vegetated so only small sections of each bluff were available for change detection to be analyzed. Additionally, these bluffs were stabilized before the June 2012 flood and like most of the bluffs in the watershed experienced significant geomorphic change. This flood also damaged some of the stabilization structures that were installed. The stabilization project was understandably not designed to withstand a 500-year flood event.

These two bluffs still have negative retreat rates during various periods and there is no longer a bankfull bench fully intact to capture the sediment that does erode. However, the calculated retreat rates are based only on the areas that are not vegetated and the vast majority of these bluffs are currently heavily vegetated, due to the stabilization efforts (Figure 7.2). The vegetated areas likely are not experiencing any detectable geomorphic change. For this reason, it is probable that the TSS load generated by B13 and B14 has been reduced due to the stabilization efforts but the quantity of the reduction cannot be accurately determined with TLS/GCD techniques.

Figure 7.2: Study bluff B14 in November 2015 is heavily vegetated, leaving little area that can be differentiated to detect geomorphic change.

7.3 Processes Affecting Bluff Erosion

TLS analyses in this study have shown that multiple processes influence bluff erosion on North Shore streams. Flow has been shown to be a major influence on bluff erosion. Results from this study show that by far the largest volume losses of sediment on our study bluffs, since November 2011 occurred in the period that contained the June 2012, 500-year flood. The average retreat rate during this period, May to June 2012 was -4.95 m/yr., while the next highest period, November 2011 to April 2012 was -0.53 m/yr. (Table 6.16). Additionally, when examining precipitation data from November 2012 to November 2015, which was used to estimate discharge, total precipitation and number of precipitation events both trend closely with average erosion rates. For example, the periods with the largest precipitation totals and the most number of precipitation events over an inch, November 2013 to September 2014 and April 2015 to November 2015, also had the largest erosion rates.

The colorized geomorphic change maps also add support to the idea that flow events influence bluff erosion, showing that most slumps occurred lower on the bluff face and often times no sediment deposition is seen below. This shows evidence of fluvial scour, which causes over-steepening in the basal zone, resulting in mass failure events, such as slides and slumps. Fluvial processes will also result in the eventual removal of the slumped material in the basal zone, which occurs when the flow has enough force to dislocate and transport the deposited sediment.

Although, our results show that peak flow events cause significant bluff retreat rate, the effect of these high flow events appear to be brief. In the periods detecting geomorphic change directly following the 500-year flood event, average retreat rates

were negligible. From June to November 2012, the average retreat rate was 0.02 m/yr. and from November 2012 to November 2013 the average retreat rate was -0.05 m/yr. These results provide evidence that there is a quick relaxation in geomorphic change on bluffs post-flood events.

Results also indicate other processes besides flows influence bluff erosion rates. However, besides scans conducting from November 2011 to November 2012 by Neitzel (2014), scans were taken between seven and 12 months of one another. Therefore, it is difficult to pinpoint the exact process or set of processes causing bluff erosion but the results show that geomorphic change did occur even when there were no large flow events. For example, from September 2014 to April 2015 there was only 5.62 inches of precipitation and only one precipitation event that resulted in over an inch of precipitation, which fell over a four-day period. However, there was geomorphic change still detected on most of the bluffs. These data indicates that despite likely not having any peak flow events, other processes were influencing bluffs resulting in erosion, such as freeze-thaw.

Additionally, geomorphic features are present on bluffs that are indicative of other erosion processes, such as rills and gullies that have formed on some bluffs due to surface water runoff. An example of this process is the gully formation on study site B2 that increased in size from April 2015 to November 2015 and deposited the eroded sediment at the bottom (Figure 7.3). In Figure 7.3, small rills are visible to the right of the indicated gully, in the November 2015 photograph, which also provides evidence that surface flow is resulting in erosion of sediment on this bluff.

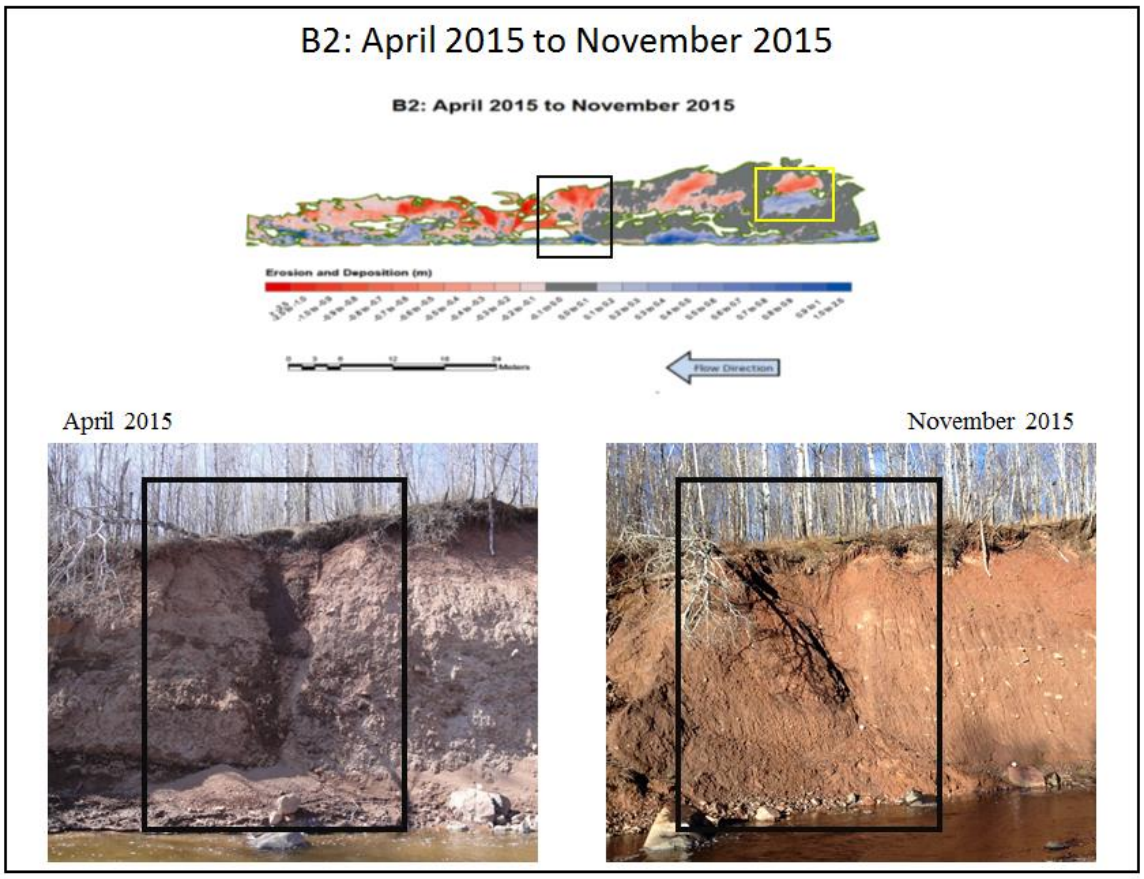

Figure 7.3: The colorized geomorphic change map of site B2 shows the location of a gully marked with a black square and the location of a slump marked by a yellow square. The pictures below show the marked gully area in April 2015 on the left and in November 2015 on the right, where the gully is wider and the pile of sediment at the base has grown.

Freeze-thaw action and groundwater-driven processes also impact bluff erosion. This can usually be seen by the presence of slides or slumps, occurring higher on bluffs, in locations that likely would not be impacted by fluvial scour especially during periods where no high flow events were recorded. Figure 7.3 shows an area marked with a yellow square where a slump has occurred but fluvial scour likely did not cause this particular slump due to the distance above the stream and no high flow events occurring from April 2015 to November 2015. Therefore, freeze-thaw action or groundwater seepage were likely the processes that caused the instability, which resulted in the seen failure.

The location of the bluffs within their given watershed also appear to influence their sediment volume loss. The three bluffs studied for a four-year period with the greatest drainage area, B9 (4.46 km^2), B7 (9.67 km^2) and B2 (9.88 km^2), also have the largest unvegetated area (Table 6.8). A bigger drainage area results in an increase in shear stress and stream power. Stream power is the product of the specific weight of water, channel slope and unit discharge, which is the total discharge divided by the channel width. As one moves downstream discharge increases and commonly on North Shore streams, channel slope also increases (Figure 2.3). Therefore, stream power and shear stress will increase downstream, resulting in more incision and higher relief. This results in sizable bluffs, which means that there is will be more sediment loss from these bluffs due to larger areas.

7.4 Retrospectives: TLS, Vegetation, Control Points

For this study, TLS did seem like the appropriate technique to use over other, more traditional techniques. The spatial and temporal range of TLS allowed for the collection of accurate, high resolution data. The data collection itself was quick, much faster than other techniques for detecting geomorphic change, such as total station instruments. It also collected large, dense point clouds, which allowed for the highly spatially variable bluff faces to be captured. Also, due to the production of the colorized geomorphic change maps using the GCD software showing the location of change, a deeper understanding could be gained on the processes affecting geomorphic change on bluffs.

However, there were some problems with using TLS technology to calculate geomorphic change of riverine bluffs. One issue is that with the TLS process, DEMs are

created of each bluffs and these are differentiated to determine net change between periods. However, a DEM reduces the 3D bluff to a "2.5D" dataset. This is problematic when a bluff has an overhanging ledge at the top (Figure 7.4). The front of the ledge will be compared and any change to the underside of the ledge will not be detected, thereby making a smaller area over which change can be differentiated on the bluff surface.

Figure 7.4: Overhanging ledge on site B15, which prevents geomorphic change from being detected underneath the ledge.

Another complication with using TLS is in removing vegetation. The collection of TLS datasets is a relatively quick, smooth process but the most intensive work is in post-processing the data, including manually removing vegetation. Due to this workload but also to the fact that heavily vegetated areas have to be removed from the dataset, bluffs cannot be extensively vegetated in order for this process to work. Most of the study bluffs in this project were relatively bare, but as discussed earlier the stabilized bluffs, B13 and

B14, were heavily vegetated (Figure 7.3). These bluffs, due to the small area on them that could be differentiated for geomorphic change did not provide much or highly accurate data to calculate an average retreat distance. Study site B12 also has patches of heavy vegetation and a fallen tree that both serve to reduce the area over which change can be detected (Figure 7.5).

Figure 7.5: Study site B12 in November 2015, showing areas that are becoming vegetated as well as an area in the center of the bluff that is blocked by the downing of a large tree.

Another issue that arose with using TLS technology was registering scans from single campaigns and from successive campaigns. Neitzel (2014) installed three control points using rebar posts in 2011 at eight of the ten bluffs in this study and control points were added at the other two bluffs in 2014. However, many of these rebar posts became buried, bent, unable to be found or covered with vegetation over the years. When three spheres are present between scans, the scans can be automatically registered but in no instance in this study were at least three spheres present between campaigns. Therefore, at all of the bluffs successive scanning campaigns had to be manually registered. This was a time-consuming process and led to reduced accuracy (i.e. higher reference tension values) in scan registration. Installing more rebar control points would be helpful so in situations where destruction occurs there would be a higher probability of other points available for use. Additionally, installing control points at higher elevations when

possible would likely help in the retention of control points between years, since at higher elevations on the bluffs the control would be less likely to be impacted by fluvial action. Lastly, control points could be added that are not on rebar but instead on seemingly permanent objects located on the bluff, such as marking a specific spot on a large rock with spray paint.

7.5 Subsequent Work

This study shows, through the use of TLS and GCD technologies, that bluffs are major sources of sediment to North Shore streams. Thereby it provides support that stabilization projects to control bluff erosion are critical to reducing the fine sediment load in these streams in order to improve the water quality in this region. These data are important to know because the current bluff stabilization projects occurring on the North Shore require a lot of money to complete. For example, Lake County Soil and Water Conservation District (SWCD) stabilized two bluffs on the Knife River, one of which is a study site, BHHR and the other was scanned but not included in this project. Lake County SWCD had two grants for this stabilization work, one funded by the Minnesota Board of Water and Soil Resources totaling $282,633 and the other funded by the Great Lakes Commission through the Sediment Control Program totaling $293,000 (Lake County SWCD 2014). Therefore, by being able to quantify the amount of sediment retained through these stabilization efforts and with a stronger understanding of the processes that are causing erosion, resources available for North Shore stream restoration can be most efficiently allocated.

Although bluff erosion is shown to be a major contributor of sediment there are other sources of fine-grained particles that are causing turbidity impairments. The University of Minnesota with funding and collaboration from the Minnesota Pollution Control Agency (MPCA), is currently working on the “Lake Superior Streams Sediment Stressor

Investigation", which began in August 2014 and will be completed by July 2016 (Nieber 2014). The investigation is looking to determine and quantify the main sources of sediment to the North Shore streams (Nieber 2014). Preliminary research in this study has shown that the geology and land use of the region are important.

Land use practices as well as the surficial geology, which includes clay-rich soils, create slow infiltration rates in the region. Infiltration tests were run on three sites, with each site containing an agricultural field, and a forested region. Within the forest regions holes were dug to a foot-deep, where a clay layer was present. At each of the three sites, 20 infiltration tests were conducted in the field, in the forested region and in the foot-deep clay layer for a total of 180 infiltration tests. Infiltration rates were found to be the highest in forested areas but when the top foot of top soil was removed, a clay layer was reached, which had very slow infiltration rates (Table 7.2). Therefore, it was surmised that water will infiltrate quickly in forested regions but then will hit the clay layer, which will restrict downward flow and the water will move laterally. Infiltration rates were also taken in agricultural areas. The rates on this land use were slower than the rates from forested areas but faster than when the top 12 inches of top soil was removed from the forested regions (Table 7.2). Slow infiltration rates will mean that there will be more occurrences of overland flow and near-surface flow. This is a faster pathway for water to travel, meaning that a greater volume of water will enter streams. Also, overland and near-surface flow pick-up sediment as the water travels, being more sediment-rich than groundwater inputs.

Table 7.2: North Shore Infiltration Rates by Land Use (cm/min)

Site	Forested	Agricultural Field	Clay Layer
1	57.7	5.78	0.02
2	48.7	6.7	0.009
3	31	2.65	0.04
Average	45.8	5.04	0.02

The geology of the region also leads to the formation of ravines in areas that do not contain a lot of bedrock. Ravines can serve as quick pathways for water to reach streams during precipitation events. During storm events, water quickly travels through these ravines, picking up and carrying fine-grained particles as the water flows to the streams. Some watersheds in this region are highly impacted by ravines, such as the Knife River watershed (Figure 7.6), which in its lower reach flows through lacustrine and fine-grained till deposits and lacks substantial areas of bedrock. The ravines in this watershed could have a notable influence on TSS. Other watersheds in the region have significantly fewer ravines. For example, the Sucker River watershed (Figure 7.7) is highly bedrock- controlled and has few ravines. Therefore, ravine flow would have a minimal impact on TSS loads within that watershed.

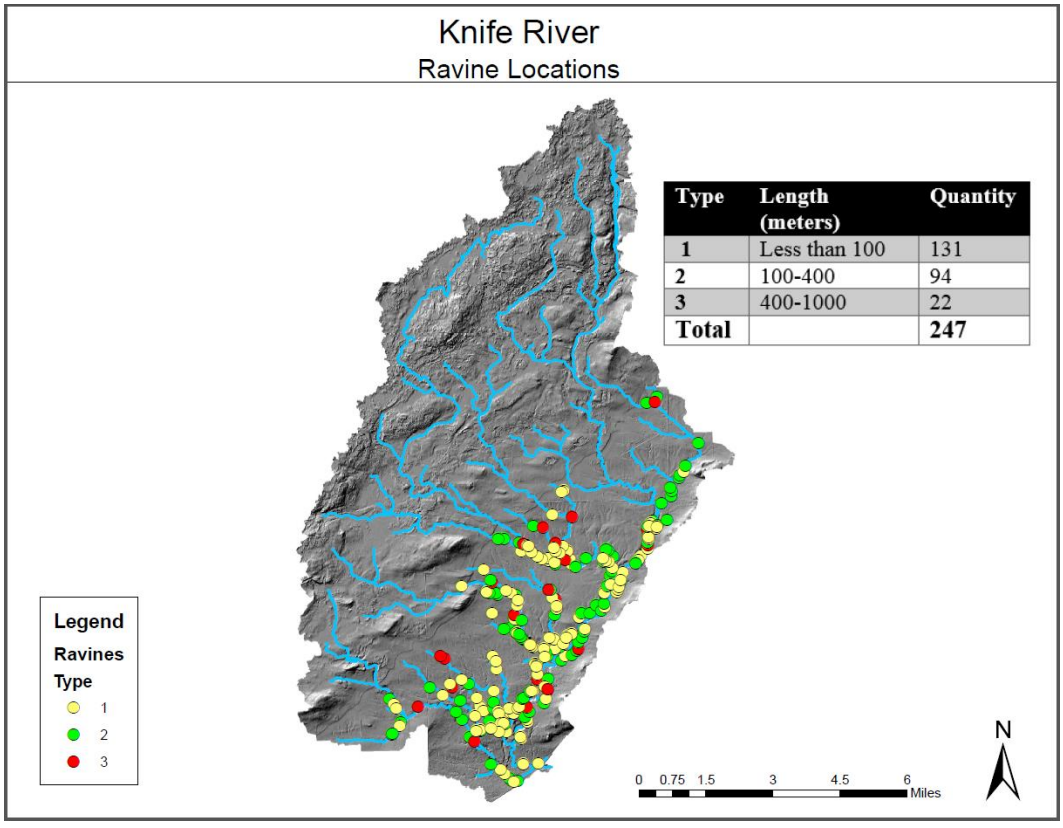

Figure 7.6: Knife River watershed with dots showing the location of all 247 ravines within the watershed.

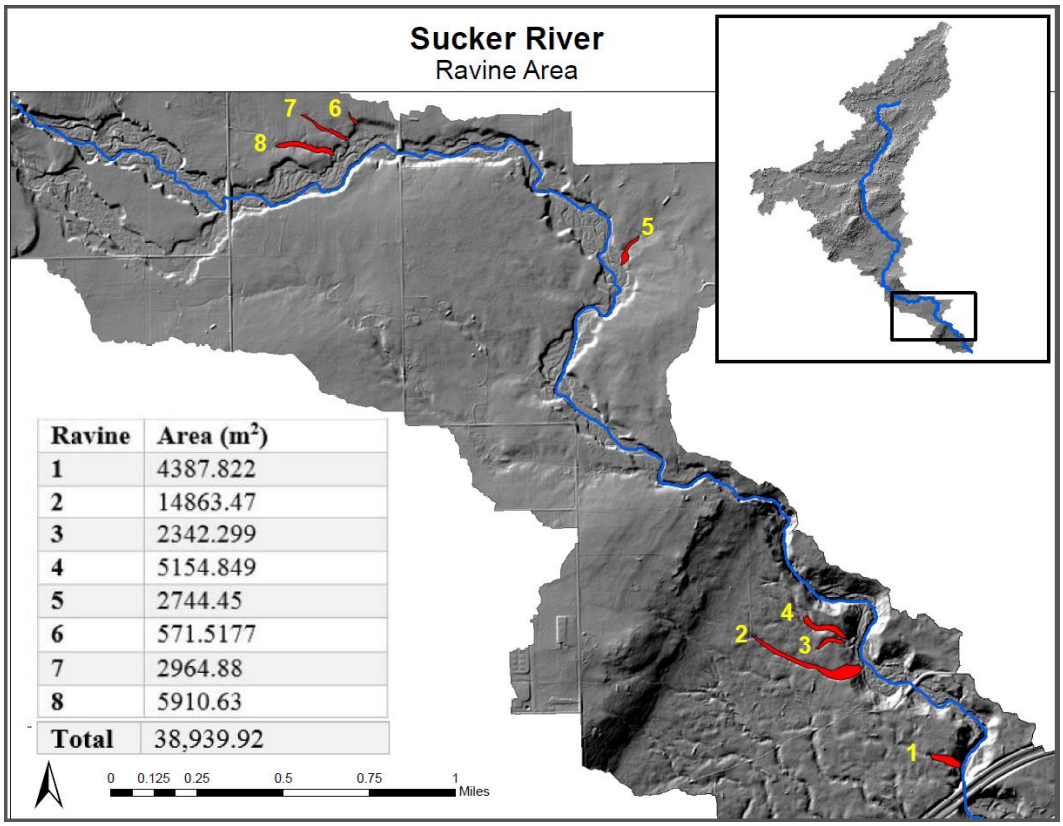

Ravine	Area (m^2)
1	4387.822
2	14863.47
3	2342.299
4	5154.849
5	2744.45
6	571.5177
7	2964.88
8	5910.63
Total	38,939.92

Figure 7.7: Sucker River watershed showing in red the area of the seven ravines within the watershed.

Past and current land use practices within the North Shore region also have negatively affected the water resources in the area, including draining wetlands, increasing the number of impervious surfaces and installing ditches. These practices increase the volume of water reaching the streams and concentrate this volume. The water coming off these land use practices will contain more sediment and more water volume in the stream will cause the stream power to increase, leading to more in-channel and near-channel sediment erosion.

Therefore, in order to restore water quality standards in the region, bluff stabilization is one effective mechanism but decreasing the amount of water reaching streams by overland flow will also work to improve water conditions within the region. This can be accomplished

by installing more wetlands and retention ponds to increase storage capacity in the watershed and will serve to decrease peak flows. Increasing infiltration capacity in the region would also be beneficial. This could be accomplished with the installation of rain gardens or replacing impervious surface with pervious surface.

REFERENCES

Anderson, K. 2010. Amity Creek bank stabilization and habitat restoration. In Proceedings of the Northland Innovative Stormwater Management Conference. Duluth, Minnesota, 2010.

Andrews, S.C., Christensen, R.G., Wilson, C.D. 1980. Impact of nonpoint pollution control on Western Lake Superior: Red Clay Project Final Report Part II. Prepared for U.S. Environmental Protection Agency.

Asare, S.N., Rudra, R.P., Dickinson, W.T., and Wall, G.J. 1997. Frequency of freezethaw cycles, bulk density and saturation effects on soil surface shear and stability in resisting water erosion. *Canadian Agricultural Engineering*. 39(4): 273-279.

Beckman Coulter, Inc. LS13 320 instruction manual. 2003.

Bedaiwy, M. N. 2012. A simplified approach for determining the hydrometer's dynamic settling depth in particle-size analysis. *Catena*. 97: 95-103.

Bitelli, G., Dubbini, M., and Zanutta, A. 2004. Terrestrial laser scanning and digital photogrammetry techniques to monitor landslide bodies. *In Proceedings of the 20th ISPRS congress*. Istanbul, Turkey, 2004

Blasone, G., Cavalli, M., Marchi, L., and Cazorzi, F. 2014. Monitoring sediment source areas in a debris-flow catchment using terrestrial laser scanning. *Catena*. 123: 23-36.

Bourke, M., Viles, H., Nicoli, J., Lyew-Ayee, P., Ghent, R., and Holmlund, J. 2008. I Innovative applications of laser scanning and rapid prototype printing to rock breakdown experiments. *Earth Surface Processes and Landforms*. 33(10): 1614-1621.

Bouyoucos, G. J. 1927. Directions for determining the colloidal material of soils by the hydrometer method. *Science*. 66(1696):16-17.

Bouyoucos, G. J. 1928. The hydrometer method for studying soils. *Soil Science*. 25(5): 365-370.

Bouyoucos, G. J. 1928. The hydrometer method for making a very detailed mechanical analysis of soils. *Soil Science*. 26(3): 233-238.

Bouyoucos, G. J. 1962. Hydrometer method improved for making particle size analyses of soils. *Agronomy Journal*. 54(5): 464-465.

Brasington, J., Vericat, D., and Rychkov, I. 2012. Modeling river bed morphology, roughness, and surface sedimentology using high resolution terrestrial laser scanning. *Water Resources Research*. 48(W11519): 1-18.

Brooks, K.N., Ffolliott, P.F., Magner, J.A. 2013. *Hydrology and the Management of Watersheds*. 4th edition. Ames, Iowa: Wiley-Blackwell.

Buckley, S.J., Howell, J.A., Enge, H.D., and Kurz, T.H. 2008. Terrestrial laser scanning in geology: data acquisition, processing and accuracy considerations. *Journal of the Geological Society, London*. 165: 625-638.

Cancienne, R.M., Fox, G.A., and Simon, A. 2008. Influence of seepage undercutting on the stability of root-reinforced streambanks. *Earth Surface Processes and Landforms*. 33: 1769-1786.

Casagli, N., Rinaldi, M., Gargini, A., and Curini, A. 1999. Pore water pressure and streambank stability: results from a monitoring site on the Sieve River, Italy. *Earth Surface Processes and Landforms*. 24: 1095-1114.

Charlton, M.E., Large A.R.G., and Fuller, I.C. 2003. Application of airborne LiDAR in river environments: The River Coquet, Northumberland, UK. *Earth Surface Processes and Landforms*. 28: 299-306.

Coveney, S., and Fotheringham, A.S. 2011. Terrestrial laser scan error in the presence of dense ground vegetation. *The Photogrammetric Record*. 26(135): 307-324.

Couper, P.R., and Maddock, I.P. 2001. Subaerial river bank erosion processes and their interaction with other bank erosion mechanisms on the River Arrow, Warwickshire, UK. *Earth Surface Processes and Landforms*. 26: 631-646.

Couper, P.R., Stott, T., & Maddock, I. 2002. Insights into river bank erosion processes derivedfrom analysis of negative erosion-pin recordings: Observations from three recent UK studies. *Earth Surface Processes and Landforms*. 27(1): 59-79.

Day, R. and Axten, G. 1989. Surficial stability of compacted clay slopes. *Journal of Geotechnical Engineering*. 115(4): 577 – 580.

Day, S.S., Gran, K.B., Belmont, P., and Wawrzyniec, T. 2012. Measuring bluff erosion part 1: terrestrial laser scanning methods for change detection and determining bluff erosion processes. *Earth Surface Processes and Landforms*. 38 (10): 1055-1067.

Day, S.S., Gran, K.B., Belmont, P., and Wawrzyniec, T. 2013. Measuring bluff erosion part 2: pairing aerial photographs and terrestrial laser scanning to create a watershed scale sediment budget. *Earth Surface Processes and Landforms*. 38 (10): 1068-1082.

Dietrich, W.E., and Gallinatti, J.D. 1991. Fluvial Geomorphology. *In Field Experiments and Measurement Programs in Geomorphology*, Slaymaker, O. (ed). Balkema: Rotterdam.

Faro Focus 3-D Laser Scanner. Tech Sheet. Web.

Farrand, W.R. 1969. The Quaternary history of Lake Superior. *In Proceedings of the 12th Conference on Great Lakes Research*. 181-197.

Farrand, W.R., and Drexler, C.W. 1985. Late Wisconsinan and Holocene history of the L Lake Superior Basin. *In Quaternary Evolution of the Great Lakes*, Karrow, P.F., Calkin, P.E. (eds). Geological Association of Canada Special Paper. 30: 17-32.

Fitzpatrick, F.A., Peppler, M.C., DePhilip, M.M., and Lee, K.E. 2006. U.S. Geological Survey; U.S. Department of the Interior. Geomorphic characteristics and classification of Duluth-area streams, Minnesota. Scientific Investigations Report 2006-5029.

Fox, G.A., Wilson, G.V., Simon, A., and Langendoen, E.J. 2007. Measuring streambank erosiondue to ground water seepage: correlation to bank pore water pressure, precipitation and stream stage. *Earth Surface Processes and Landforms*. 32: 1158-1573.

Grabbelaar, J. U. 2009. Turbidity. In *The Encyclopedia of Inland Waters*. Amsterdam: Elsevior. 699-704.

Grayson, R., Holden, J., Jones, R., Carle, J., & Lloyd, A. 2012. Improving particulate carbon loss estimates in eroding peatlands through the use of terrestrial laser scanning. *Geomorphology*. 179: 240-248.

Heritage, G., and Hetherington, D. 2007. Towards a protocol for laser scanning in fluvial geomorphology. *Earth Surface Processes and Landforms*. 32: 66-74.

Hobbs, H.C., and Goebel, J.E. 1982. Geologic map of Minnesota, Quaternary geology. Minnesota Geological Survey.

Hobbs, H.C. 2003. Surficial Geology of the Two Harbors quadrangle, Lake County, Minnesota. Minnesota Geological Survey.

Hobbs, H.C. 2004. Late Wisconsinan Superior-Lobe deposits in the Superior Basin northeast of Duluth. Institute on Lake Superior Geology, 4-9 May, 2004. Field Trip 3: 86-98.

Hobbs, H.C., and Breckenridge, A. 2011. Ice advances and retreats, inlets and outlets, sediments and strandlines of the western Lake Superior Basin. The Geological Society of America Field Guide. 24: 299-315.

Jones, R., Kokkalas, S., and McCaffrey, K. J. 2009. Quantitative analysis and visualization of nonplanar fault surfaces using terrestrial laser scanning (LIDAR)—The Arkitsa fault, central Greece, as a case study. *Geosphere*. 5(6): 465-482.

Kok, H., and McCool, D.K. 1989. Freeze-thaw induced variability of soil shear strength. ASAE Paper No. 89-2189. St. Joseph, MI: ASAE.

Lake County SWCD. 2014. 2015 Annual Plan of Work. Lake County, Minnesota Soil and Water Conservation District.

Lake Superior Streams. 2009. Lake Superior Streams: Community Partnerships for Understanding Water Quality and Stormwater Impacts at the Head of the Great Lakes (http://lakesuperiorstreams.org). University of Minnesota-Duluth, Duluth, MN.

Lawler, D.M. 1992. Process dominance in bank erosion systems. In *Lowland Floodplain Rivers: Geomorphological Perspectives*. Wiley, New York. 119-141.

Lawler, D.M. 1993. The measurement of river bank erosion and lateral channel change: a review.*Earth Surface Processes and Landforms*. 18: 777-821.

Letortu, P., Costa, S., Maquaire, O., Delacourt, C., Augereau, E., Davidson, R., Suanez, S., and Nabucet, J. 2015. Retreat rates, modalities and agents responsible for erosion along the coastal chalk cliffs of Upper Normandy: The contribution of terrestrial laser scanning. *Geomorphology*. 245: 3-14.

Lim, M., Rosser, N. J., Allison, R. J., and Petley, D. N. 2010. Erosional processes in the h hard rock coastal cliffs at Staithes, North Yorkshire. *Geomorphology*. 114(1-2): 12-21.

Munsell Color. 1975. Munsell Soil Color Charts. MacBeth Division of Kollmorgen Corp., Maryland USA.

Nasermoaddeli, M.H., and Pasche, E. 2008. Application of terrestrial 3D laser scanner in quantification of the riverbank erosion and deposition. In *Proceedings of Riverflow 2008*. 3: 2407-2416.

Neitzel, G.D. 2014. Monitoring event-scale stream bluff erosion with repeat terrestrial laser scanning: Amity Creek, Duluth, MN. M.S thesis. University of Minnesota – Duluth.

Nieber, J.L. 2014. Lake Superior Streams Sediment Stressor Investigation: Project Work Plan. University of Minnesota prepared for Minnesota Pollution Control Agency.

Nieber, J. L., Wilson, B. N., Ulrich, J. S., Hansen, B. J., and Canelon, D. J. 2008. Assessment of streambank and bluff erosion in the Knife River watershed. Final Report Submitted to Minnesota Pollution Control Agency. Department of Bioproducts and Biosystems Engineering, University of Minnesota.

Olsen, M. J. 2015. In situ change analysis and monitoring through terrestrial laser scanning. *Journal of Computing in Civil Engineering*. 29(2): 04014040-1-04014040-10.

O'Neal, M. A., and Pizzuto, J. E. 2010. The rates and spatial patterns of annual riverbank erosionrevealed through terrestrial laser-scanner surveys of the South River, Virginia. *Earth Surface Processes and Landforms.* 36(5): 695-701.

Pyle, C. J., Richards, K. S., and Chandler, J. H. 1997. Digital photogrammetric monitoring of river bank erosion. *The Photogrammetric Record*. 15(89): 753-764.

Resop, J.P., and Hession, W.C. 2010. Terrestrial laser scanning for monitoring streambank retreat: comparison with traditional surveying techniques. *Journal of Hydraulic Engineering*. 136(10): 794-798.

Rinaldi, M., Casagli, N., Daporto, S., and Gargini, A. 2004. Monitoring and modeling pore water pressure changes and riverbank stability during flow events. *Earth S Surface Processes and Landforms*. 29: 237-254.

Rosgen, D.L. 2006. The Cross-Vane, W-Weir and J-Hook Vane structures: their d description, design and application for stream stabilization and river restoration. Wildland Hydrology, Inc., Ft. Collins, CO.

Rosgen, D.L. 2011. The Trail Creek watershed master plan for stream restoration and sediment reduction. Wildland Hydrology, Inc., Ft. Collins, CO.

Rosser, N., Petley, D., Lim, M., Dunning, S., and Allison, R. 2005. Terrestrial laser scanning for monitoring the process of hard rock coastal cliff erosion. *Quarterly Journal of Engineering Geology and Hydrogeology*. 38(4): 363-375.

Schubert, J. E., Gallien, T. W., Majd, M. S., and Sanders, B. F. 2015. Terrestrial laser scanning of anthropogenic beach berm erosion and overtopping. *Journal of Coastal Research*. 299: 47-60.

Simon, A., Curini, A., Darby, S.E., and Langendoen, E.J. 1999. Streambank mechanics and therole of bank and near-bank processes in incised channels. In *Incised River Channels: Processes, Forms, Engineering and Management*, Darby, S.D., Simon, A. (eds). John Wiley and Sons: New York.

Simon, A., Curini, A., Darby, S.E., and Langendoen, E.J. 2000. Bank and near-bank processes in an incised channel. *Geomorphology*. 35: 193-217.

Sims, P.K., and Morey, G.B. 1972. Geology of Minnesota: a centennial volume. Minnesota Geological Survey. 632.

Teza, G., Pesci, A., Genevois, R., and Galgaro, A. 2008. Characterization of landslide ground surface kinematics from terrestrial laser scanning and strain field computation. *Geomorphology*. 97(3-4): 424-437.

Vosselman, G., & Maas, H. 2010. *Airborne and terrestrial laser scanning*. Dunbeath: Whittles Publishing.

Wawrzyniec, T. F., Mcfadden, L. D., Ellwein, A., Meyer, G., Scuderi, L., Mcauliffe, J., and Fawcett, P. 2007. Chronotopographic analysis directly from point-cloud data: Amethod for detecting small, seasonal hillslope change, Black Mesa Escarpment, NE Arizona. *Geosphere*. 3(6): 550-567.

Wheaton, J.M., Brasington, J., Darby, S. E., David, S.A., 2009. Accounting for uncertainty in DEMs from repeat topographic surveys: improved sediment budgets. *Earth Surface Processes and Landforms*. 35: 136-156.

Wick, M.J. 2013. Identifying erosional hotspots in streams along the North Shore of Lake Superior, Minnesota using high-resolution elevation and soils data. M.S. thesis. University of Minnesota – Duluth.

Wilson, G.V., Periketi, R.K., Fox, G.A., Dabney, S.M., Shields, F.D., and Cullum, R.F. 2007. Soil properties controlling seepage erosion contributions to streambank failure. *Earth Surface Processes and Landforms*. 32: 447-459.

Wright, H.E. 1971. Retreat of the Laurentide ice sheet from 14,000 to 9,000 years ago. *Quaternary Research*. 1(3): 316-330.

Wynn, T., and Mostaghimi, S. 2006. The effects of vegetation and soil type on streambank erosion, southwestern Virginia, USA. *Journal of the American Water Resources Association*. 42(1): 69-82.

Appendix A: Geomorphic Change Detection Maps

B9: November 2012 to November 2013

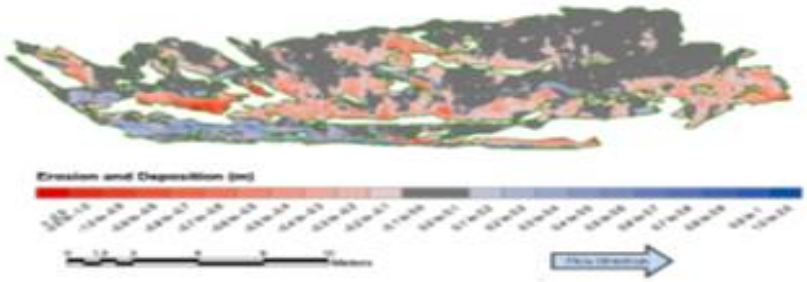

B9: November 2013 to September 2014

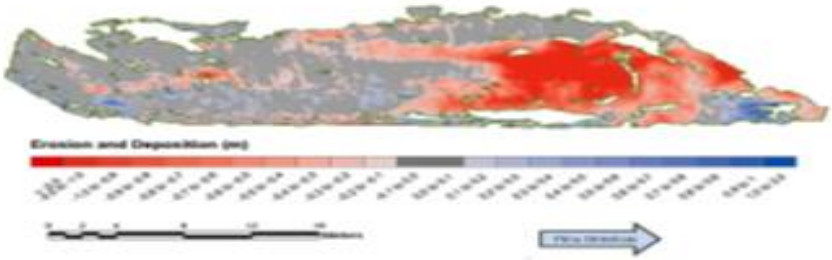

B9: September 2014 to April 2015

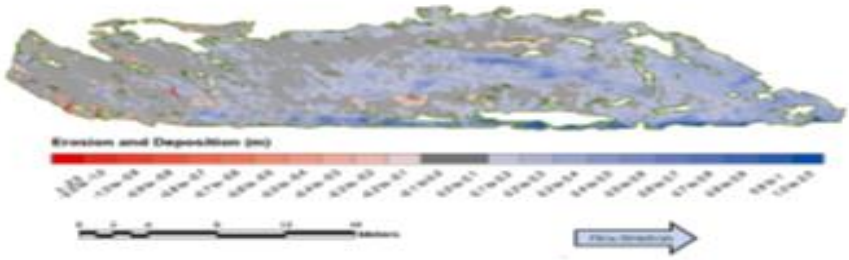

B9: November 2012 to November 2015

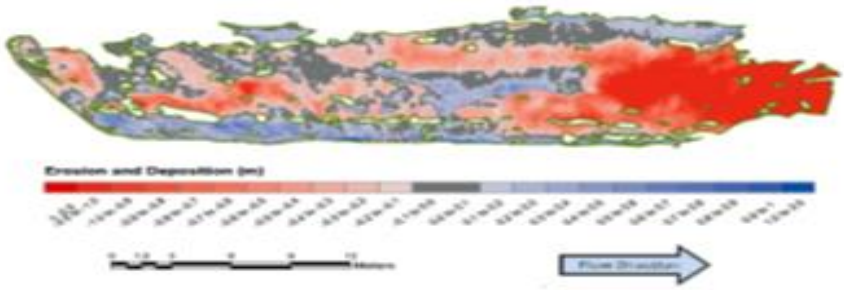

B12: September 2014 to April 2015

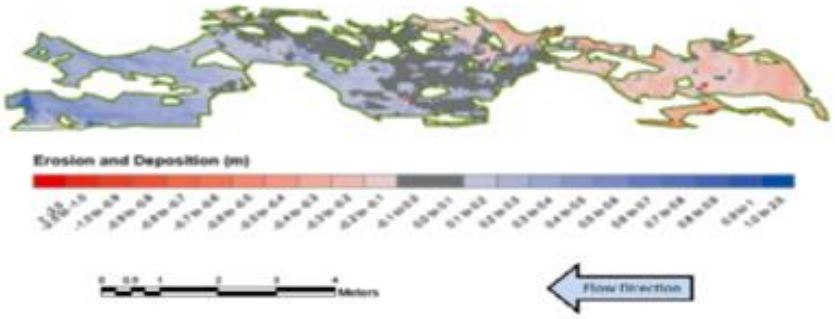

B12: April 2015 to November 2015

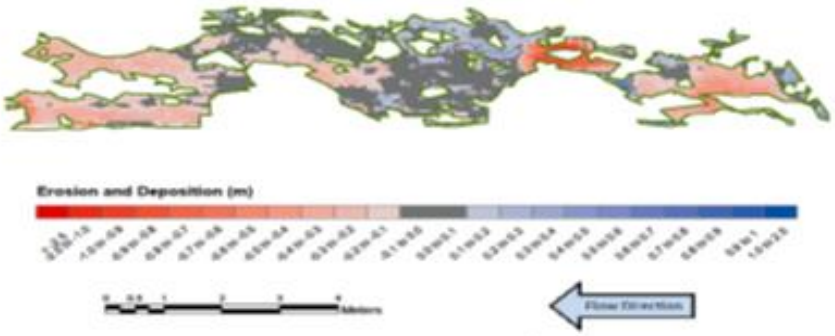

B12: November 2012 to November 2015

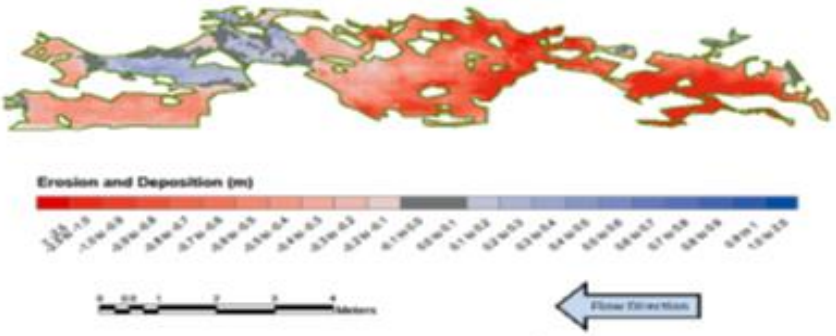

B13: November 2012 to November 2013

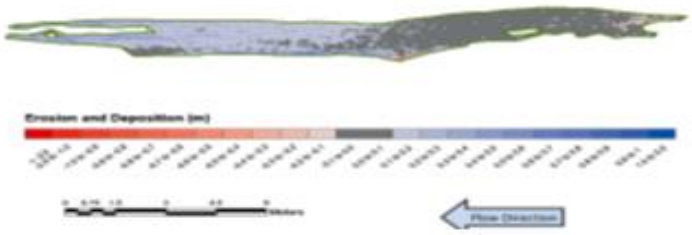

B13: November 2013 to September 2014

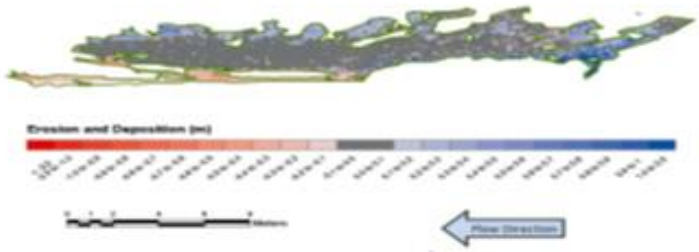

B13: April 2015 to November 2015

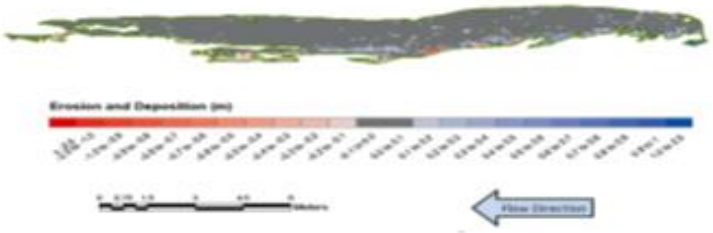

B13: April 2012 to November 2015

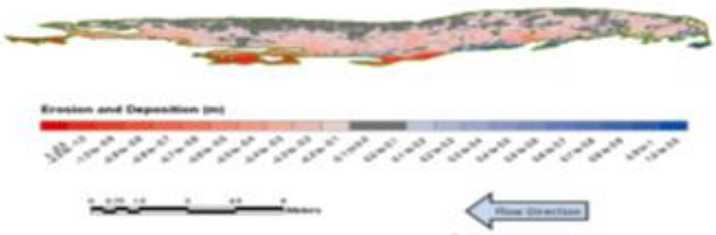

B14: November 2012 to November 2013

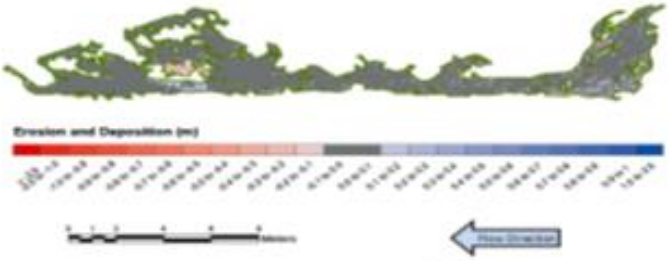

B14: November 2013 to April 2015

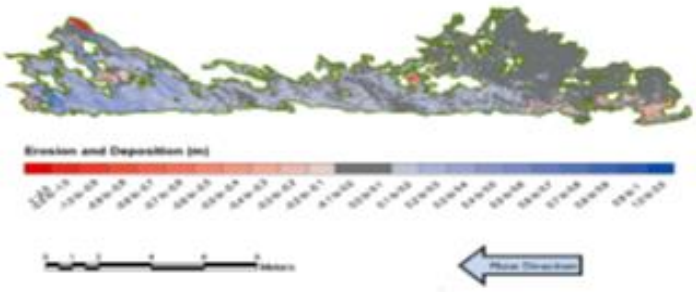

B14: April 2015 to November 2015

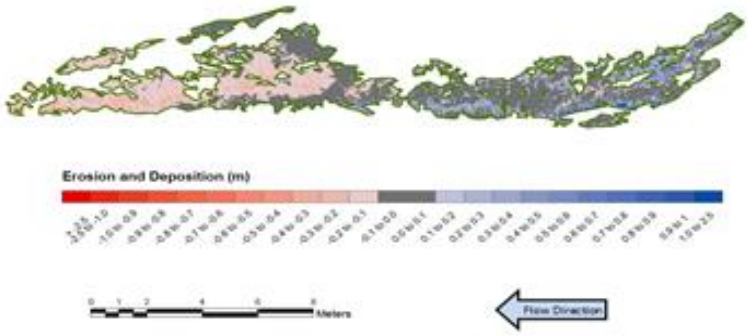

B14: November 2012 to November 2015

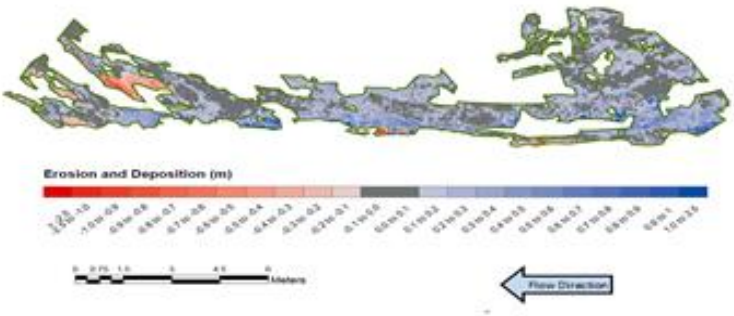

B15: November 2012 to November 2013

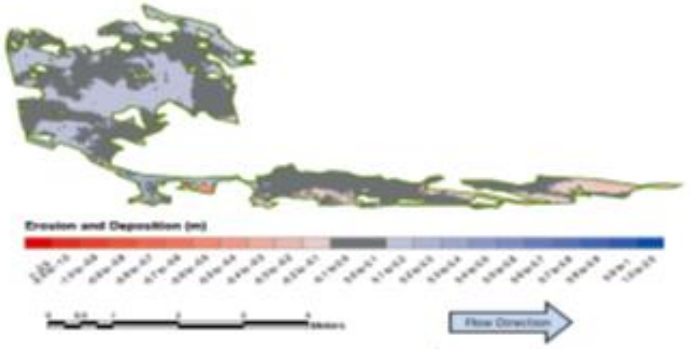

B15: November 2013 to September 2014

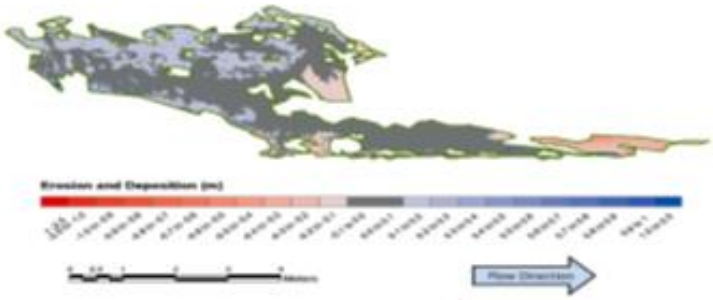

B15: September 2014 to April 2015

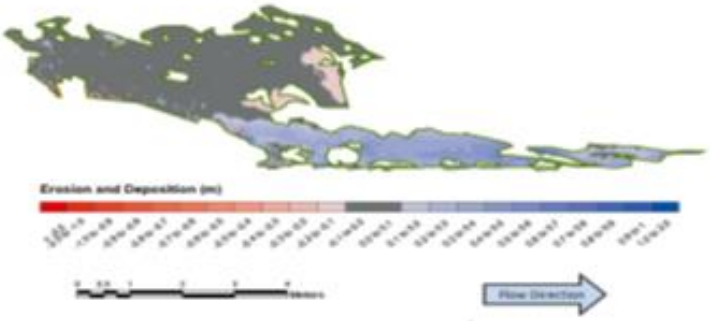

B15: November 2012 to November 2015

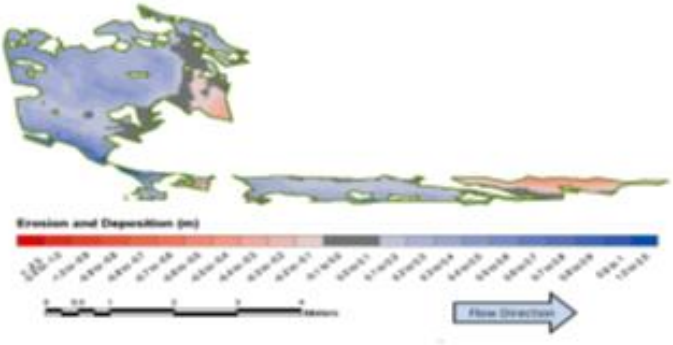

B20: November 2012 to November 2013

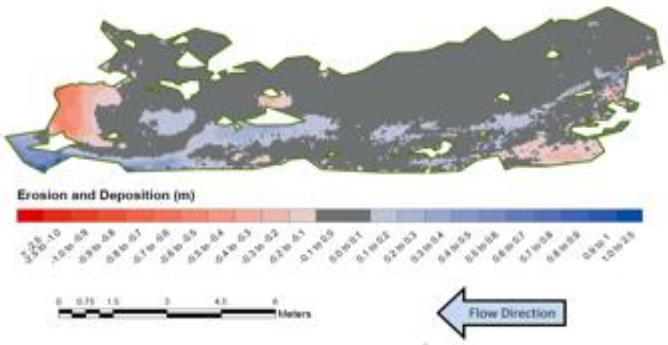

B20: November 2013 to September 2014

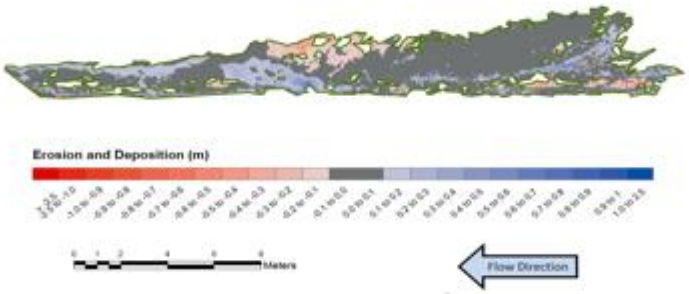

B20: April 2015 to November 2015

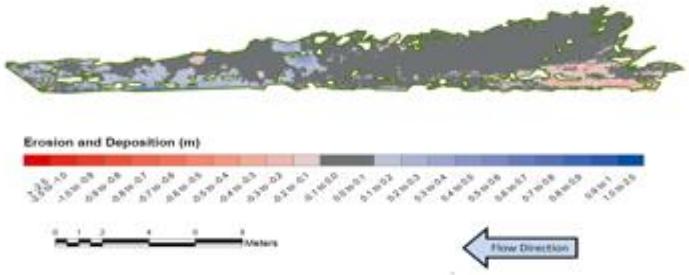

B20: November 2012 to November 2015

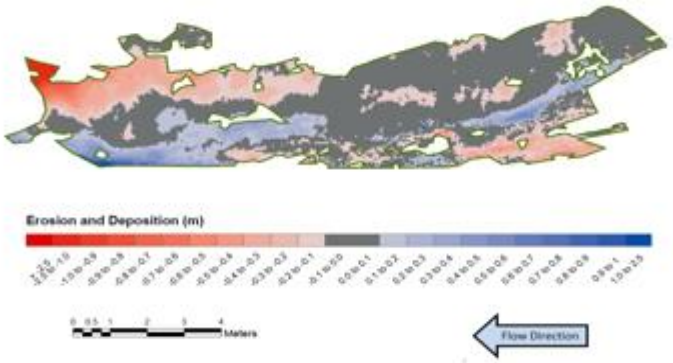

B2: November 2012 to November 2013

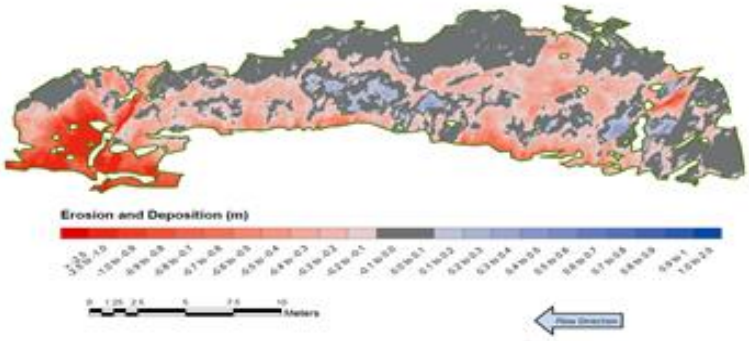

B2: September 2014 to April 2015

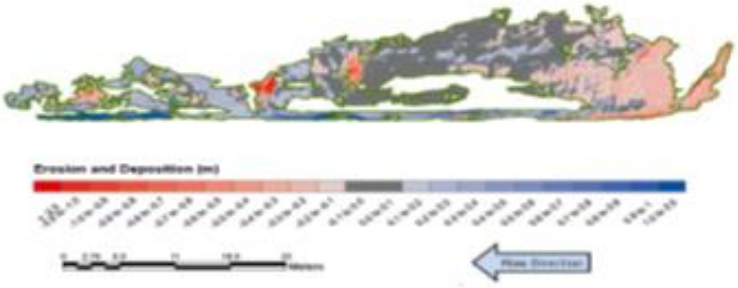

B2: April 2015 to November 2015

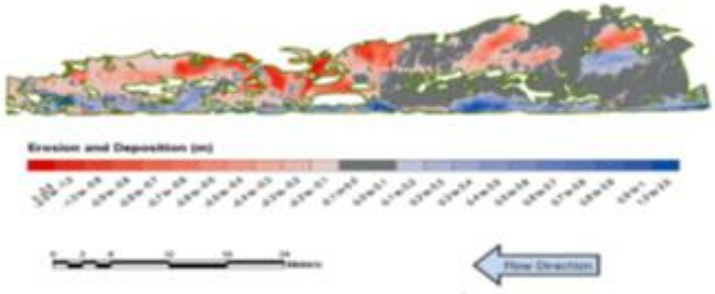

B2: November 2012 to November 2015

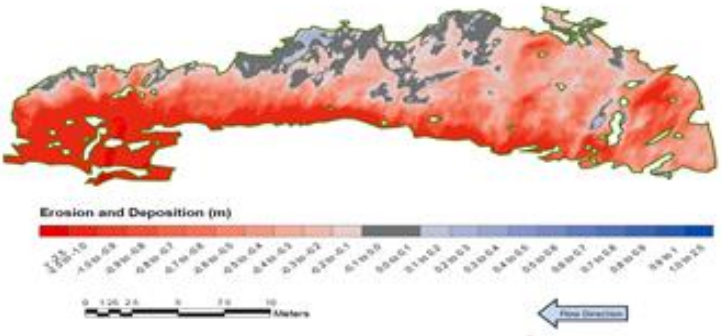

B7: November 2012 to November 2013

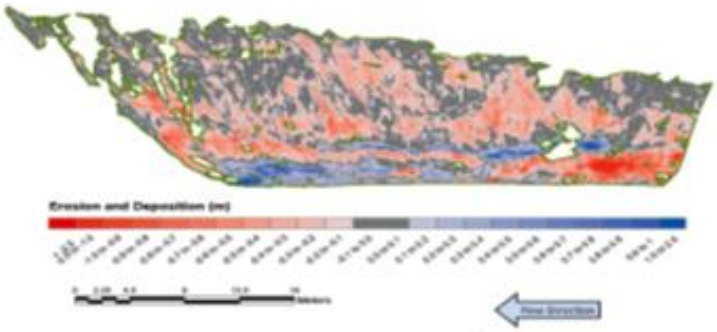

B7: September 2014 to April 2015

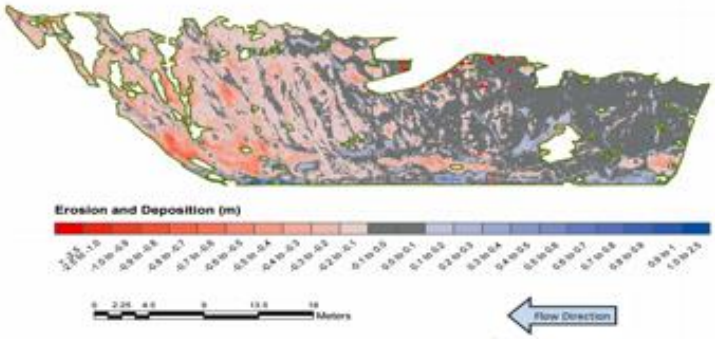

B7: April 2015 to November 2015

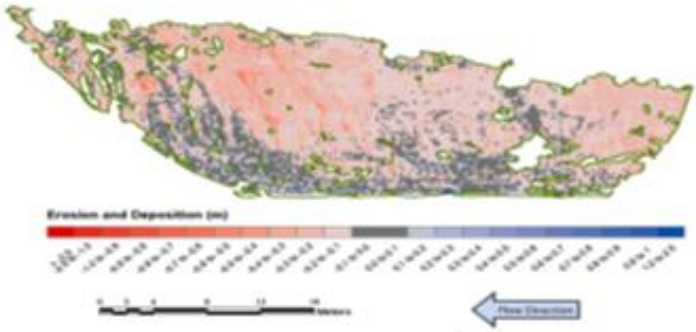

B7: November 2012 to November 2015

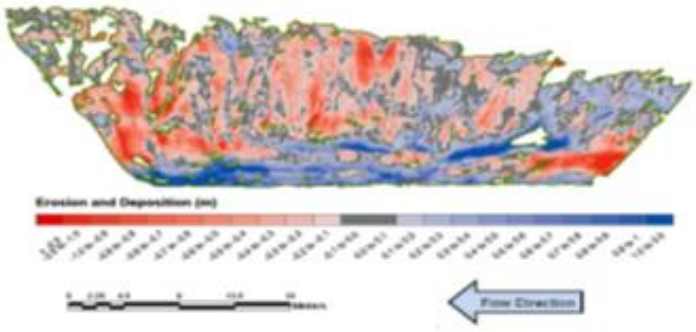

Hawk Hill Road: September 2014 to April 2015

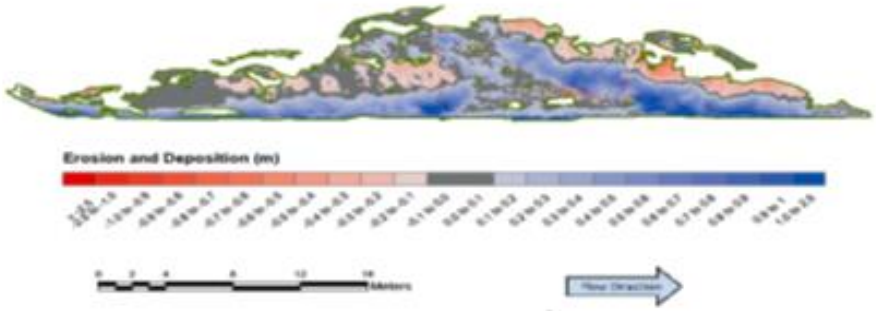

Hawk Hill Road: April 2015 to November 2015

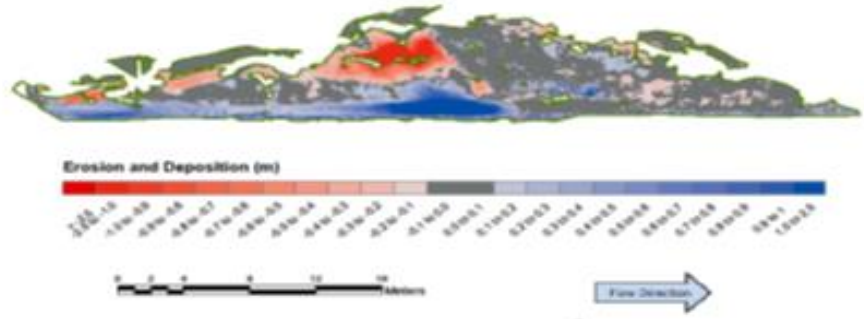

Hawk Hill Road: September 2014 to November 2015

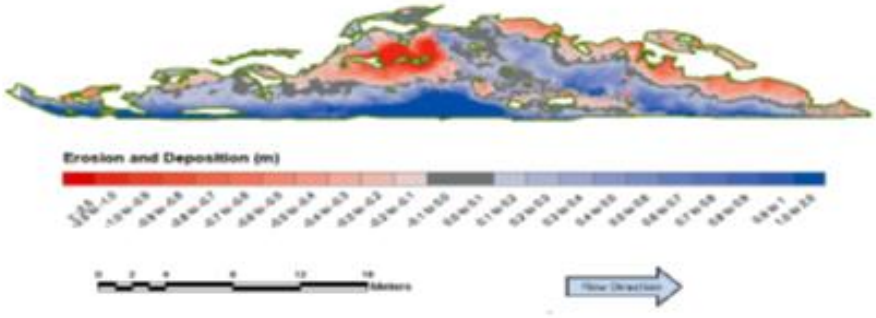

BSWCD: September 2014 to April 2015

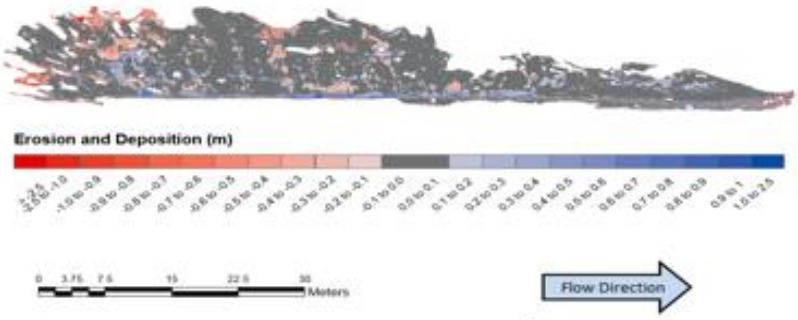

BSWCD: April 2015 to November 2015

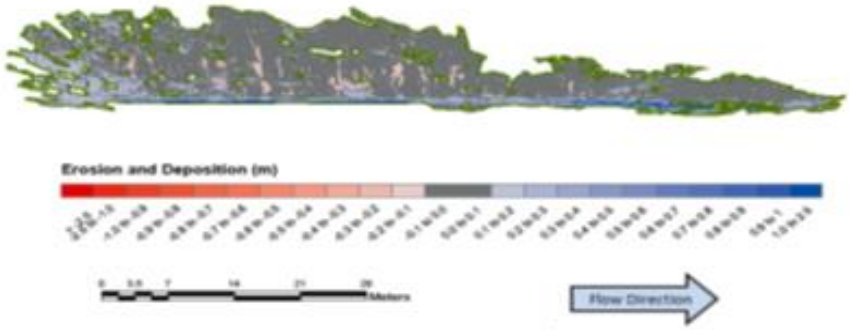

BSWCD: September 2014 to November 2015

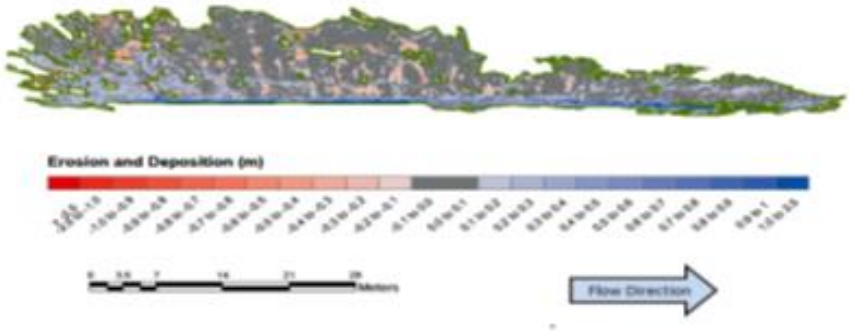

Appendix B: GCD Summary File Results

B9

November 2012 to November 2013

Attribute	Raw	Thresholded DoD Estimate:	± Error Volume	% Error
AREAL:				
Total Area of Erosion (m²)	141	70		
Total Area of Deposition (m²)	56	9		
VOLUMETRIC:				
Total Volume of Erosion (m³)	23	20	± 8	38%
Total Volume of Deposition (m³)	6	3	± 2	51%
Total Volume of Difference (m³)	29	23	± 9	40%
Total Net Volume Difference (m³)	-17	**-17**	**± 8**	-48%

November 2013 to September 2014

Attribute	Raw	Thresholded DoD Estimate:	± Error Volume	% Error
AREAL:				
Total Area of Erosion (m²)	251	251		
Total Area of Deposition (m²)	94	26		
VOLUMETRIC:				
Total Volume of Erosion (m³)	97	97	± 20	21%
Total Volume of Deposition (m³)	14	10	± 4	38%
Total Volume of Difference (m³)	111	107	± 24	23%
Total Net Volume Difference (m³)	-83	**-87**	**± 21**	-24%

September 2014 to April 2015

Attribute	Raw	Thresholded DoD Estimate:	± Error Volume	% Error
AREAL:				
Total Area of Erosion (m²)	58	58		
Total Area of Deposition (m²)	287	98		
VOLUMETRIC:				
Total Volume of Erosion (m³)	6	6	± 2	25%
Total Volume of Deposition (m³)	53	35	± 19	55%
Total Volume of Difference (m³)	59	41	± 21	50%
Total Net Volume Difference (m³)	47	**28**	**± 19**	67%

April 2015 to November 2015

Attribute	Raw	Thresholded DoD Estimate:	± Error Volume	% Error
AREAL:				
Total Area of Erosion (m²)	185	185		
Total Area of Deposition (m²)	30	0		
VOLUMETRIC:				
Total Volume of Erosion (m³)	21	21	± 8	38%
Total Volume of Deposition (m³)	3	1	± 1	65%
Total Volume of Difference (m³)	24	22	± 9	39%
Total Net Volume Difference (m³)	-19	**-20**	**± 8**	-40%

November 2012 to November 2015

Attribute	Raw	Thresholded DoD Estimate:	± Error Volume	% Error
AREAL:				
Total Area of Erosion (m²)	209	209		
Total Area of Deposition (m²)	96	49		
VOLUMETRIC:				
Total Volume of Erosion (m³)	106	106	± 17	16%
Total Volume of Deposition (m³)	20	17	± 6	37%
Total Volume of Difference (m³)	126	123	± 23	19%
Total Net Volume Difference (m³)	-87	**-90**	**± 18**	-20%

B12

September 2014 to April 2015

Attribute	Raw	Thresholded DoD Estimate:	± Error Volume	% Error
AREAL:				
Total Area of Erosion (m²)	6	5		
Total Area of Deposition (m²)	10	5		
VOLUMETRIC:				
Total Volume of Erosion (m³)	1	1	± 1	44%
Total Volume of Deposition (m³)	2	2	± 1	47%
Total Volume of Difference (m³)	3	3	± 1	46%
Total Net Volume Difference (m³)	1	**0**	**± 1**	228%

April 2015 to November 2015

Attribute	Raw	Thresholded DoD Estimate:	± Error Volume	% Error
AREAL:				
Total Area of Erosion (m²)	10	9		
Total Area of Deposition (m²)	5	2		
VOLUMETRIC:				
Total Volume of Erosion (m³)	2	2	± 1	35%
Total Volume of Deposition (m³)	1	0	± 0	47%
Total Volume of Difference (m³)	3	3	± 1	37%
Total Net Volume Difference (m³)	-2	**-2**	**± 1**	-47%

November 2012 to November 2015

Attribute	Raw	Thresholded DoD Estimate:	± Error Volume	% Error
AREAL:				
Total Area of Erosion (m²)	13	12		
Total Area of Deposition (m²)	2	1		
VOLUMETRIC:				
Total Volume of Erosion (m³)	8	8	± 1	16%
Total Volume of Deposition (m³)	0	0	± 0	57%
Total Volume of Difference (m³)	9	9	± 1	17%
Total Net Volume Difference (m³)	-8	**-8**	**± 1**	-17%

B13

November 2012 to November 2013

Attribute	Raw	Thresholded DoD Estimate:		
AREAL:				
Total Area of Erosion (m^2)	4	2		
Total Area of Deposition (m^2)	19	11		
VOLUMETRIC:			± Error Volume	% Error
Total Volume of Erosion (m^3)	0	0	± 0	29%
Total Volume of Deposition (m^3)	3	2	± 1	48%
Total Volume of Difference (m^3)	3	3	± 1	46%
Total Net Volume Difference (m^3)	3	**2**	**± 1**	53%

November 2013 to September 2014

Attribute	Raw	Thresholded DoD Estimate:		
AREAL:				
Total Area of Erosion (m^2)	34	34		
Total Area of Deposition (m^2)	27	15		
VOLUMETRIC:			± Error Volume	% Error
Total Volume of Erosion (m^3)	3	3	± 1	29%
Total Volume of Deposition (m^3)	7	7	± 1	21%
Total Volume of Difference (m^3)	10	10	± 2	23%
Total Net Volume Difference (m^3)	4	**4**	**± 2**	43%

September 2014 to April 2015

Attribute	Raw	Thresholded DoD Estimate:		
AREAL:				
Total Area of Erosion (m^2)	36	36		
Total Area of Deposition (m^2)	38	8		
VOLUMETRIC:			± Error Volume	% Error
Total Volume of Erosion (m^3)	13	13	± 2	19%
Total Volume of Deposition (m^3)	4	2	± 1	59%
Total Volume of Difference (m^3)	17	15	± 4	25%
Total Net Volume Difference (m^3)	-8	**-10**	**± 3**	-27%

April 2015 to November 2015

Attribute	Raw	Thresholded DoD Estimate:		
AREAL:				
Total Area of Erosion (m^2)	12	4		
Total Area of Deposition (m^2)	14	2		
VOLUMETRIC:			± Error Volume	% Error
Total Volume of Erosion (m^3)	1	1	± 0	34%
Total Volume of Deposition (m^3)	1	1	± 0	32%
Total Volume of Difference (m^3)	2	1	± 0	33%
Total Net Volume Difference (m^3)	0	**0**	**± 0**	311%

November 2012 to November 2015

Attribute	Raw	Thresholded DoD Estimate:		
AREAL:				
Total Area of Erosion (m^2)	24	21		
Total Area of Deposition (m^2)	2	1		
VOLUMETRIC:			± Error Volume	% Error
Total Volume of Erosion (m^3)	5	5	± 2	31%
Total Volume of Deposition (m^3)	1	1	± 0	16%
Total Volume of Difference (m^3)	6	6	± 2	29%
Total Net Volume Difference (m^3)	-5	**-5**	**± 2**	-36%

B14

November 2012 to November 2013

Attribute	Raw	Thresholded DoD Estimate:		
AREAL:				
Total Area of Erosion (m^2)	29	29		
Total Area of Deposition (m^2)	19	3		
VOLUMETRIC:			± Error Volume	% Error
Total Volume of Erosion (m^3)	2	2	± 0	21%
Total Volume of Deposition (m^3)	1	1	± 0	39%
Total Volume of Difference (m^3)	3	2	± 1	27%
Total Net Volume Difference (m^3)	0	**-1**	**± 0**	-47%

November 2013 to April 2015

Attribute	Raw	Thresholded DoD Estimate:		
AREAL:				
Total Area of Erosion (m^2)	15	4		
Total Area of Deposition (m^2)	48	12		
VOLUMETRIC:			± Error Volume	% Error
Total Volume of Erosion (m^3)	2	2	± 0	27%
Total Volume of Deposition (m^3)	8	5	± 3	53%
Total Volume of Difference (m^3)	10	6	± 3	46%
Total Net Volume Difference (m^3)	6	**3**	**± 3**	82%

April 2015 to November 2015

Attribute	Raw	Thresholded DoD Estimate:		
AREAL:				
Total Area of Erosion (m^2)	28	22		
Total Area of Deposition (m^2)	15	7		
VOLUMETRIC:			± Error Volume	% Error
Total Volume of Erosion (m^3)	3	3	± 2	49%
Total Volume of Deposition (m^3)	3	2	± 1	32%
Total Volume of Difference (m^3)	6	5	± 2	42%
Total Net Volume Difference (m^3)	-1	**-1**	**± 2**	-213%

November 2012 to November 2015

Attribute	Raw	Thresholded DoD Estimate:		
AREAL:				
Total Area of Erosion (m^2)	7	7		
Total Area of Deposition (m^2)	37	15		
VOLUMETRIC:			± Error Volume	% Error
Total Volume of Erosion (m^3)	1	1	± 0	27%
Total Volume of Deposition (m^3)	8	6	± 2	38%
Total Volume of Difference (m^3)	9	7	± 3	36%
Total Net Volume Difference (m^3)	7	**5**	**± 2**	47%

B15

November 2012 to November 2013

Attribute	Raw	Thresholded DoD Estimate:		
AREAL:				
Total Area of Erosion (m²)	3	2		
Total Area of Deposition (m²)	7	3		
VOLUMETRIC:			± Error Volume	% Error
Total Volume of Erosion (m³)	0	0	± 0	39%
Total Volume of Deposition (m³)	1	0	± 0	69%
Total Volume of Difference (m³)	1	1	± 0	58%
Total Net Volume Difference (m³)	0	**0**	**± 0**	154%

November 2013 to September 2014

Attribute	Raw	Thresholded DoD Estimate:		
AREAL:				
Total Area of Erosion (m²)	3	2		
Total Area of Deposition (m²)	12	4		
VOLUMETRIC:			± Error Volume	% Error
Total Volume of Erosion (m³)	0	0	± 0	41%
Total Volume of Deposition (m³)	1	1	± 0	68%
Total Volume of Difference (m³)	2	1	± 1	56%
Total Net Volume Difference (m³)	1	**0**	**± 0**	289%

September 2014 to April 2015

Attribute	Raw	Thresholded DoD Estimate:		
AREAL:				
Total Area of Erosion (m²)	3	1		
Total Area of Deposition (m²)	12	5		
VOLUMETRIC:			± Error Volume	% Error
Total Volume of Erosion (m³)	0	0	± 0	43%
Total Volume of Deposition (m³)	2	2	± 0	32%
Total Volume of Difference (m³)	2	2	± 1	33%
Total Net Volume Difference (m³)	2	**1**	**± 0**	37%

April 2015 to November 2015

Attribute	Raw	Thresholded DoD Estimate:		
AREAL:				
Total Area of Erosion (m²)	3	2		
Total Area of Deposition (m²)	12	6		
VOLUMETRIC:			± Error Volume	% Error
Total Volume of Erosion (m³)	0	0	± 0	41%
Total Volume of Deposition (m³)	1	1	± 1	61%
Total Volume of Difference (m³)	2	1	± 1	55%
Total Net Volume Difference (m³)	1	**1**	**± 1**	103%

November 2012 to November 2015

Attribute	Raw	Thresholded DoD Estimate:		
AREAL:				
Total Area of Erosion (m²)	1	1		
Total Area of Deposition (m²)	7	6		
VOLUMETRIC:			± Error Volume	% Error
Total Volume of Erosion (m³)	0	0	± 0	37%
Total Volume of Deposition (m³)	2	2	± 1	33%
Total Volume of Difference (m³)	2	2	± 1	34%
Total Net Volume Difference (m³)	2	**2**	**± 1**	39%

B20

November 2012 to November 2013

Attribute	Raw	Thresholded DoD Estimate:		
AREAL:				
Total Area of Erosion (m²)	24	10		
Total Area of Deposition (m²)	30	7		
VOLUMETRIC:			± Error Volume	% Error
Total Volume of Erosion (m³)	2	2	± 1	31%
Total Volume of Deposition (m³)	3	2	± 1	44%
Total Volume of Difference (m³)	4	3	± 1	37%
Total Net Volume Difference (m³)	1	**0**	**± 1**	198%

November 2013 to September 2014

Attribute	Raw	Thresholded DoD Estimate:		
AREAL:				
Total Area of Erosion (m²)	24	24		
Total Area of Deposition (m²)	40	4		
VOLUMETRIC:			± Error Volume	% Error
Total Volume of Erosion (m³)	2	2	± 1	35%
Total Volume of Deposition (m³)	4	1	± 1	82%
Total Volume of Difference (m³)	6	4	± 2	54%
Total Net Volume Difference (m³)	2	**-1**	**± 1**	-207%

September 2014 to April 2015

Attribute	Raw	Thresholded DoD Estimate:		
AREAL:				
Total Area of Erosion (m²)	27	27		
Total Area of Deposition (m²)	41	9		
VOLUMETRIC:			± Error Volume	% Error
Total Volume of Erosion (m³)	2	2	± 0	20%
Total Volume of Deposition (m³)	5	3	± 1	50%
Total Volume of Difference (m³)	7	5	± 2	37%
Total Net Volume Difference (m³)	3	**1**	**± 2**	191%

April 2015 to November 2015

Attribute	Raw	Thresholded DoD Estimate:		
AREAL:				
Total Area of Erosion (m²)	31	6		
Total Area of Deposition (m²)	32	4		
VOLUMETRIC:			± Error Volume	% Error
Total Volume of Erosion (m³)	2	1	± 1	48%
Total Volume of Deposition (m³)	3	2	± 1	63%
Total Volume of Difference (m³)	5	3	± 2	57%
Total Net Volume Difference (m³)	1	**0**	**± 1**	342%

November 2012 to November 2015

Attribute	Raw	Thresholded DoD Estimate:		
AREAL:				
Total Area of Erosion (m²)	33	33		
Total Area of Deposition (m²)	17	8		
VOLUMETRIC:			± Error Volume	% Error
Total Volume of Erosion (m³)	5	5	± 2	32%
Total Volume of Deposition (m³)	2	2	± 1	38%
Total Volume of Difference (m³)	7	7	± 2	34%
Total Net Volume Difference (m³)	-2	**-3**	**± 2**	-65%

B2

November 2012 to November 2013

Attribute	Raw	Thresholded DoD Estimate:		
AREAL:				
Total Area of Erosion (^{2})	188	136		
Total Area of Deposition (^{2})	62	6		
VOLUMETRIC:			± Error Volume	% Error
Total Volume of Erosion (^{3})	54	52	± 14	28%
Total Volume of Deposition (^{3})	4	1	± 1	83%
Total Volume of Difference (^{3})	58	53	± 16	29%
Total Net Volume Difference (^{3})	-50	**-50**	**± 15**	-29%

November 2013 to September 2014

Attribute	Raw	Thresholded DoD Estimate:		
AREAL:				
Total Area of Erosion (m^2)	381	381		
Total Area of Deposition (m^2)	83	19		
VOLUMETRIC:			± Error Volume	% Error
Total Volume of Erosion (m^3)	196	196	± 43	22%
Total Volume of Deposition (m^3)	26	20	± 5	25%
Total Volume of Difference (m^3)	222	215	± 48	22%
Total Net Volume Difference (m^3)	-170	**-176**	**± 43**	-24%

September 2014 to April 2015

Attribute	Raw	Thresholded DoD Estimate:		
AREAL:				
Total Area of Erosion (m^2)	251	251		
Total Area of Deposition (m^2)	214	29		
VOLUMETRIC:			± Error Volume	% Error
Total Volume of Erosion (m^3)	48	48	± 17	35%
Total Volume of Deposition (m^3)	51	29	± 13	46%
Total Volume of Difference (m^3)	99	77	± 30	39%
Total Net Volume Difference (m^3)	3	**-19**	**± 21**	-110%

April 2015 to November 2015

Attribute	Raw	Thresholded DoD Estimate:		
AREAL:				
Total Area of Erosion (m^2)	379	379		
Total Area of Deposition (m^2)	205	82		
VOLUMETRIC:			± Error Volume	% Error
Total Volume of Erosion (m^3)	107	107	± 25	24%
Total Volume of Deposition (m^3)	50	42	± 12	28%
Total Volume of Difference (m^3)	157	149	± 37	25%
Total Net Volume Difference (m^3)	-58	**-65**	**± 28**	-43%

November 2012 to November 2015

Attribute	Raw	Thresholded DoD Estimate:		
AREAL:				
Total Area of Erosion (^{2})	234	234		
Total Area of Deposition (^{2})	17	3		
VOLUMETRIC:			± Error Volume	% Error
Total Volume of Erosion (^{3})	158	158	± 25	16%
Total Volume of Deposition (^{3})	1	1	± 0	85%
Total Volume of Difference (^{3})	160	159	± 25	16%
Total Net Volume Difference (^{3})	-157	**-158**	**± 25**	-16%

B7

November 2012 to November 2013

Attribute	Raw	Thresholded DoD Estimate:		
AREAL:				
Total Area of Erosion (m^2)	465	465		
Total Area of Deposition (m^2)	168	69		
VOLUMETRIC:			± Error Volume	% Error
Total Volume of Erosion (m^3)	108	108	± 32	29%
Total Volume of Deposition (m^3)	29	25	± 7	28%
Total Volume of Difference (m^3)	137	133	± 39	29%
Total Net Volume Difference (m^3)	-80	**-84**	**± 32**	-39%

November 2013 to September 2014

Attribute	Raw	Thresholded DoD Estimate:		
AREAL:				
Total Area of Erosion (m^2)	444	444		
Total Area of Deposition (m^2)	169	9		
VOLUMETRIC:			± Error Volume	% Error
Total Volume of Erosion (m^3)	91	91	± 29	32%
Total Volume of Deposition (m^3)	71	55	± 7	12%
Total Volume of Difference (m^3)	161	145	± 35	24%
Total Net Volume Difference (m^3)	-20	**-36**	**± 29**	-82%

September 2014 to April 2015

Attribute	Raw	Thresholded DoD Estimate:		
AREAL:				
Total Area of Erosion (m^2)	460	460		
Total Area of Deposition (m^2)	138	3		
VOLUMETRIC:			± Error Volume	% Error
Total Volume of Erosion (m^3)	99	99	± 26	27%
Total Volume of Deposition (m^3)	14	3	± 4	151%
Total Volume of Difference (m^3)	113	101	± 30	30%
Total Net Volume Difference (m^3)	-85	**-96**	**± 27**	-28%

April 2015 to November 2015

Attribute	Raw	Thresholded DoD Estimate:		
AREAL:				
Total Area of Erosion (m^2)	470	470		
Total Area of Deposition (m^2)	37	13		
VOLUMETRIC:			± Error Volume	% Error
Total Volume of Erosion (m^3)	84	84	± 38	45%
Total Volume of Deposition (m^3)	4	3	± 1	39%
Total Volume of Difference (m^3)	88	87	± 40	45%
Total Net Volume Difference (m^3)	-80	**-81**	**± 38**	-47%

November 2012 to November 2015

Attribute	Raw	Thresholded DoD Estimate:		
AREAL:				
Total Area of Erosion (m^2)	418	337		
Total Area of Deposition (m^2)	253	134		
VOLUMETRIC:			± Error Volume	% Error
Total Volume of Erosion (m^3)	131	127	± 36	28%
Total Volume of Deposition (m^3)	87	76	± 20	26%
Total Volume of Difference (m^3)	218	203	± 56	28%
Total Net Volume Difference (m^3)	-44	**-51**	**± 41**	-81%

BSWCD

September 2014 to April 2015

Attribute	Raw	Thresholded DoD Estimate:		
AREAL:				
Total Area of Erosion (m^2)	308	308		
Total Area of Deposition (m^2)	375	18		
VOLUMETRIC:			± Error Volume	% Error
Total Volume of Erosion (m^3)	38	38 ±	10	26%
Total Volume of Deposition (m^3)	32	10 ±	8	75%
Total Volume of Difference (m^3)	70	49 ±	18	37%
Total Net Volume Difference (m^3)	-6	**-28 ±**	**13**	-46%

April 2015 to November 2015

Attribute	Raw	Thresholded DoD Estimate:		
AREAL:				
Total Area of Erosion (m^2)	195	195		
Total Area of Deposition (m^2)	460	49		
VOLUMETRIC:			± Error Volume	% Error
Total Volume of Erosion (m^3)	11	11 ±	3	24%
Total Volume of Deposition (m^3)	63	36 ±	14	38%
Total Volume of Difference (m^3)	74	47 ±	16	35%
Total Net Volume Difference (m^3)	52	**25 ±**	**14**	55%

September 2014 to November 2015

Attribute	Raw	Thresholded DoD Estimate:		
AREAL:				
Total Area of Erosion (m^2)	221	221		
Total Area of Deposition (m^2)	435	48		
VOLUMETRIC:			± Error Volume	% Error
Total Volume of Erosion (m^3)	27	27 ±	8	29%
Total Volume of Deposition (m^3)	75	41 ±	17	42%
Total Volume of Difference (m^3)	102	68 ±	25	37%
Total Net Volume Difference (m^3)	48	**14 ±**	**19**	134%

BHHR

September 2014 to April 2015

Attribute	Raw	Thresholded DoD Estimate:		
AREAL:				
Total Area of Erosion (m^2)	69	69		
Total Area of Deposition (m^2)	136	75		
VOLUMETRIC:			± Error Volume	% Error
Total Volume of Erosion (m^3)	12	12 ±	4	33%
Total Volume of Deposition (m^3)	46	41 ±	10	23%
Total Volume of Difference (m^3)	58	53 ±	14	26%
Total Net Volume Difference (m^3)	35	**30 ±**	**10**	35%

April 2015 to November 2015

Attribute	Raw	Thresholded DoD Estimate:		
AREAL:				
Total Area of Erosion (m^2)	117	117		
Total Area of Deposition (m^2)	109	52		
VOLUMETRIC:			± Error Volume	% Error
Total Volume of Erosion (m^3)	24	24 ±	5	21%
Total Volume of Deposition (m^3)	35	32 ±	7	21%
Total Volume of Difference (m^3)	59	56 ±	12	21%
Total Net Volume Difference (m^3)	11	**8 ±**	**8**	108%

September 2014 to November 2015

Attribute	Raw	Thresholded DoD Estimate:		
AREAL:				
Total Area of Erosion (m^2)	85	85		
Total Area of Deposition (m^2)	121	71		
VOLUMETRIC:			± Error Volume	% Error
Total Volume of Erosion (m^3)	31	31 ±	7	23%
Total Volume of Deposition (m^3)	66	60 ±	11	18%
Total Volume of Difference (m^3)	97	91 ±	18	19%
Total Net Volume Difference (m^3)	35	**29 ±**	**13**	44%

Appendix C: Post-Processing Procedures

A) Faro Scene

- Create a new project in Faro Scene and add all the scan (.fls) files from a campaign. This can be done by dragging the files from the Windows folder to Faro Scene.

- Pre-process scans: Right-click on the "Scans" folder at the top of the structure tree on the left of the screen. Selected "Operations" → "Preprocessing" → "Process Scans". A dialogue box will appear – select "Spheres" under the "Detect Artificial References" and "Place Scans", then click "OK". Make sure that the lights next to the "ScanFit" folders for each scan are all green. If they are not green, check the "AutoFeatures" → "Sphere Container" folder. Make sure only actual spheres are being located by the software, which can be done by right-clicking on the individual scan (i.e. B2_Scan1) and selecting "View" → "Planar View" and then right-clicking on the individuals sphere and selecting "Locate 'Sphere'". If the software is finding another object, such as a round rock, right-click on the sphere in the structure tree and select "Delete 'Sphere'". Check all the spheres in each scan folder and then right-click on the "Scans" folder select "Operations" → "Registration" → "Place Scans" and then "OK".

- Remove unnecessary areas from the point cloud dataset: Right-click the "Scans" folder again and select "View" → "3D View". Using the "Polygon Selector" tool, which is shown as the button on top with the image of a yellow polygon, remove areas that are unnecessary to the point cloud. This can be done by clicking to make a polygon around an area not of the bluff and then double click. This will produce a polygon that is yellow. Right-click on this yellow polygon and select "Delete Inside Selection".

- Remove vegetation: Vegetation must be removed from each scan file. Right-click on an individual scan file and select "View" → "Planar View". Using the "Rectangular Selector" tool, select a vertical slice of the bluff, starting at one end. Right-click on the vertical rectangle and selected "View" → "3D View". Rotate the section of the bluff laterally using the "Set Rotation Point" tool and then using the "Polygon Selector" tool again select vegetation, right-click and delete inside/outside selection. Continue this process for the rest of the scan and for all the scans encompassing the campaign.

- Register campaigns together: Create a new project in Faro Scene and create a new folder for each campaign in the structure tree. New folders can be made by right-clicking on "Models" and then selecting "New" → "Folder". In the dialogue box give it a name and in the "Layer" box, select "Scans". Bring in all the processed scan files to each campaign folder. This can be done by opening the Windows folder where the processed scans are being saved to and dragging them into the structure tree of the new project. Once each campaign has all its scan (.fls) files registered, register all the campaigns together. This can be done by going to the top folder on the structure tree (i.e. Scans_All), right-clicking and selecting "Operations" → "Registration" → "Place Scans" and then "OK".

- Register scans with manually selected objects: If not enough or no control points (i.e. spheres) are available between campaigns then campaigns can be registered manually. To do this, selected "Correspondence Split View" and drag in scan (.fls) files from different campaigns. It helps if scans are in color, which can be done by right-clicking on the scan file and selecting "Operations" → "Color/Pictures" → "Colorize Scan". Next, locate objects between the scans from different campaigns that appear to be the same, such as corners of large rocks or cracks in rocks. Once a point is found select "Mark a scan point", click on the point in one scan, give it a name (i.e. Red_Rock_Corner) and then select the same point in the second scan. Next, select "Force Correspondence" and click the marked point in each scan, which should give the points the same name in each scan. After multiple points are found between the two scans, select "Force current correspondences between shown scans". Continue this process for different variations of scans. Once manual targets are found right-click the top folder (Scans_All) selected "Operations" → "Registration" → "Place Scans". In the dialogue box, just check "Force correspondences by manual target names" and "Calculate scan point based statistics".

- Check accuracy of scan registration by target tension values: To check the accuracy of the scan registration, right-click the top "Scan Manager" in the structure tree. This will bring up a dialogue box with multiple tabs. Under the "Target Tension" tab, it shows the points that are being used to register the scans together and the tension between the points. If the tension is high, the points can be deleted by right-clicking on the points and selecting "Set Anti Correspondence", then select "Apply" and "OK".

- Check accuracy of scan registration visually: Right-click on top scan folder, select "Operations" → "View" → "Correspondence View". This shows all the scan campaigns in a different color and shows if scans are close to being aligned properly.

- Align scans on proper coordinate plane: In "Correspondence View", use the rotation tools to confirm the bluff scans are aligned so that the z-axis is perpendicular to the face of the bluff and the y-axis would be perpendicular to the Earth's surface. If this is not the case, click the tag with the name of the scan campaign. This will bring up arrows, use these arrows to rotate the scans. After the scan campaigns are all rotated, go back and register the campaigns again. Confirm in "Correspondence View" that the orientation of the scans is now correct.

- Export point cloud: Right-click on a campaign folder, select "Import/Export" → "Export Scan Points". Export as a .pts file, provide a name and destination for the file, and then select "Export".

B) ToPCAT

- Create a new folder (easy to have it on the desktop as you are working on this process) and within the folder create a folder for each campaign (i.e. each .pts file exported from Faro Scene).

- In each campaign folder place the .pts file, pcgrid.exe file, pctools.bat file, pctools.dll file, pctools.py file and a run.bat file.

- Right-click the "run" file and edit it to read: 'pcgrid "name".pts --xres 0.05 --yres 0.05 --nmin 4 --*zmin0 --*zmean 1 --*stdev 0 @pause' and then save. Double click the "run" file back in the folder to run the decimation process. Note: the 'xres' and the 'yres' can be changed based on what you want to use to decimate the point cloud (e.g. 0.05 = 5 cm). Also, make sure the "name" exactly matches the .pts file name. This process will produce 7 additional files in the folder.

C) ArcMap/GCD

- Import files: In ArcMap select "File" → "Add Data" → "Add XY Data". In the dialogue box, locate the .zmin file produced for the campaign using ToPCAT, in the "Y Field" select 'zmin' and in the "Z Field" select 'y'. Also, add a coordinate system, such as NAD_1983_UTM_Zone_15N. Import all the campaigns for a specific bluff.

- Export data as a point shapefile: Right-click on the .txt file and select "Data" → "Export Data". In the dialogue box, give it a name and in the "Save as type" box select 'Shapefile'. Once complete add the .shp to the map and the .txt can be removed. Export all the campaigns to shapefiles.

- Create common extent shapefiles for each campaign: In ArcCatalog, create new polygon shapefiles for each campaign and using the editor tool create a polygon that outlines the boundary of each campaign's point shapefile. Next turn on all the polygons and create a new polygon shapefile that exceeds the boundary of all the campaign polygons.

- Create a polygon that only includes areas where geomorphic change can be detected on all the campaigns: Select "Geoprocessing" → "Clip" and in the "Input Feature" box put the large polygon. In the "Clip Features" box insert the polygon that encompasses the extent of the earliest scanning campaign. Next, do this step again using the output polygon shapefile generated from running the process the first time and now in the "Clip Features" box insert the polygon that encompasses the extent of the second to the earliest scanning campaign. Continue this step until a polygon is available that is clipped to include only the area where all the campaigns that are being compared overlap. After a polygon is available that is clipped to the boundaries, overlay the point shapefiles one at a time from each campaign to it and clip out holes. This can be done by right-clicking on the polygon in the Table of Contents, selecting "Edit Feature" → "Start Editing". Then in the "Create Feature" box, click on the shapefile and in the "Construction Tools" box click on polygon. Create a polygon on the main polygon, around the hole in the point shapefile. Close the polygon, go to "Editor" → "Clip" → "OK" (make sure "Discard the area that

intersects" is checked) and then go to "Edit" → "Delete". Continue this process for all the holes in every point shapefile.

- Create a TIN: In ArcToolbox, go to "3D Analyst Tools" → "Data Management" → "TIN" → "Create TIN". Use one of the point shapefiles as your first "Input Feature Class" and specify 'y' in the Height Field, 'Mass_Points' as the SF type, and '<None>' for the Tag Field. Use the clipped polygon shapefile for the second input feature class; specify '<None>' for the Height Field, 'Hard_Clip' as the SF type, and '<None>' for the Tag Field. Create a TIN for each campaign.

- Create a DEM: In ArcToolbox, go to "3D Analyst Tools" → "Conversion" → "From TIN" → "TIN to Raster". Input TIN, specify 'Float' under "Output Data Type" and 'Natural Neighbors' under "Method". To define DEM resolution, manually enter the same resolution as used in the decimation of the point cloud in ToPCAT (e.g. 0.05) under "Sampling Distance". Under "Environments" (within Tin to Raster tool) go to "Processing Extent" and define the "Extent" as the polygon shapefile created of the boundary of this point shapefile (not the one that was clipped to fit the extent of all the campaigns). Next, round the top and right extents up to nearest whole number and the bottom and left extents down to the nearest whole number. Create a DEM for each campaign. Note: When creating the rest of the DEMs, the DEM that was created first can be used as the processing extent for each successive DEM generated.

- Detect geomorphic change: Using the GCD Add-In, go to "Project" → "New" and give the project a name and destination to be saved. Next, go to "Data Preparation" → "Survey Library" and add each DEM, making sure to select "Single method survey" and "TLS". Then go to "GCD Analysis" → "Change Detection". In the Change Detection tool, pick the older DEM as the "New Survey" and the newer DEM as the "Old Survey". Make sure the "Simple minimum level of detection" is selected and click "Calculate". Using the threshold slider bar on the right side, move the arrow to 0.10 m and click "Save".